Scaffolding cooperation in human groups with deep reinforcement learning

Kevin R. McKee[1,*], Andrea Tacchetti[1], Michiel Bakker[1], Jan Balaguer[1], Lucy Campbell-Gillingham[1], Richard Everett[1] and Matt Botvinick[1,2]

[1]DeepMind, London, UK, [2]Gatsby Computational Neuroscience Unit, University College London, London, UK, [*]Corresponding author

Altruism and selfishness are highly transmissible. Either can easily cascade through human communities. Effective approaches to encouraging group cooperation—while also mitigating the risk of spreading defection—are still an open challenge. Here, we apply recent advances in deep reinforcement learning to structure networks of human participants playing a group cooperation game. We leverage deep reinforcement learning and simulation methods to train a "social planner" capable of making recommendations to create or break connections between group members. This social planner learns a strategy from scratch, through repeated trial and error. The strategy that it develops succeeds at encouraging prosociality in networks of human participants (N = 208 participants in 13 groups) playing the group cooperation game for real monetary stakes. Under the social planner, groups finished the game with an average cooperation rate of 77.7%, compared to 42.8% in static networks (N = 176 participants in 11 groups). In contrast to prior strategies that separate defectors from cooperators (tested here with N = 384 participants in 24 groups), the social planner learns to take a conciliatory approach to defectors, encouraging them to act prosocially by moving them to small, highly-cooperative neighborhoods. Three follow-up studies (N = 624 participants in 39 groups) validate that this encouraging approach can scaffold group cooperation absent the "black box" of deep learning. Deep learning can help explore and identify new approaches to support human cooperation and prosociality.

Keywords: cooperation, social networks, deep reinforcement learning, social contagion, assortativity

Introduction

Cooperation is contagious. Social contact and interaction can spread prosociality from one person to another (Christakis and Fowler, 2013; Keizer et al., 2013; Tsvetkova and Macy, 2014). This property can cause cascades of cooperation in community settings, catalyzing the accumulation of amity within groups and networks (Fowler and Christakis, 2008; Hatfield et al., 1993). However, antisocial behavior is also contagious (Tsvetkova and Macy, 2015). Social networks thus have a corresponding tendency to propagate selfishness and other negative phenomena (Cacioppo et al., 2009; Hill et al., 2010). Such contagion dynamics pervade both personal social networks and contemporary social media (Lerman and Ghosh, 2010; Ugander et al., 2012), where an increasing amount of interpersonal interactions unfold (Auxier and Anderson, 2021; Lenhart, 2015; Shklovski et al., 2004). Social planners face a challenge: How can one structure a community to scaffold and support cooperation, while mitigating the risk that defection will take hold?

Assortative mixing—a network phenomenon in which cooperators connect preferentially with other cooperators, and defectors with other defectors—is central to many prior solutions.[1] For example, Rand et al. (2011) provide individuals with random opportunities to make or break links to other community members, showing that link updates both cause clustering among individuals sharing the same strategy and mitigate the natural decline in group cooperation. Similarly, Shirado and Christakis (2020) embed cooperative "bots" throughout networks in order to foster homophilic clusters and promote cooperation. This research contends that assortative mixing prevents antisocial contagion from corrupting altruistic behavior by partitioning cooperators from defectors. It also frames assortment mechanisms in terms of punishment or ostracism: specifically, assortment threatens defectors with exclusion from the benefits of cooperative relationships (Rand et al., 2011; Shirado and Christakis, 2020; Shirado et al., 2013; Wang et al., 2012). In combination, these effects are believed to protect existing cooperators and punish defectors to incentivize changes to their behavior. Indeed, studies of modern hunter-gatherer tribes indicate that cooperative assortment may trace back to early epochs of human evolutionary history (Apicella et al., 2012; Smith et al., 2018).

[1]Studies refer to assortative mixing by a number of terms, including assortativity (Apicella et al., 2012; Santos et al., 2006), assortment (Eshel and Cavalli-Sforza, 1982), clustering (Rand et al., 2014), and homophily (Centola, 2013; Shirado and Christakis, 2020).

Corresponding author: kevinrmckee@deepmind.com

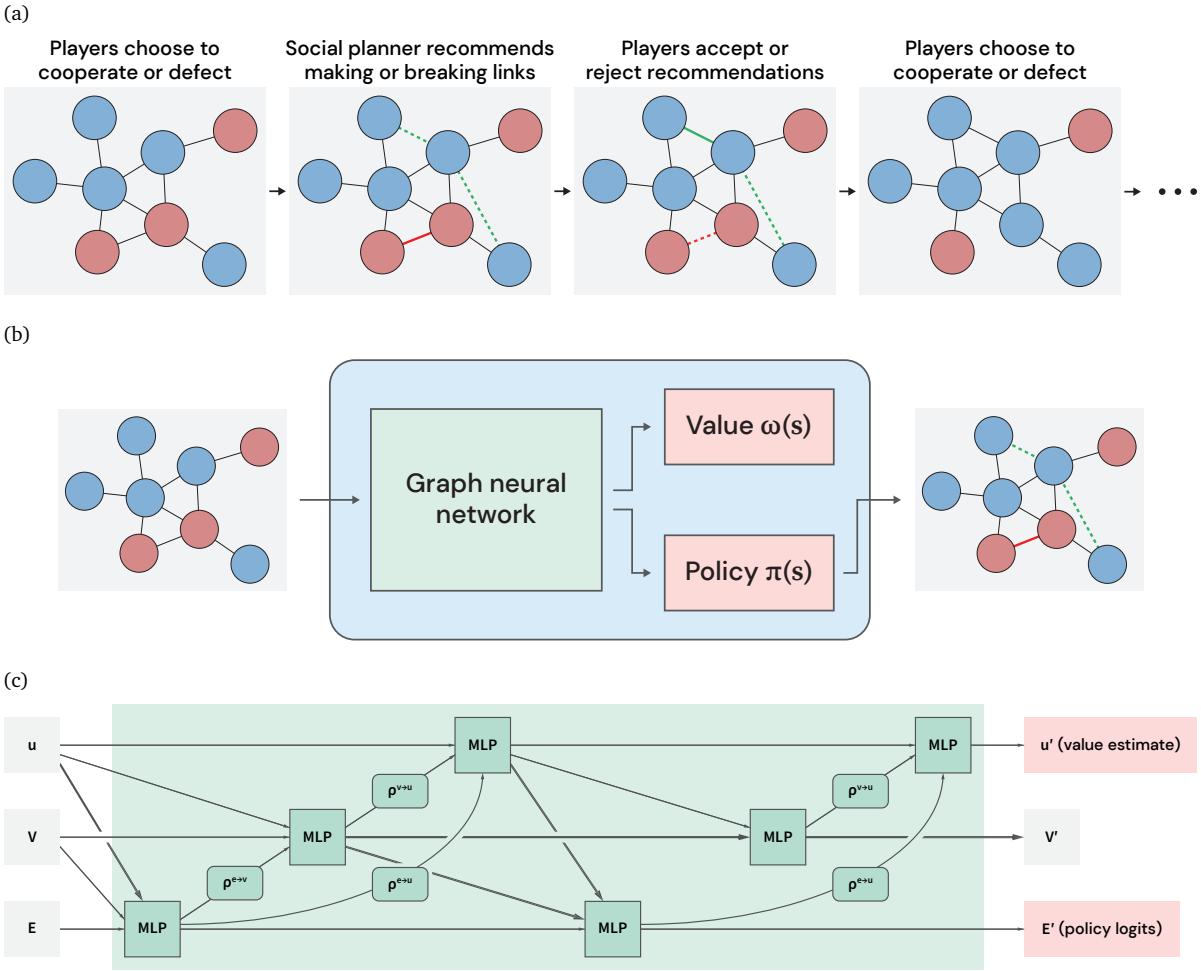

Figure 1. Overview of the network cooperation game and our social-planning agent. (a) In this cooperation game, players are connected on a network and decide to cooperate with or defect from their neighbors. A social planner observes the players' decisions and the network structure, and then recommends changes to the network. Players choose to accept or reject the recommendations to their connections, and then a new turn begins. (b) Our agent learns to act as the social planner and make rewiring recommendations through a graph neural network (a "GraphNet"). We optimize the GraphNet through reinforcement learning, producing a value function $\omega(s)$ and policy function $\pi(s)$. (c) GraphNets explicitly encode graph structure in their computations. In this cooperation game, social planners observe the entire network of players and their cooperation decisions from the most recent round. The GraphNet in our social planning agent observes this information and processes the graph's global features (u), node features (V), and edge features (E) with a sequence of multilayer perceptrons (MLPs) and summation functions (ρs), producing policy logits (E') and a value estimate (u'). See Section S5 in supporting information for more detail.

Several recent research efforts propose using machine learning to identify novel solutions to social challenges (e.g., Dafoe et al., 2020; Zheng et al., 2020). Artificial intelligence and machine learning systems increasingly suffuse everyday social processes (Wagner et al., 2021), so it seems natural to ask how they might support beneficial outcomes for human communities. For network-based problems, the application of machine learning is especially fitting: algorithms play a key role mediating the structure of online social networks (Sanz-Cruzado and Castells, 2019; Sanz-Cruzado et al., 2018; Su et al., 2016). Algorithms make recommendations to connect users, thus changing the structure of the underlying social graph.

Bringing these lines of research together, we aim to construct a social planner with deep learning that maximizes cooperation among human participants in a network cooperation game (Figure 1a; Rand et al., 2011; Shirado and Christakis, 2020; see also Section S1 in supporting information). Players are positioned on the vertices of a graph; edges represent active interpersonal links between players (see Figure S3). Players accumulate (or lose) capital through turn-based interactions with their neighbors. On each turn, players choose to cooperate or defect. Cooperation exacts a constant cost $c = 0.05$ per linked neighbor from a player's capital. Each neighbor receives a constant benefit $b = 0.1$, generating net benefits for the neighborhood at personal cost to the cooperator. Thus, group welfare is highest when everyone cooperates, but for each group member it is tempting to free-ride on the prosociality of others. Every turn, the social planner observes the graph structure and the players' most recent decisions (i.e., their choice to cooperate or defect in the previous round). The planner then makes recommendations to the

players as to which edges should be established or broken. Players decide whether to accept or reject the recommendations, resulting in changes to the graph connectivity. Subsequently, another turn begins. The game imposes no constraints on graph structure aside from precluding self-loops: with the right circumstances and recommendations, a social planner can produce outcomes as extreme as network isolates or fully connected graphs.

Here we leverage deep reinforcement learning and simulation methods to develop a new social planner capable of scaffolding cooperation among groups of interacting humans. The deep neural network tunes its parameters through repeated simulations of the cooperation game. Through this "training" stage, the network refines its "policy": a mapping from the state of the game (e.g., the connectivity between players and their recent choices) to a probability distribution over actions for the planner to take (e.g., recommendations to make to players). The policy starts out as a random mapping at the beginning of training, with the planner making random recommendations to players. Through reinforcement learning—and in particular, optimization through trial and error in simulation—the policy iteratively improves until the social planner is able to maintain cooperation at high levels in games with real human participants (the "evaluation" stage). Neural networks can learn through interaction with real human groups, but the amount of trial-and-error experience needed for deep reinforcement learning takes a generally prohibitive amount of time to accumulate. Interactions with simulated human groups enable our social planning agent to gain a large amount of experience in a short period of time.

In specific terms, we construct a reinforcement learning agent with a graph neural network (a "GraphNet"; Battaglia et al., 2018). GraphNets explicitly encode graph structure into their computations (Figure 1b & 1c). On a given turn of the network cooperation game, the GraphNet computes policy logits (representing a probability distribution over possible actions to take) and a value estimate (representing a prediction of future reward, given the current state of the game). Our reinforcement learning agent uses advantage actor-critic (A2C; Mnih et al., 2016) as its learning algorithm.

The GraphNet-based agent trains to make rewiring recommendations by repeatedly playing as the social planner in simulation. Through games with simulated human players (see *Methods*), the agent learns to effectively scaffold group cooperation. Across different random initializations of its neural network, the agent reliably converges to a high level of performance by the end of training (Figure S7). We select one of these high-performing agents to evaluate in 16-player games with human participants (the "GraphNet social planner" condition; $N = 208$ participants across 13 groups).

To better contextualize the capabilities and behavior of the GraphNet social planner, we compare its performance against several baseline strategies:

- In the "static network" condition, the social planner never recommends any changes to the graph ($N = 176$ participants over 11 groups).
- In the "random recommendations" condition, on each turn the social planner randomly samples 30% of the graph's possible edges and recommends that they be changed, creating edges if they are not active and breaking edges if they are already established (Rand et al., 2011; $N = 208$ participants across 13 groups).
- Finally, in the "cooperative clustering" condition, the social planner uses a rule-based system to cluster cooperators ($N = 176$ participants across 11 groups). On each turn, the cooperative-clustering social planner makes recommendations that first disengage defectors from cooperators, and secondarily that connect cooperators with other cooperators (Shirado and Christakis, 2020).[2] Following prior implementation, the cooperative-clustering planner selects an additional 5% of the graph's possible edges at random and recommends that they be changed.

Across the GraphNet planner condition and all baseline conditions, we recruit $N = 768$ participants in 48 groups. Each group consists of 16 participants playing 15 rounds of the cooperative network game for real monetary stakes.

Results

Across all four conditions, groups began the game with an average cooperation rate of 69.5%. As expected, cooperation degrades substantially in the static network condition (generalized linear mixed model[3]; coeff = −0.24, $p < 0.001$; Figure 2a). Without the opportunity to update their connections, groups quickly succumb to the tragedy of the commons: cooperation levels decline to 42.8% by the time the game ends in round 15. The random-recommendation baseline (coeff = −0.13, $p < 0.001$; Figure 2b) and cooperative-clustering baseline (coeff = −0.07, $p < 0.001$; Figure 2c) mitigate the initial decline of cooperation, concluding the game with higher cooperation rates than observed on static networks. Nonetheless, cooperation still declines over time, ending at 57.0% with random recommendations and 61.2% with cooperative clustering.

[2] To implement this clustering algorithm, Shirado and Christakis (2020) embed cooperative, computer-controlled bots throughout the network as players to give recommendations to humans (a distributed, embodied approach). Given our motivation of studying non-embodied algorithms as network mediators, we re-implement their algorithm with a centralized, non-embodied approach. See Section S4 in supporting information for more details.

[3] Following past studies (Rand et al., 2011, 2014; Shirado and Christakis, 2020; Shirado et al., 2013), we employ generalized linear mixed models to analyze cooperation decisions at the individual level, with random effects for participants nested in groups. Linear models of cooperation at the group level echo the results from these individual-level models (results reported in Section S6.2 in supporting information). For all other game outcomes analyzed in the main text, we implement group-level linear models. Detailed model specifications are provided in the supporting information and within our analysis scripts available at https://osf.io/8ahkg/.

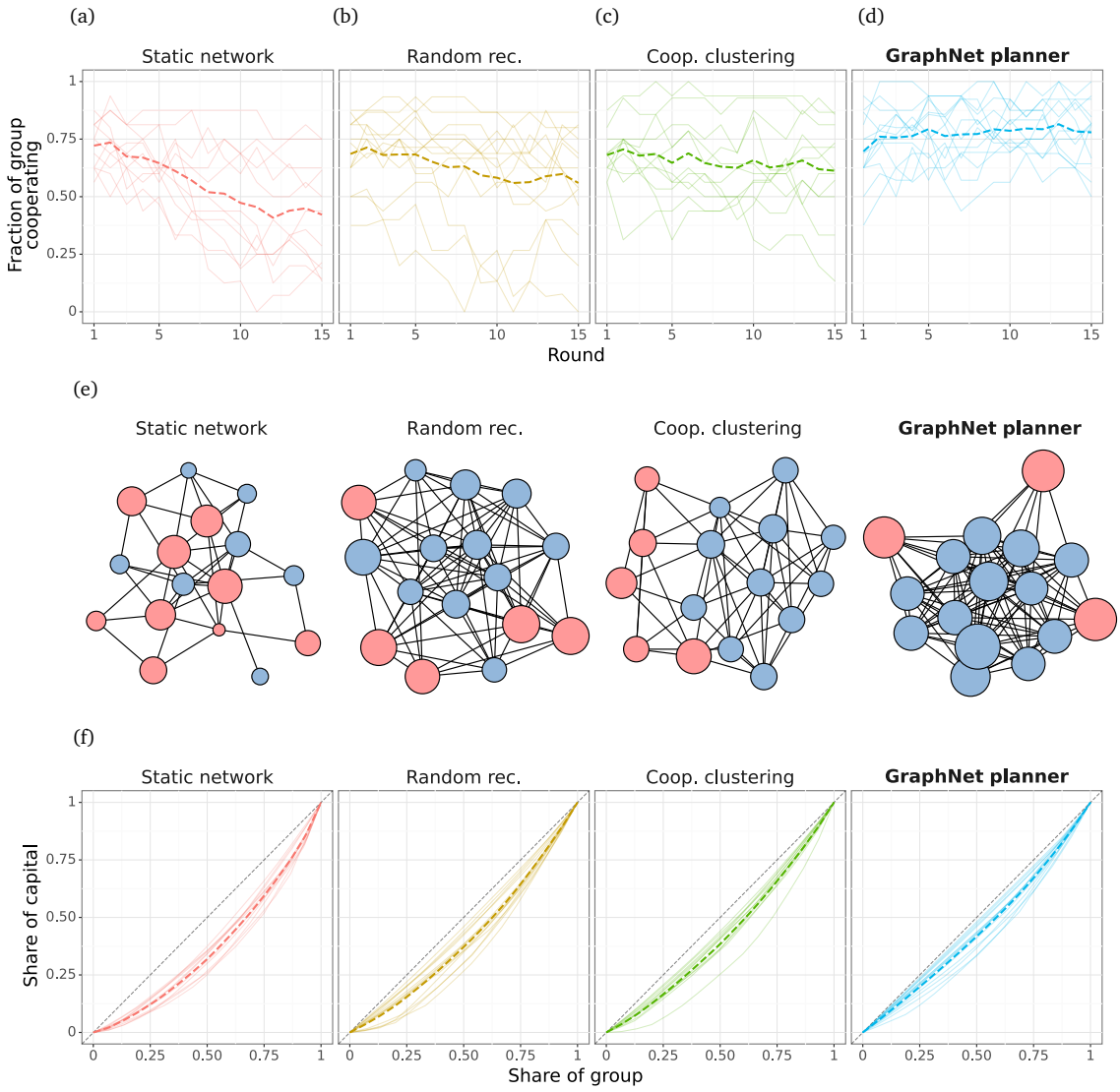

Figure 2. Group outcomes fostered across different conditions. Bold dotted lines represent the mean level across groups. Solid lines reflect the levels in individual groups. (a) Cooperation levels tend to devolve in static networks. (b) Random recommendations mitigate the decline of cooperation. (c) Similarly, the cooperative-clustering social planner stabilizes cooperation levels. (d) In contrast, the GraphNet social planner strengthens cooperation above starting levels. (e) These networks illustrate representative games from round 10 of each condition. Node color represents the participant's previous choice (blue, cooperate; red, defect). Node size reflects cumulative cooperative capital (larger nodes indicate a greater amount of capital). (f) The GraphNet planner reduces group inequality relative to our baselines. These Lorenz curves display the cumulative share of capital held by the group in the final round of the game, with the dashed 45° line reflecting perfect equality.

In contrast, under the GraphNet social planner, cooperation rates increase significantly over the course of the game (coeff = 0.04, $p = 0.007$; Figure 2d). Groups conclude the game in round 15 with a cooperation rate of 77.7%. Comparing directly against the other rewiring strategies, the GraphNet planner supports significantly higher rates of cooperation than do static networks ($p < 0.001$), random recommendations ($p < 0.001$), and cooperative clustering ($p < 0.001$), respectively (Figure S8). To help illustrate the divergent outcomes fostered by the GraphNet and baseline planners, Figure 2e provides graphical illustrations of networks from each condition. With the support of the GraphNet planner, groups enjoy high levels of capital relative to the other conditions (Figure S1b), as well as minimal inequality (Figure 2f; see also Figure S1d).

To better understand the GraphNet planner's strategy, we analyze each planner's recommendations by valence (connect or disconnect) and by the cooperation decisions of the players involved (cooperate-cooperate, cooperate-defect, or defect-defect). The random-recommendation planner is not designed to take player choices into account when generating recommendations. Indeed, its behavior in the actual groups provides no empirical evidence that participant choice affects its recommendations,

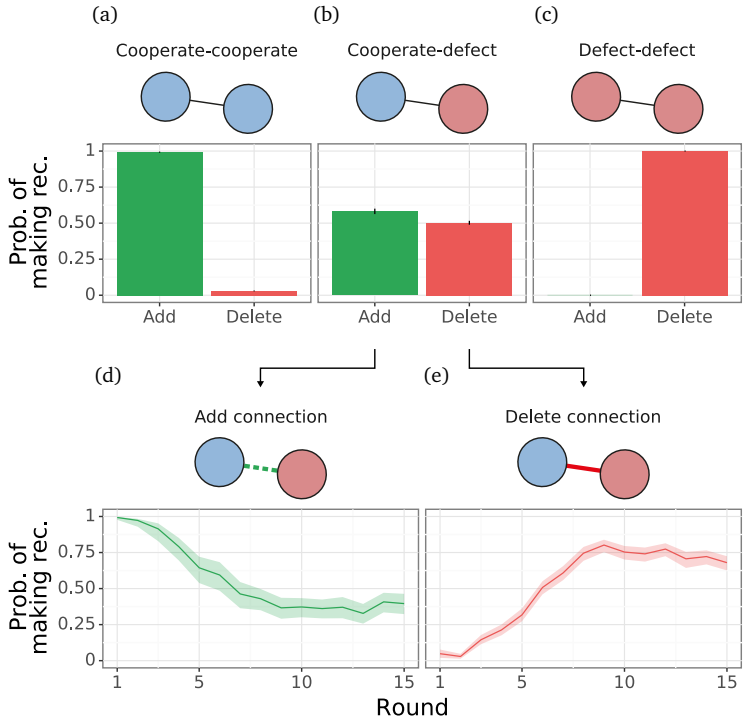

Figure 3. Recommendations from the GraphNet planner as a function of the cooperation choices of the participants involved (cooperate-cooperate, cooperate-defect, or defect-defect) and the change recommended (add or delete). The GraphNet planner conditions its recommendations on participants' cooperation choices from the past round, $p < 0.001$. Error bars and bands represent 95% confidence intervals. (a) Like the cooperative clustering algorithm, the GraphNet planner recommends adding cooperator-cooperator links. (b) Uniquely, the GraphNet planner recommends a mixture of adding and removing cooperator-defector links. (c) It also suggests removing defector-defector links. (d) The GraphNet planner is much more likely to suggest adding cooperator-defector links at the beginning of the game. (e) Moving toward the end of the game, it increasingly recommends removing cooperator-defector connections.

$\chi^2(2) = 0.9$, $p = 0.64$ (likelihood ratio test). The cooperative-clustering planner, in contrast, explicitly incorporates player choices into its planning algorithm: empirically, participant choices exert a significant influence on its recommendation patterns, $\chi^2(2) = 92.0$, $p < 0.001$.

We empirically find that the GraphNet planner learns a conditional approach to its recommendations, taking into account the cooperation decisions of the participants involved on each edge, $\chi^2(2) = 3451.8$, $p < 0.001$ (Figure 3). A representation analysis (e.g., Sanchez-Lengeling et al., 2020; Zambaldi et al., 2018) provides convergent evidence that the social planner learns to encode and track the cooperativeness of the human participants in its neural network (Figure S9; see Section S6.2 in supporting information).

The GraphNet planner virtually always recommends establishing links between cooperators (Figure 3a). Unlike the cooperative-clustering baseline, the planner also recommends breaking existing links between defectors (Figure 3c). This approach diminishes clustering among defectors; defectors rarely connect with one another under the GraphNet planner, as exemplified in Figure 2e. The GraphNet planner also suggests a mix of making and breaking connections involving one cooperator and one defector (Figure 3b). The nuance of these cooperate-defect link recommendations becomes clearer when examining the planner's strategy over time. The GraphNet planner discovers a strategy that initially takes a conciliatory stance toward defectors, establishing numerous cooperate-defect links at the beginning of the game (Figure 3d). As the game progresses, it grows increasingly protective of cooperators, recommending a greater number of deletions for cooperate-defect links (Figure 3e). The planner sends the average defector 1.4 recommendations (interdecile range: 0–4) to connect with cooperators in each of the first four rounds, compared with 0.9 recommendations (interdecile range: 0–3) in each of the last four rounds.

This conciliatory approach produces distinct patterns of network assortativity compared to the other conditions (Figure 4). In particular, the GraphNet planner induces near-zero assortment between cooperators and defectors (linear model; $\beta = -0.06$, $p = 0.13$; Figure 4a). In contrast, and as expected, cooperative clustering induces positive choice assortativity by the end of the game, reflecting a positive tendency for cooperators to cluster with cooperators and defectors to cluster with defectors

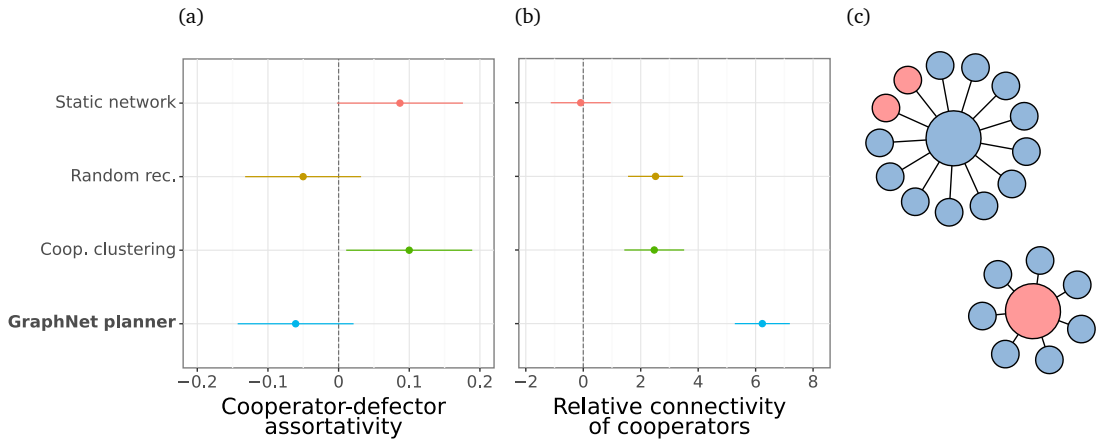

Figure 4. Mixing patterns induced by the different social planners. Error bars indicate 95% confidence intervals. (a) Network rigidity and cooperative clustering produce significant choice assortativity, visualized here at the end of the game: cooperators tend to connect with cooperators, and defectors with defectors. The GraphNet planner, in contrast, induces non-assortativity between cooperators and defectors. (b) The GraphNet planner maximizes the relative connectivity of cooperators in the network game, as measured by the difference in the average degree of cooperating participants and defecting participants (i.e., the mean degree bias toward cooperators; visualized for the final round). (c) The mixing patterns engineered by the GraphNet precipitate drastically different experiences for cooperators and defectors. On expectation, cooperators inhabit large neighborhoods with a mix of cooperators and defectors. In contrast, defectors experience small neighborhoods with virtually only cooperators. The neighborhoods here depict the median cooperator and defector counts for cooperators' and defectors' neighborhoods partway through the game, on round 10.

($\beta = 0.10$, $p = 0.023$). These patterns are robust to multiple specifications for calculating assortative mixing (see Section S6.2 in supporting information). Remarkably, the GraphNet planner's non-assortative strategy does not blunt the connectivity of cooperators (linear model; $\beta = 6.2$, $p < 0.001$; Figure 4b). The relative degree for cooperators under the GraphNet planner significantly exceeds the levels seen on static networks ($p < 0.001$), under the random-recommendations planner ($p < 0.001$), and under the cooperative-clustering planner ($p < 0.001$). Under the GraphNet planner, participants enjoy non-assortative interactions, with cooperators exerting an outsize influence throughout the graph.

These patterns—non-assortativity and high connectivity for a subset of nodes in a graph—are characteristic of a core-periphery structure (Borgatti and Everett, 2000). Consequently, we investigate the possibility that the GraphNet planner organizes communities into core-periphery networks. To do so, we estimate the degree to which networks in each condition manifest a core-periphery structure (de Jeude et al., 2019; see also Section S6.2 in supporting information). Groups receiving the GraphNet planner's recommendations exhibit significant levels of core-periphery structure (linear model; $\beta = 0.46$, $p < 0.001$). Within the GraphNet planner condition, cooperators comprise on average 96.7% of the network core, and defectors 61.2% of the periphery. This pattern is extremely unlikely to emerge by chance, $p < 0.001$ (permutation test). Rather than punish defectors with exclusion, the planner recommends they move into small, highly cooperative neighborhoods (Figure 4c). Visual inspection of networks formed by the different groups of participants underscores how consistently this core-periphery pattern emerges (Figure S11).

This approach represents a substantial departure from prior studies, in which "decentralized ostracism" reduces the relative payoffs for defectors and—as the argument goes—incentivizes them to begin cooperating (Rand et al., 2011, 2014; Shirado and Christakis, 2020). For example, cooperative clustering decreases the mean payoff for defectors over time, causing the relative payoff advantage of defection to gradually disappear. In contrast, under the GraphNet social planner, the average payoff for defectors never declines below the average payoff for cooperation (Figure S10). In spite of this payoff gap, the planner is still able to maintain cohesive group cooperation, with minimal group inequality relative to the other conditions (measured through the Gini coefficient; see Figure 2f).[4] Our application of deep reinforcement learning breaks from prior approaches and converges on an encouraging, conciliatory approach toward defectors.

Deep learning methods are often criticized for their lack of "interpretability" (Heuillet et al., 2021; von Eschenbach, 2021; but see also Holm, 2019). In particular, it is difficult to know what exactly drives the behavior of deep neural networks, given the inherent complexity, opacity, and high non-linearity of the solutions they learn (the "black box" problem). We test whether the conciliatory patterns we observe are sufficient to explain the GraphNet planner's performance. Alternatively, its success may stem from the black box of deep learning—that is, from a mechanism more difficult for us to interpret. To test these

[4] Exploratory bootstrap analysis suggests that this inequality effect stems from two separate factors: first, the rarity of defection in each group, and second, the higher average level of capital throughout each group relative to the other conditions.

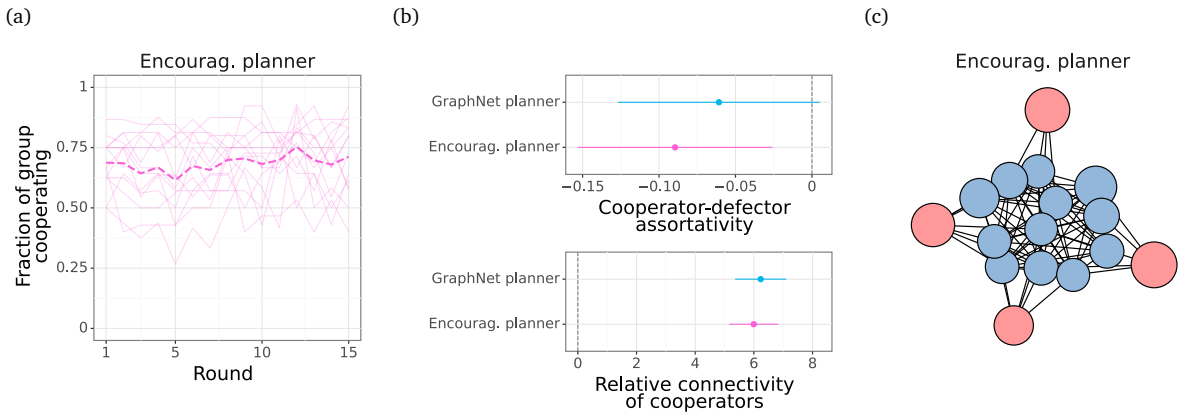

Figure 5. Group cooperation levels and network structure cultivated by the "encouragement" social planner. Based on our analysis of the GraphNet planner's conciliatory approach to defectors, the encouragement planner makes recommendations as a simple function of player cooperation choices and the round number. (a) The encouragement planner stabilizes cooperation levels among human groups. (b) The encouragement planner reproduces the patterns of assortativity engineered by the GraphNet planner, visualized here for the final round. Error bars indicate 95% confidence intervals. (c) This network shows a representative game under the encouragement planner in round 10. Like the GraphNet planner, the encouragement planner tends to recommend a core-periphery structure for groups.

alternatives, we construct a new "encouragement" social planner based on our analysis of the GraphNet planner's policy (i.e., the patterns depicted in Figure 3). In contrast with the GraphNet planner's complex, opaque computations, the encouragement planner makes recommendations as a simple function of player cooperation choices and the round number (Tables S5–S7). For example, when faced with a connection between a cooperator and a defector in round 1, the encouragement planner will recommend removing the link with 4.8% probability; faced with a similar pair in the final round, it will recommend removing the link with 72.2% probability.

A follow-up study with human groups (N = 224 participants across 14 groups) validates the effectiveness of the conciliatory approach we observe from the GraphNet planner. The encouragement planner significantly improves group cooperation levels over the course of the game (generalized linear mixed model; coeff = 0.04, p = 0.005; Figure 5a). A direct comparison shows that the encouragement approach significantly outperforms static networks ($p < 0.001$), random recommendations ($p < 0.001$), and cooperative clustering ($p < 0.001$) at supporting group cooperation (Figure S12). The encouragement planner enhances group cooperation to a similar extent as the GraphNet planner (p = 1.00) and exerts similar effects on network assortativity (Figure 5b), consistently engineering a core-periphery structure for groups (Figure 5c; see also Figure S14).

The recommendations from both the GraphNet planner and the encouragement planner produce networks with notably high density, especially relative to the baseline conditions (see Figure S1b). Under the GraphNet planner, for example, several groups reached full networked connectivity (see Figure S11). To evaluate the possibility that high density alone drives the success of these planners—without the need for an encouraging approach—we run two additional follow-up studies (N = 400 participants across 25 groups). First, we build a "neutral" social planner that aims to recreate the connectivity dynamics observed under the GraphNet planner, without regard for player's choices (i.e., dispensing with the encouraging approach to defectors; N = 192 participants across 12 groups). As intended, this planner generates levels of network connectivity to a similar extent as the GraphNet planner (linear model; p = 0.47). Nonetheless, its choice-agnostic approach degrades group cooperation significantly over time (generalized linear mixed model; coeff = −0.17, $p < 0.001$). As a further test of whether network density drives the high cooperation rates seen with the GraphNet planner, we construct another social planner that seeks to maximize network connectivity as much as possible (N = 208 participants across 13 groups). This strategy generates levels of network density that significantly exceed those produced by the GraphNet planner ($p < 0.001$). However, this also causes a precipitous decline in cooperation (coeff = −0.51, $p < 0.001$). On its own, network density does not offer a compelling explanation for the high cooperation rates supported by the GraphNet planner.

Overall, these three follow-up studies help to validate the value and sufficiency of an encouraging approach to defectors.

Discussion

How can a social planner best support group cooperation and mitigate the spread of defection? Prior methods focus on increasing the assortment of strategy types within a networked group. This approach protects cooperators from antisocial

contagion and simultaneously punishes defectors for their selfishness.

We build a social planner that learns for itself how to scaffold cooperation, through deep reinforcement learning and repeated trial and error in simulation. Our social planner proves capable of not only stabilizing, but also enhancing cooperation over time. The planner's strategy validates several characteristics of prior approaches, including a tendency for cooperators to connect with other cooperators. It does not, however, partition defectors away from cooperators ("decentralized ostracism"; Rand et al., 2011, 2014; Shirado and Christakis, 2020). Instead, the planner recommends a core-periphery structure for the community. Though defecting participants move to the periphery of the graph, they remain well-connected to cooperators. This encouraging, conciliatory approach fosters prosocial contagion while minimizing the spread of defection. Echoing dynamics observed in collective action (Centola, 2013), a critical mass of cooperative individuals can draw cynical outsiders into the fold.

Prior studies in this domain emphasize higher relative payoffs for cooperation as central to incentivizing players to abandon defection (Rand et al., 2014; Sohn et al., 2020). Our social planner succeeds at encouraging group cooperation, but unexpectedly, the networks that it engineers consistently reward defectors more than cooperators. This discrepancy indicates that short-term utility calculus can provide only a partial explanation for participants behavior in this network game. Future studies should draw inspiration from psychology research to better understand participants' motivation and thinking. Non-economic factors such as preferences for fairness (Ketelaar and Tung Au, 2003) and conformity (Bardsley and Sausgruber, 2005; Cialdini and Trost, 1998) likely contribute to the contagiousness of cooperation. Overall, deep reinforcement learning discovers a novel approach to the challenge of scaffolding community cooperation.

Our social planner learns to make its recommendations through a graph neural network. Multiple experiments have demonstrated the effectiveness of graph neural networks in solving physical problems (e.g., Bapst et al., 2019; Cranmer et al., 2020; Sanchez-Gonzalez et al., 2020). Notably, social scientists have long argued that social systems are well-modeled through physics ("social physics"; Comte, 1825). This consonance may explain the GraphNet planner's effectiveness, and additionally suggests that our approach may prove applicable to other graphical games (Kearns et al., 2001) modeling community dilemmas. The combination of graph neural networks, reinforcement learning, and simulation could uncover novel solutions to challenges such as resource sharing (Shirado et al., 2019) and efficient innovation and discovery (Mason and Watts, 2012; Mason et al., 2008).

Developments in machine learning indicate several promising directions for future research. The design of graph neural networks allows them to generalize to large-scale problems. Several teams, for example, have applied graph neural networks to so-called "web-scale" challenges, involving millions of nodes and potentially billions of edges (Hu et al., 2021; Ying et al., 2018). These successes hint at a path to scaffolding cooperation in expansive networks: can an encouraging approach support community cohesion at large scales? Another potential path concerns interpretability. Recent work demonstrates that large language models (e.g., Brown et al., 2020; Devlin et al., 2019) may be capable of generating explanations for algorithmic decision making (Wiegreffe et al., 2022). With the support of a language model, our social planner could explain its policy to group members in natural language, helping them to understand the possible consequences of any choices that they might make.

Ethicists and policymakers emphasize human autonomy as a central value for the development and deployment of artificial intelligence (AI; Heer, 2019; Jobin et al., 2019). Nonetheless, modern AI research does not always afford human participants much control or power within the context of their interaction with AI systems. In our experiments, our agent's actions are entirely recommendation-based: participants have the option to accept or reject the decisions that the agent makes. These decisions to accept or reject system advice reflect a revealed preference within human-AI interaction (McKee et al., 2022). In addition to recommendation-based approaches, future interaction research can support autonomy through other revealed-preference frameworks, perhaps including the choice of entirely opting out of interactions with the agent in question (an "exit option"; Dobbe et al., 2021). The deployment of agents to assist with social planning raises additional questions concerning consent and governance. Which stakeholders should direct, steer, and fund AI systems in this domain? The application of participatory and democratic methods will be particularly important for such technology (Birhane et al., 2022; Garvey, 2018). It is imperative that technologists preserve the ability of communities that will be affected by AI to engage with it on their own terms—whether that is to withdraw from, contribute to, steer, or potentially resist the deployment of these systems.

Artificial intelligence increasingly infuses everyday life. As a result, people enjoy a growing range of relationships with AI systems, forming "hybrid societies" of human and algorithmic actors (Christakis, 2019; McKee et al., in revision). Some applications of AI technology call for a physical, embodied presence to interact with humans (Shirado and Christakis, 2020; Traeger et al., 2020; Weidinger et al., in press). Others, like the algorithmic social planner in our study, may be less visible to the communities with which they interact, yet no less influential. Both categories merit expanded research and study. Overall, our results contribute to a growing body of evidence that agents trained with deep reinforcement learning can enhance collaboration and cooperation (Carroll et al., 2019; Strouse et al., 2021; Zheng et al., 2020; see also Dafoe et al., 2020; Paiva et al., 2018). Artificial intelligence can prove a positive, beneficial force to support human communities.

Methods

We trained an artificial agent to act as a social planner in the cooperative network game through reinforcement learning and simulation methods. The agent comprised a graph neural network (a "GraphNet"; Battaglia et al., 2018) with two message-passing steps (Figure 1c). The architecture was non-recurrent. The agent optimized for a combination of capital level and recommendation quality (see Section S5.3 in supporting information), and used advantage-actor critic (Mnih et al., 2016) as its learning algorithm over a distributed framework (Espeholt et al., 2018). See Section S5 in supporting information for more detail on the agent design and parameterization.

We constructed bots to simulate human cooperation and recommendation-acceptance decisions for the agent's training (Equations 1 & 2). Each bot i randomly sampled a cooperative disposition parameter $\theta_i \sim \mathcal{N}(\mu_\theta, \sigma_\theta)$ upon its initialization. Bots made cooperation choices through two logistic functions, conditional on the current round number t. In the initial round, when a bot had no information about the behavior of its neighbors, it randomly sampled an action (cooperate or defect) as a logistic function of its disposition parameter θ_i and two parameters shared by all bots: β'_0 and β'_1. In subsequent rounds, the bot chose to cooperate as a logistic function of its current neighborhood size x_s, its current number of cooperating neighbors x_n, the current rate of cooperation in its neighborhood x_r, its disposition parameter θ_i, and four parameters shared by all bots: β_0, β_1, β_2, and β_3:

$$P_{\text{coop.}}(t,i) = \begin{cases} \dfrac{1}{1+e^{-(\beta'_0+\beta'_1\cdot\theta_i)}} & \text{if } t=1 \\ \dfrac{1}{1+e^{-(\beta_0+\beta_1\cdot x_s+\beta_2\cdot x_n+\beta_3\cdot x_r+\theta_i)}} & \text{otherwise} \end{cases} \tag{1}$$

The bot accepted or rejected recommendations from the social planner as a function of the recommendation valence $a_{\text{SP}}(i,j) \in \{-1,1\}$ (where -1 signifies "break link" and 1 reflects "make link") and the referent neighbor's previous cooperation decision $a_j^0 \in \{0,1\}$ (where 0 denotes defection and 1 represents cooperation):

$$P_{\text{accept rec.}}\left(a_{\text{SP}}(i,j), a_j^0\right) = \begin{cases} \varphi_0 & \text{if } a_{\text{SP}}(i,j)=-1 \text{ and if } a_j^0=0 \\ \varphi_1 & \text{if } a_{\text{SP}}(i,j)=-1 \text{ and if } a_j^0=1 \\ \varphi_2 & \text{if } a_{\text{SP}}(i,j)=1 \text{ and if } a_j^0=0 \\ \varphi_3 & \text{if } a_{\text{SP}}(i,j)=1 \text{ and if } a_j^0=1 \end{cases} \tag{2}$$

To select the μ_θ, σ_θ, β, and φ parameters for the bots, we fit models to behavioral data collected in the baseline conditions of the group experiments. See Section S5.5 in supporting information for fitted values and more information on the bot design.

We trained 30 replicates of the agent for a maximum of 5×10^7 simulated game rounds, using a different random initialization for the neural network in each replicate. Across multiple random network initializations, the social planner learned qualitatively and quantitatively similar policies that scaffolded high levels of cooperation with simulated groups. We selected one of these high-performing policies to evaluate with human participants.

We recruited participants from Prolific (Peer et al., 2021) for our group experiments. In addition to the summary provided here, see Section S3 in supporting information for full details of the study design. The experiments employed a between-participants design: that is, participants joined a single group (with no participant experiencing multiple conditions). The experiments were also incentive compatible: that is, participants (knowingly) made decisions in the cooperative network game for real monetary stakes. Participants first read detailed study and game instructions, played a short tutorial round, and subsequently completed a comprehension test on the game rules. We required participants to answer all three questions correctly to continue. The majority of participants (74.2%) passed the test and were randomly sorted into groups of $n = 16$. We provided the remainder a show-up payment for their time. The final sample comprised $N = 1392$ participants (mean age of 36.7, $sd = 12.7$; 44.9% female, 52.6% male, and 1.4% non-binary, trans, genderqueer, demigender, agender, asexual, and aromantic).

Each group consisted of 16 participants and played 15 rounds of the cooperative network game (see Figures S31–S37). To avoid end-game effects, participants were not told how many rounds to expect. Each stage of the game (e.g., choosing to cooperate or receiving recommendations from the planner) waited a preset amount of time for participant input. Participants that did not respond were removed from the experiment; we subsequently provided these participants with a debrief questionnaire including questions about any technical problems they may have encountered. The tutorial explicitly detailed these rules for participants, and the main game interface displayed a timer at the bottom of every page counting down the time remaining for the current choice. Empirically, the groups experienced a very low dropout rate among participants, ending with a mean of 14.6 participants (median = 15). After completing the game, participants completed a short questionnaire and then received their compensation for the study.

Acknowledgements

We thank Zafarali Ahmed, Felix Fischer, and Miteyan Patel for providing technical support for the project; Shakir Mohamed for offering general support; and Ian Gemp, Gracie Reinecke, Brendan Tracey, and Karl Tuyls for offering feedback on the manuscript.

Author contributions

K.R.M. proposed the research idea; K.R.M. and M. Botvinick designed the research; K.R.M. coded and developed the baselines and agents, with assistance from A.T., J.B., and R.E.; K.R.M. coded the study, collected data, and conducted statistical analysis; K.R.M. interpreted results, with assistance from A.T., M. Bakker, J.B., L.C.G., R.E., and M. Botvinick; and K.R.M. wrote the paper, with assistance from A.T., M. Bakker, J.B., L.C.G., R.E., and M. Botvinick.

Funding

This research was funded by DeepMind. The authors declare no competing interests.

Data availability

The data and analysis scripts necessary for reproducing all analyses and figures are available at https://osf.io/8ahkg/.

References

C. L. Apicella, F. W. Marlowe, J. H. Fowler, and N. A. Christakis. Social networks and cooperation in hunter-gatherers. *Nature*, 481(7382):497–501, 2012.

B. Auxier and M. Anderson. Social media use in 2021, 2021.

V. Bapst, A. Sanchez-Gonzalez, C. Doersch, K. Stachenfeld, P. Kohli, P. Battaglia, and J. Hamrick. Structured agents for physical construction. In *International Conference on Machine Learning*, pages 464–474. PMLR, 2019.

N. Bardsley and R. Sausgruber. Conformity and reciprocity in public good provision. *Journal of Economic Psychology*, 26(5): 664–681, 2005.

P. W. Battaglia, J. B. Hamrick, V. Bapst, A. Sanchez-Gonzalez, V. Zambaldi, M. Malinowski, A. Tacchetti, D. Raposo, A. Santoro, R. Faulkner, et al. Relational inductive biases, deep learning, and graph networks. *arXiv preprint arXiv:1806.01261*, 2018.

A. Birhane, W. Isaac, V. Prabhakaran, M. Díaz, M. C. Elish, I. Gabriel, and S. Mohamed. Power to the people? Opportunities and challenges for participatory AI. *Equity and Access in Algorithms, Mechanisms, and Optimization*, pages 1–8, 2022.

S. P. Borgatti and M. G. Everett. Models of core/periphery structures. *Social Networks*, 21(4):375–395, 2000.

T. Brown, B. Mann, N. Ryder, M. Subbiah, J. D. Kaplan, P. Dhariwal, A. Neelakantan, P. Shyam, G. Sastry, A. Askell, et al. Language models are few-shot learners. *Advances in Neural Information Processing Systems*, 33:1877–1901, 2020.

J. T. Cacioppo, J. H. Fowler, and N. A. Christakis. Alone in the crowd: The structure and spread of loneliness in a large social network. *Journal of Personality and Social Psychology*, 97(6):977, 2009.

M. Carroll, R. Shah, M. K. Ho, T. Griffiths, S. Seshia, P. Abbeel, and A. Dragan. On the utility of learning about humans for human-AI coordination. *Advances in Neural Information Processing Systems*, 32, 2019.

D. M. Centola. Homophily, networks, and critical mass: Solving the start-up problem in large group collective action. *Rationality and Society*, 25(1):3–40, 2013.

N. A. Christakis. *Blueprint: The evolutionary origins of a good society*. Hachette, 2019.

N. A. Christakis and J. H. Fowler. Social contagion theory: Examining dynamic social networks and human behavior. *Statistics in Medicine*, 32(4):556–577, 2013.

R. B. Cialdini and M. R. Trost. *Social influence: Social norms, conformity and compliance*. McGraw-Hill, 1998.

A. Comte. V. Considérations philosophiques sur les sciences et les savants. *Le Producteur, Journal Philosophique de l'Industrie, des Sciences et des Beaux Arts*, 1825.

M. Cranmer, A. Sanchez Gonzalez, P. Battaglia, R. Xu, K. Cranmer, D. Spergel, and S. Ho. Discovering symbolic models from deep learning with inductive biases. *Advances in Neural Information Processing Systems*, 33:17429–17442, 2020.

A. Dafoe, E. Hughes, Y. Bachrach, T. Collins, K. R. McKee, J. Z. Leibo, K. Larson, and T. Graepel. Open problems in Cooperative AI. *arXiv preprint arXiv:2012.08630*, 2020.

J. v. L. de Jeude, G. Caldarelli, and T. Squartini. Detecting core-periphery structures by surprise. *Europhysics Letters*, 125(6): 68001, 2019.

J. Devlin, M.-W. Chang, K. Lee, and K. Toutanova. BERT: Pre-training of deep bidirectional transformers for language understanding. In *Proceedings of the 2019 Conference of the North American Chapter of the Association for Computational Linguistics: Human Language Technologies*, pages 4171–4186, 2019.

R. Dobbe, T. K. Gilbert, and Y. Mintz. Hard choices in artificial intelligence. *Artificial Intelligence*, 300:103555, 2021.

P. Erdős and A. Rényi. On random graphs. I. *Publicationes Mathematicae*, 6:290–297, 1959.

I. Eshel and L. L. Cavalli-Sforza. Assortment of encounters and evolution of cooperativeness. *Proceedings of the National Academy of Sciences*, 79(4):1331–1335, 1982.

L. Espeholt, H. Soyer, R. Munos, K. Simonyan, V. Mnih, T. Ward, Y. Doron, V. Firoiu, T. Harley, I. Dunning, et al. IMPALA: Scalable distributed deep-RL with importance weighted actor-learner architectures. In *International Conference on Machine Learning*, pages 1407–1416, 2018.

J. H. Fowler and N. A. Christakis. Dynamic spread of happiness in a large social network: Longitudinal analysis over 20 years in the framingham heart study. *British Medical Journal*, 337, 2008.

J. Fox. *Applied regression analysis and generalized linear models*. Sage Publications, 2015.

C. Garvey. A framework for evaluating barriers to the democratization of artificial intelligence. In *Proceedings of the AAAI Conference on Artificial Intelligence*, volume 32, 2018.

L. H. Gilpin, D. Bau, B. Z. Yuan, A. Bajwa, M. Specter, and L. Kagal. Explaining explanations: An overview of interpretability of machine learning. In *2018 IEEE 5th International Conference on Data Science and Advanced Analytics*, pages 80–89. IEEE, 2018.

M. Gori, G. Monfardini, and F. Scarselli. A new model for learning in graph domains. In *Proceedings of the IEEE International Joint Conference on Neural Networks*, volume 2, pages 729–734. IEEE, 2005.

J. B. Hamrick, K. R. Allen, V. Bapst, T. Zhu, K. R. McKee, J. B. Tenenbaum, and P. W. Battaglia. Relational inductive bias for physical construction in humans and machines. In *Proceedings of the 40th Annual Conference of the Cognitive Science Society*, 2018.

E. Hatfield, J. T. Cacioppo, and R. L. Rapson. Emotional contagion. *Current Directions in Psychological Science*, 2(3):96–100, 1993.

J. Heer. Agency plus automation: Designing artificial intelligence into interactive systems. *Proceedings of the National Academy of Sciences*, 116(6):1844–1850, 2019.

A. Heuillet, F. Couthouis, and N. Díaz-Rodríguez. Explainability in deep reinforcement learning. *Knowledge-Based Systems*, 214: 106685, 2021.

A. L. Hill, D. G. Rand, M. A. Nowak, and N. A. Christakis. Emotions as infectious diseases in a large social network: The SISa model. *Proceedings of the Royal Society B: Biological Sciences*, 277(1701):3827–3835, 2010.

J. Hindriks and G. D. Myles. *Intermediate public economics*. MIT Press, 2013.

E. A. Holm. In defense of the black box. *Science*, 364(6435):26–27, 2019.

W. Hu, M. Fey, H. Ren, M. Nakata, Y. Dong, and J. Leskovec. OGB-LSC: A large-scale challenge for machine learning on graphs. In *Proceedings of the Neural Information Processing Systems Track on Datasets and Benchmarks*, 2021.

A. Jobin, M. Ienca, and E. Vayena. The global landscape of AI ethics guidelines. *Nature Machine Intelligence*, 1(9):389–399, 2019.

M. Kearns, M. L. Littman, and S. Singh. Graphical models for game theory. In *Proceedings of the Seventeenth Conference on Uncertainty in Artificial Intelligence*, pages 253–260, 2001.

K. Keizer, S. Lindenberg, and L. Steg. The importance of demonstratively restoring order. *PLoS ONE*, 8(6):e65137, 2013.

T. Ketelaar and W. Tung Au. The effects of feelings of guilt on the behaviour of uncooperative individuals in repeated social bargaining games: An affect-as-information interpretation of the role of emotion in social interaction. *Cognition and Emotion*, 17(3):429–453, 2003.

A. Lenhart. Teens, social media & technology, 2015.

K. Lerman and R. Ghosh. Information contagion: An empirical study of the spread of news on Digg and Twitter social networks. In *Fourth International AAAI Conference on Weblogs and Social Media*, 2010.

A. Mas-Colell, M. Whinston, and J. Green. *Microeconomic Theory*. Oxford University Press, 1995.

W. A. Mason and D. J. Watts. Collaborative learning in networks. *Proceedings of the National Academy of Sciences*, 109(3): 764–769, 2012.

W. A. Mason, A. Jones, and R. L. Goldstone. Propagation of innovations in networked groups. *Journal of Experimental Psychology: General*, 137(3):422, 2008.

K. R. McKee, X. Bai, and S. T. Fiske. Warmth and competence in human-agent cooperation. In *Proceedings of the 21st International Conference on Autonomous Agents and MultiAgent Systems*, 2022.

K. R. McKee, X. Bai, and S. T. Fiske. Humans perceive warmth and competence in artificial intelligence. *iScience*, in revision. doi: 10.31234/osf.io/5ursp.

V. Mnih, A. P. Badia, M. Mirza, A. Graves, T. Lillicrap, T. Harley, D. Silver, and K. Kavukcuoglu. Asynchronous methods for deep reinforcement learning. In *Proceedings of the International Conference on Machine Learning*, pages 1928–1937, 2016.

R. O. Murphy, K. A. Ackermann, and M. Handgraaf. Measuring social value orientation. *Judgment and Decision Making*, 6(8): 771–781, 2011.

M. E. J. Newman. Mixing patterns in networks. *Physical Review E*, 67(2):026126, 2003.

R. M. O'Brien. A caution regarding rules of thumb for variance inflation factors. *Quality & Quantity*, 41:673–690, 2007.

A. Paiva, F. Santos, and F. Santos. Engineering pro-sociality with autonomous agents. In *Proceedings of the AAAI Conference on Artificial Intelligence*, volume 32, 2018.

E. Peer, D. Rothschild, A. Gordon, Z. Evernden, and E. Damer. Data quality of platforms and panels for online behavioral research. *Behavior Research Methods*, pages 1–20, 2021.

M. Pielot, K. Church, and R. De Oliveira. An in-situ study of mobile phone notifications. In *Proceedings of the 16th International Conference on Human-Computer Interaction with Mobile Devices & Services*, pages 233–242, 2014.

D. G. Rand, S. Arbesman, and N. A. Christakis. Dynamic social networks promote cooperation in experiments with humans. *Proceedings of the National Academy of Sciences*, 108(48):19193–19198, 2011.

D. G. Rand, M. A. Nowak, J. H. Fowler, and N. A. Christakis. Static network structure can stabilize human cooperation. *Proceedings of the National Academy of Sciences*, 111(48):17093–17098, 2014.

A. Sanchez-Gonzalez, J. Godwin, T. Pfaff, R. Ying, J. Leskovec, and P. Battaglia. Learning to simulate complex physics with graph networks. In *International Conference on Machine Learning*, pages 8459–8468. PMLR, 2020.

B. Sanchez-Lengeling, J. Wei, B. Lee, E. Reif, P. Wang, W. W. Qian, K. McCloskey, L. Colwell, and A. Wiltschko. Evaluating attribution for graph neural networks. *Advances in Neural Information Processing Systems*, 33:5898–5910, 2020.

F. C. Santos, J. M. Pacheco, and T. Lenaerts. Cooperation prevails when individuals adjust their social ties. *PLoS Computational Biology*, 2(10):e140, 2006.

J. Sanz-Cruzado and P. Castells. Contact recommendations in social networks. In *Collaborative Recommendations: Algorithms, Practical Challenges and Applications*, pages 519–569. World Scientific, 2019.

J. Sanz-Cruzado, S. M. Pepa, and P. Castells. Structural novelty and diversity in link prediction. In *Companion Proceedings of the 2018 Web Conference*, pages 1347–1351, 2018.

F. Scarselli, M. Gori, A. C. Tsoi, M. Hagenbuchner, and G. Monfardini. The graph neural network model. *IEEE Transactions on Neural Networks*, 20(1):61–80, 2008.

H. Shirado and N. A. Christakis. Network engineering using autonomous agents increases cooperation in human groups. *iScience*, 23(9):101438, 2020.

H. Shirado, F. Fu, J. H. Fowler, and N. A. Christakis. Quality versus quantity of social ties in experimental cooperative networks. *Nature Communications*, 4(1):1–8, 2013.

H. Shirado, G. Iosifidis, L. Tassiulas, and N. A. Christakis. Resource sharing in technologically defined social networks. *Nature Communications*, 10(1):1–10, 2019.

I. Shklovski, R. Kraut, and L. Rainie. The Internet and social participation: Contrasting cross-sectional and longitudinal analyses. *Journal of Computer-Mediated Communication*, 10(1):JCMC1018, 2004.

K. M. Smith, T. Larroucau, I. A. Mabulla, and C. L. Apicella. Hunter-gatherers maintain assortativity in cooperation despite high levels of residential change and mixing. *Current Biology*, 28(19):3152–3157, 2018.

Y. Sohn, J.-K. Choi, and T.-K. Ahn. Core–periphery segregation in evolving prisoner's dilemma networks. *Journal of Complex Networks*, 8(1):cnz021, 2020.

D. Strouse, K. R. McKee, M. Botvinick, E. Hughes, and R. Everett. Collaborating with humans without human data. *Advances in Neural Information Processing Systems*, 34:14502–14515, 2021.

J. Su, A. Sharma, and S. Goel. The effect of recommendations on network structure. In *Proceedings of the 25th International Conference on World Wide Web*, pages 1157–1167, 2016.

A. Tacchetti, H. F. Song, P. A. M. Mediano, V. Zambaldi, J. Kramár, N. C. Rabinowitz, T. Graepel, M. Botvinick, and P. W. Battaglia. Relational forward models for multi-agent learning. In *Proceedings of the International Conference on Learning Representations*, 2018.

R. H. Thaler and C. R. Sunstein. Libertarian paternalism. *American Economic Review*, 93(2):175–179, 2003.

M. L. Traeger, S. Strohkorb Sebo, M. Jung, B. Scassellati, and N. A. Christakis. Vulnerable robots positively shape human conversational dynamics in a human–robot team. *Proceedings of the National Academy of Sciences*, 117(12):6370–6375, 2020.

M. Tsvetkova and M. W. Macy. The social contagion of generosity. *PLoS One*, 9(2):e87275, 2014.

M. Tsvetkova and M. W. Macy. The social contagion of antisocial behavior. *Sociological Science*, 2:36–49, 2015.

J. Ugander, L. Backstrom, C. Marlow, and J. Kleinberg. Structural diversity in social contagion. *Proceedings of the National Academy of Sciences*, 109(16):5962–5966, 2012.

W. J. von Eschenbach. Transparency and the black box problem: Why we do not trust AI. *Philosophy & Technology*, 34(4): 1607–1622, 2021.

C. Wagner, M. Strohmaier, A. Olteanu, E. Kıcıman, N. Contractor, and T. Eliassi-Rad. Measuring algorithmically infused societies. *Nature*, pages 1–6, 2021.

J. Wang, S. Suri, and D. J. Watts. Cooperation and assortativity with dynamic partner updating. *Proceedings of the National Academy of Sciences*, 109(36):14363–14368, 2012.

L. Weidinger, K. R. McKee, R. Everett, S. Huang, T. O. Zhu, M. J. Chadwick, C. Summerfield, and I. Gabriel. Using the veil of ignorance to align AI systems with principles of justice. *Proceedings of the National Academy of Sciences*, in press.

S. Wiegreffe, J. Hessel, S. Swayamdipta, M. Riedl, and Y. Choi. Reframing human-AI collaboration for generating free-text explanations. In *Proceedings of the 2022 Conference of the North American Chapter of the Association for Computational Linguistics: Human Language Technologies*, pages 632–658, 2022.

R. Ying, R. He, K. Chen, P. Eksombatchai, W. L. Hamilton, and J. Leskovec. Graph convolutional neural networks for web-scale recommender systems. In *Proceedings of the 24th ACM SIGKDD International Conference on Knowledge Discovery & Data Mining*, pages 974–983, 2018.

V. Zambaldi, D. Raposo, A. Santoro, V. Bapst, Y. Li, I. Babuschkin, K. Tuyls, D. Reichert, T. Lillicrap, E. Lockhart, et al. Deep reinforcement learning with relational inductive biases. In *International Conference on Learning Representations*, 2018.

S. Zheng, A. Trott, S. Srinivasa, N. Naik, M. Gruesbeck, D. C. Parkes, and R. Socher. The AI economist: Improving equality and productivity with AI-driven tax policies. *arXiv preprint arXiv:2004.13332*, 2020.

(a) **Average cooperation rate in group.**

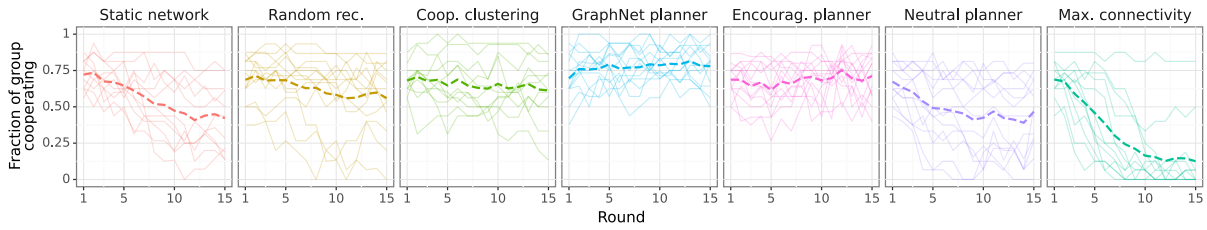

(b) **Group connectivity.**

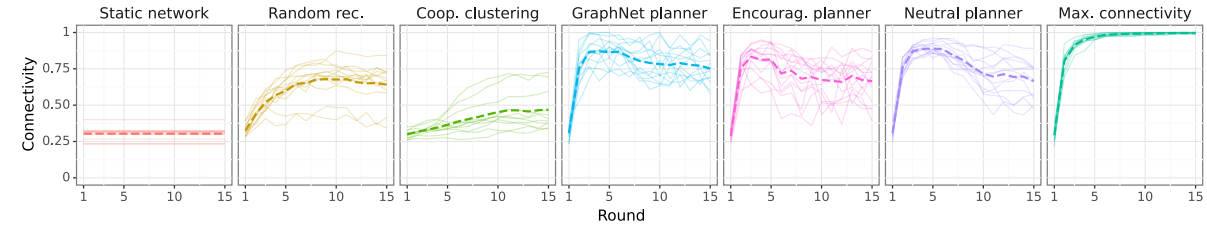

(c) **Average accumulated capital in group.**

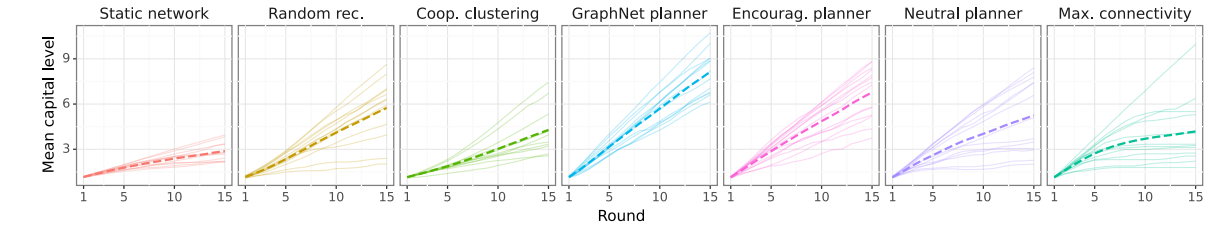

(d) **Inequality of capital distribution within group.**

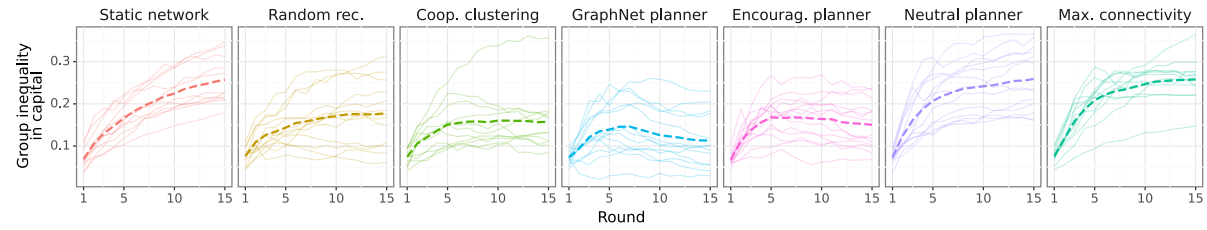

Figure S1. Group outcomes over time. Bold dotted lines represent the mean level across sessions. Solid lines reflect the levels in individual sessions.

(a) **Assortative mixing between cooperators and defectors.**

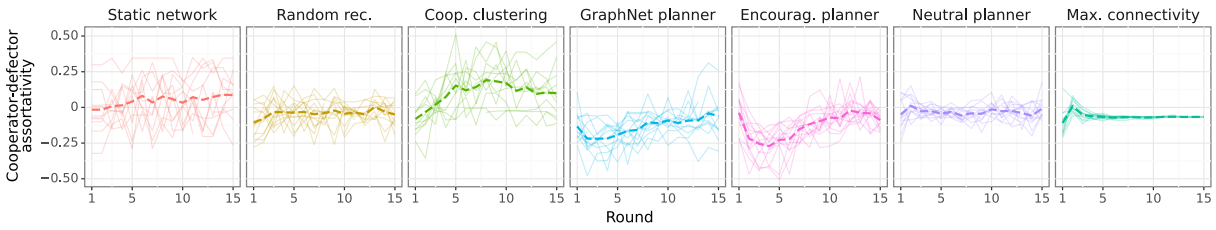

(b) **Disassortative separation between defectors.**

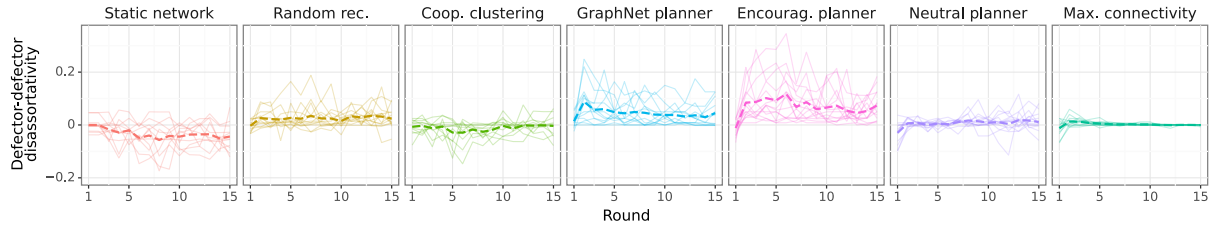

(c) **Relative degree of cooperators.**

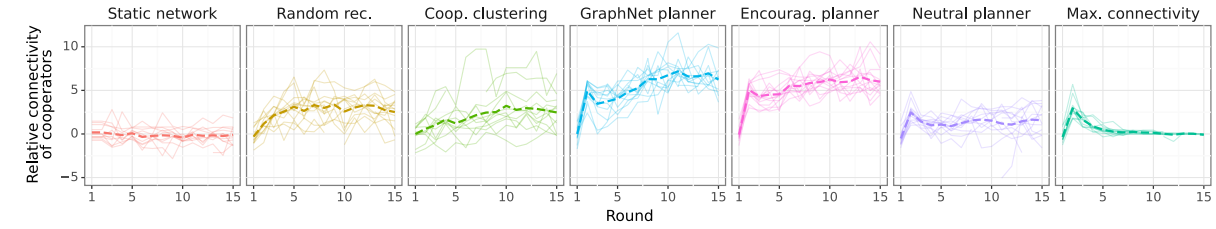

(d) **Core-periphery structure.**

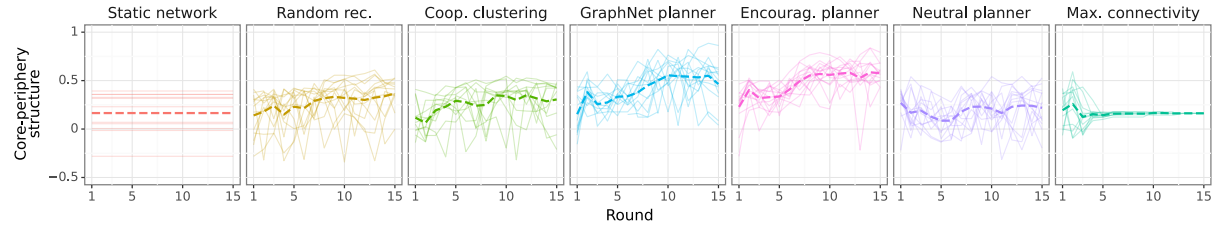

Figure S2. Network outcomes over time. Bold dotted lines represent the mean level across sessions. Solid lines reflect the levels in individual sessions.

S1. Formal game model

We model social relations and social connectivity through a network-based game (see Figure 1a). In this task, individuals occupy nodes, with edges representing active interpersonal relationships. Individuals in active relationships can choose to act either generously (*cooperation*, representing the provision of cooperative capital) or disobligingly (*defection*, representing the withholding of cooperative capital).

Formally, this *cooperative network game* is a graphical game (Kearns et al., 2001) played by n node players and overseen by one social-planner player. The node players occupy the vertices $V = \{0, 1, \ldots, n-2, n-1\}$ in an undirected and loop-free graph $G = (V, E)$. The graph edges $E = \{(i, j) \mid i, j \in V\}$ reflect active social connections between node players.

Each round of the cooperative network game is split between the node players and the social planner. The following subsections provide formal details of the game, from both of these perspectives.

S1.1. The node player perspective

At any given time during the game, each node player i observes and interacts with a subset of the full graph's nodes, N_i (their neighborhood; see Figure S3). The set of active social connections on the graph, E, defines the neighborhood $N_i = \{j \mid (i, j) \in E\}$ for player i.

Each node player i has two action spaces: the first action space corresponds to a node player's decision to cooperate or defect while the second action space corresponds to a set of node player decisions on which recommendations made by the social engineer it wishes to accept or reject.

The action space corresponding to cooperation for player i is binary $a_i^0 \in \{0, 1\}$. Choosing $a_i^0 = 0$ reflects defection and imposes no direct cost on player i. Choosing $a_i^0 = 1$ represents cooperation and imposes a direct cost $c \cdot |N_i|$, where c represents a constant cost per active connection. The cost of cooperation thus scales with the size of the neighborhood of player i. While cooperation by player i imposes a cost to itself, it also generates a positive externality b for each neighbor $j \in N_i$. The positive externalities from cooperation are additive, such that the utility for player i is defined as the sum of cooperative externalities from their neighbors less the cost of their own action:

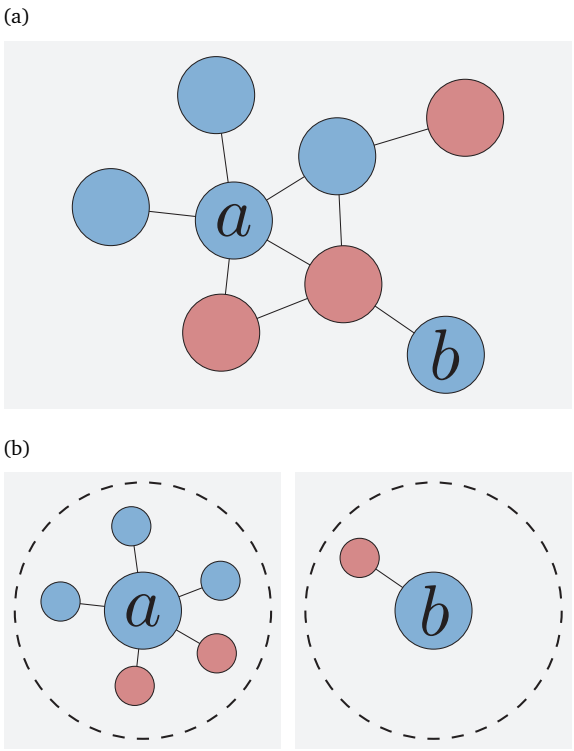

Figure S3. Node player perspective in the cooperative network game with $n = 7$. (a) Node players a and b are both situated in the game graph, but (b) receive distinct observations from their local neighborhoods.

$$U_i(\vec{a^0}, G) = \sum_{j \in N_i} (b \cdot a_j^0) - c \cdot a_i^0 \cdot |N_i| \tag{S1}$$

Each node player i possesses a level of cooperative capital d_i that can fluctuate over time. It increases when players in the neighborhood of player i cooperate and decreases if player i cooperates. Node players can only choose $a_i^0 = 1$ if they have enough capital to cover the costs of cooperation for all of their neighbors:

$$c \cdot a_i^0 \cdot |N_i| \overset{!}{\leq} d_i \tag{S2}$$

The joint action a^0 taken by all n node players can be denoted $\vec{a^0} = (a_0^0, a_1^0, \ldots, a_{n-2}^0, a_{n-1}^0) \in \{0,1\}^n$. Similarly, $\vec{d}$ denotes the vector of capital levels for all node players in the graph.

The second action space, $a_i^1 \in \{0,1\}^{n-1}$, corresponds to whether a node player i accepts or rejects the recommendation given by the social planner to add or break an active relationship with another node player j. Upon acceptance, the network changes to reflect the recommendation in the next round.

In a given round, the node player i observes their neighborhood N_i and the actions that their neighbors took in the prior round, $\{a_j^0 \mid j \in N_i\}$. They then choose their own action for the current round, $a_i^1 \in \{0,1\}$. Subsequently, the social planner recommends a set of changes to the graph a_{SP}, corresponding to either breaking an existing relationship or forming a new one, and assigns each of these edge recommendation randomly to one of the two node players that the edge is incident to. For each edge recommendation, the assigned node player i then observes which other player j the social planner recommends breaking or forming an active relationship with, together with their cooperative action a_j^0 at the current round. They then choose whether or not to accept the recommendation: $a_{i,j}^1 \in \{0,1\}$. When not receiving a recommendation for an edge change, player j's action for that edge is set to zero: $a_{j,i}^1 = 0$. Players may become fully isolated as a result of the accepted edge changes.

After all recommendations have been adjudicated, the next round starts with a cooperation decision. The joint action a^1 taken by all n node players can be denoted $\vec{a^1} = \left((a_{0,1}^1, a_{0,2}^1, \ldots, a_{0,n-1}^1), \ldots, (a_{n-1,0}^1, a_{n-1,1}^1, \ldots, a_{n-1,n-2}^1)\right) \in \{\{0,1\}^{n-1}\}^n$.

In our experiments, node players represent members of a human community. In the reinforcement learning experiments, they are simulated by hard-coded bots. In the laboratory experiments, human participants take on the node player roles.

S1.2. The social planner perspective

In the cooperative network game, the graph G (and thus node-player neighborhoods) can change over time. Prior studies have investigated, for example, the effect of random changes to the graph on the stability of group cooperation levels (Rand et al., 2011). We formalize these graph changes as a consequence of the actions of a social-planner player, or more simply a social planner.[5]

The social planner sits outside of (and can observe the entirety of) the graph G as well as the current node player cooperation decisions and capital levels. They can modify the graph by recommending changes to the set of active social connections E resulting in a modified set E'. Formally, as a result of the social planner's action a_{SP}, the game transitions from the graph $G = (V, E)$ to the graph $G' = (V, E')$. There are $m = \frac{n(n-1)}{2}$ possible edges in the (undirected and loop-free) graph. The social planner's action space is thus defined as $a_{\text{SP}} = \{-1, 0, 1\}^m$. The social planner's recommendation for a particular edge $(i, j) \in E$ is denoted as $a_{\text{SP}}(i, j) \in \{-1, 0, 1\}$, with a value of -1 representing a recommendation for the deletion of an existing edge, 0 a recommendation for no change, and 1 a recommendation for the addition of a currently nonexistent edge.

In our experiments, artificial agents—either trained with reinforcement learning or hand-crafted based on prior approaches—occupy the social planner role.

[5] In its precise, original usage, "social planner" refers to an individual or institution who can make structural decisions and who seeks to maximize social welfare (Hindriks and Myles, 2013; Mas-Colell et al., 1995). Over the years, the term has acquired a broader connotation in the social sciences. Thaler and Sunstein (2003), for example, define social planners as "anyone who must design plans for others, from human resource directors to bureaucrats to kings" (p. 178).

S2. Other game rules and parameters

At the beginning of each game, the initial network is produced with the Erdős-Rényi model for generating random graphs (Erdős and Rényi, 1959). Parameters for the initial graph generation and other game rules are summmarized in Table S1. Notably, with $n = 16$ node players in the game, the action space for the social planner is incredibly large. In each round, the social planner must recommend one of $2^{\binom{n}{2}} = 1.33 \times 10^{36}$ unique edge configurations for the network.

Game parameter	Value
Number of node players (n)	16
Episode length (T)	15
Erdős-Rényi (p)	0.3
Initial endowment of capital (d^0)	1.00
Benefit of cooperation (b)	0.10
Cost of cooperation (c)	0.05

Table S1. Parameter values used for the cooperative network game in our evaluation experiments.

S3. Study design

The protocol for the group experiments underwent independent ethical review and received a favorable opinion from the Human Behavioural Research Ethics Committee at DeepMind (#19/004). All participants provided informed consent before joining the study.

We recruited participants from the online platform Prolific (Peer et al., 2021). Inclusion criteria were residence in the U.S. and completion of at least 20 previous studies with an approval rate of 95% or more.

Each condition followed the same general study design. Participants proceeded through the following sequence of steps:

1. Read study instructions and gameplay tutorial (Figures S15–S22).
2. Play practice game (Figures S23–S27).
3. Take comprehension test (Figures S28 & S29).
4. Wait for random assignment to a game with 15 other participants (Figure S30).
5. Observe neighbors and choose to cooperate or defect (Figure S31a).
6. Wait for other participants in the game to make their choices (Figure S31b).
7. Observe neighbors' choices and own earnings (Figure S32).
8. Receive recommendations for neighborhood changes. Choose to accept or reject recommendation. Repeat for all recommendations (Figures S33 & S34).
9. Wait for other participants in the game to make their choices (Figure S35).
10. Observe changes to neighborhood (Figure S36).
11. Repeat steps 5 through 11 for 14 additional rounds. (Skip recommendations for neighborhood changes in final round.)
12. Note total earnings and transition to post-game questionnaire (Figure S37).

We required participants to answer all three questions in the comprehension test correctly to join a game session. The majority of participants (74.8%) answered all three questions correctly and were randomly sorted into sessions in groups of $n = 16$. We provided the remainder a show-up payment for the time they spent on the study tutorial and test.

Participants earned a bonus for the score they earned throughout the game and an additional bonus for finishing the entire game. Participants were not told how many rounds to expect to play of the game. Each stage of the game (e.g., choosing to cooperate or receiving recommendations from the planner) waited a preset amount of time for participant input. Participants that did not respond were removed from the experiment. We subsequently provided participants who dropped out with a debrief questionnaire including questions about technical problems they may have encountered. The tutorial explicitly detailed these rules for participants, and the main game interface displayed a timer at the bottom of every page counting down the time remaining for the current choice. Participants who dropped out were replaced with simple imitation bots for the remainder of the game. In each round, these imitation bots copied the decision making of the participants in their group from the prior round. For example, if a bot replaced a participant after a round where 12 participants cooperated and three defected, in the next round it would cooperate with 80% probability. Similarly, if the participants in its group accepted 75% of the recommendations they received in the previous round, it would accept each of its incoming recommendations with 75% probability. These imitation decisions were excluded from analysis. We observed a very low dropout rate among our participants: groups completed the final round with a mean of 14.6 participants (median = 15) out of 16 still connected.

The post-game questionnaire included the slider measure for Social Value Orientation (Murphy et al., 2011), demographic questions, two questions assessing participants' perceptions of the timing of the experiment, and two questions gathering open-ended feedback on the study.

Participants completed the study in an average of 26.5 minutes and earned an average overall payment of $11.79 for participating.

S4. Baseline studies

S4.1. Social planners

The baseline studies comprised three conditions: "static network", "random recommendations", and "cooperative clustering". This section describes the implementation of each baseline. For the purpose of comparison, we also report their performance from any prior studies that tested them with human participants.

In the static network condition, the social planner does not make any recommendations to change peer connections. Previous studies indicate that on static networks, groups gradually succumb to the tragedy of the commons. Rand et al. (2011) found that network rigidity resulted in an average cooperation rate of ∼20% after 11 rounds of the cooperative network game. Shirado et al. (2013) similarly reported that cooperation levels decline to ∼40% after 15 rounds of play on a static network.

In the random recommendations condition, the social planner recommends changing each edge with 30% probability, suggesting a deletion if the edge already exists and an addition if the edge does not exist. Rand et al. (2011) reported an average cooperation rate of ∼60% after 11 rounds of participants playing with random recommendations. Shirado et al. (2013) observed a slightly steeper decline in cooperation levels, with ∼40% of participants cooperating after 15 rounds with random recommendations.

The cooperative clustering condition draws inspiration from the "single bot" condition in Shirado and Christakis (2020). In this baseline, the social planner selects five players at random at the beginning of the game. The planner follows a set procedure for each of these focal players on each turn. First, if the focal player cooperated and one or more of their neighbors defected, the planner selects one neighbor at random and recommends that they disconnect. Second, if the focal player cooperated and none of their neighbors defected, the planner selects a player who cooperated and does not share a link with the focal player, and recommends that they connect. Third, if the focal player defected, the planner chooses a non-focal, cooperating player to replace them as a focal player in the next round. The planner chooses an additional 5% of the graph's possible edges at random and recommends that they be changed. Shirado and Christakis take a centralized, embodied approach with this algorithm: their social planner is a node player that plays the cooperation game and is connected directly to the focal players. This embedded bot generates a cooperation rate of 76.6% among human participants on round 15 in their study.

S4.2. Demographics

We recruited $N = 560$ participants (35 sessions) for the baseline conditions, with a mean age of 36.6 years ($sd = 13.2$). Approximately 48.2% of the recruited participants identified as female, 49.6% as male, and 1.0% as non-binary, genderfluid, and agender. When asked about their education, 8.8% of the sample reported completing a high school degree or equivalent, 10.8% an associate degree, 18.4% some college, 40.2% a bachelor's degree, and 21.2% a graduate degree.

S4.3. Preliminary analysis and results

We conduct an initial analysis of participant decision making to validate that participant behavior in baseline conditions resembles the behavior observed in prior studies.

We find a parsimonious model captures a substantial amount of the variance in individual decision making. We fit a generalized linear mixed model with a logistic link, regressing an individual's choice to cooperate or defect on: a joint intercept; a fixed effect for the number of neighbors they have; a fixed effect for the number of their neighbors who chose to cooperate in the previous round; a fixed effect for the fraction of their neighbors who chose to cooperate in the previous round; and a random effect reflecting the participant. For better comparability, we standardize the variables for all fixed effects. Because two of these predictors incorporate information about neighbors' cooperation decisions from the previous round, we focus this model on the second to fifteenth rounds of each game.

The joint intercept (coeff = 1.37, 95% CI $[1.03, 1.67]$, $p < 0.001$), number of neighbors a participant had (coeff = −0.75, 95% CI $[-1.01, -0.26]$, $p < 0.001$), number of cooperating neighbors (coeff = 1.16, 95% CI $[0.79, 1.68]$, $p < 0.001$), and fraction of cooperating neighbors (coeff = 0.46, 95% CI $[0.20, 0.67]$, $p < 0.001$) each had a significant effect on participants' cooperation decisions (Figure S4). To test potential multicollinearity concerns, we compute the variance inflation factor (VIF) and inspect the precision of each effect estimate (Fox, 2015; O'Brien, 2007). The VIF for each fixed effect falls below standard rules of thumb, and the effect estimates are sufficiently precise that multicollinearity is not a substantial concern for the model.

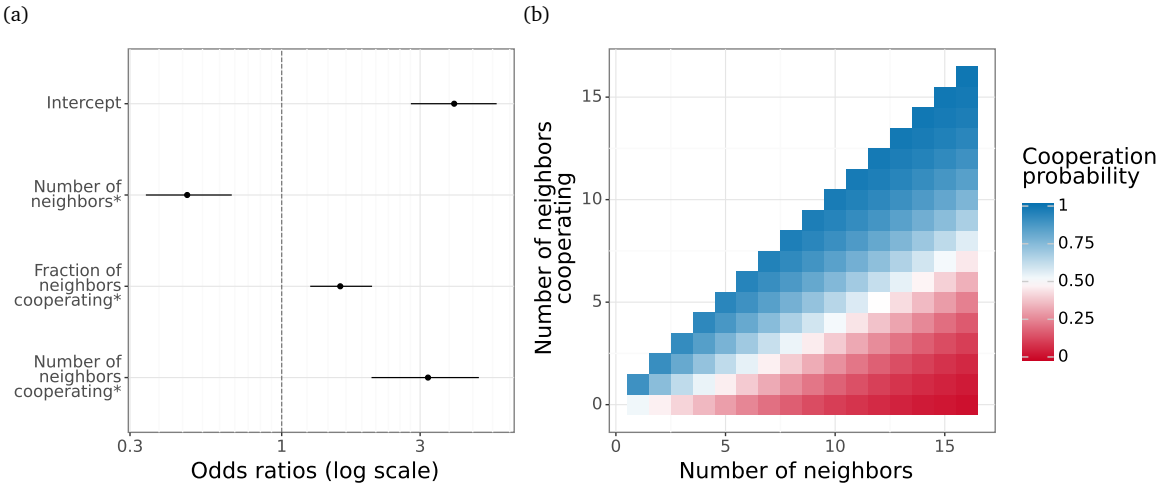

Figure S4. A generalized linear mixed model captures a substantial amount of the variance in individual cooperation decisions from round 2 and on. (a) The model regresses an individual's cooperation choice on the number of neighbors they have, the fraction of their neighborhood that chose cooperation, and the number of their neighbors that chose cooperation. Error bars represent 95% confidence intervals. Asterisks indicate that the predictor variable was standardized. (b) Predictions from the model echo behavioral dynamics observed in prior studies of the cooperative network game (see Shirado and Christakis, 2020).

We hypothesize that the random intercepts fit in the parsimonious cooperation model reflect a general cooperative disposition for each participant. We subsequently fit a simple logistic model to predict participants' decisions in the first round of the game, regressing participants' cooperation choices on a joint intercept and the random intercepts from the cooperation model for later rounds. The joint intercept (coeff = 1.55, 95% CI [1.27, 1.85], $p < 0.001$) and random intercepts (coeff = 0.78, 95% CI [0.65, 0.91], $p < 0.001$) each exhibited a significant relationship with participants' cooperation decisions (Figure S5).

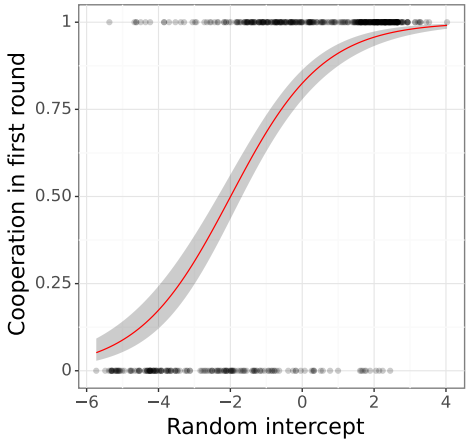

Figure S5. A simple logistic model predicts individual cooperation decisions in the first round. The model regresses cooperation decisions on the random intercepts fitted by the parsimonious cooperation model for the game's later rounds (see Figure S4). The error band indicates the 95% confidence interval.

Finally, the baseline data indicate that participant decisions to accept or reject recommendations vary as a function of the referent other's behavior (cooperate or defect) and the nature of the recommendation (add or delete). We fit a logistic model regressing participant decisions to accept or reject a recommendation on: a joint intercept; the referent other's previous cooperation choice; the recommendation valence; and the interaction between the two variables. The effects of the joint intercept (coeff = 0.15, 95% CI [0.8, 0.24], $p < 0.001$), of recommendation valence (coeff = −1.07, 95% CI [−1.15, −0.99], $p < 0.001$), of the referent other's choice (coeff = −0.20, 95% CI [−0.33, 0.07], $p < 0.001$), and the interaction (coeff = 3.41, 95% CI [3.28, 3.54], $p < 0.001$) were all significant (Figure S6).

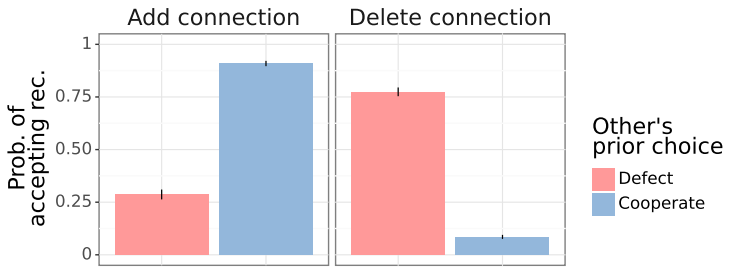

Figure S6. A logistic model indicates that participants' decisions to accept or reject recommendations vary as a function of the referent other's behavior and the nature of the recommendation. Error bars represent 95% confidence intervals.

Versions of these functions with non-standardized variables form the basis of the simulated human behavior used in agent training (see Equations 1 & 2; see also Section S5.4).

S5. Agent design and training

Over the past two decades, efforts in computer science invented a new class of computational techniques intended for graph-based applications (Gori et al., 2005; Scarselli et al., 2008). This class of techniques includes specialized neural network architectures that can—through repeated trial-and-error exploration—learn to solve graph-based problems (Battaglia et al., 2018; Hamrick et al., 2018; Tacchetti et al., 2018).

In Sections S5.1 and S5.2, we change our notation to follow common conventions from the GraphNet literature. In these sections, we define G as the tuple (u, V, E), where $u \in \mathbb{R}^{d_u}$ is a global, graph-level attribute, $V \in \mathbb{R}^{n \times d_n}$ is a matrix with each row representing a vector of node-level attributes for one node, and $E \in \mathbb{E}^{m \times d_e}$ is a matrix with each row representing a vector of edge-level attributes for one edge. The V and E matrices correspond to the V and E sets previously defined in Section S1.

S5.1. Network architecture

In our implementation, a sequence of graph neural networks (GraphNets) compose a single combined network that takes the tuple $G = (u, V, E)$ as input and outputs a tuple containing a value estimate u', unused node representations V', and policy logits E'. As a general class, GraphNets accept a directed graph $G = (u, V, E)$ and produce a similar tuple $G' = (u', V', E')$. This output represents a graph with the same topology as the input but updated global, node, and edge attributes.

Computations in a GraphNet start by invoking an edge-update function ϕ_e that computes new edge attributes based on several inputs: edge attributes, global attributes, and adjacent node attributes. The GraphNet computes updated edge attributes for the connection between sender node s and receiver node r as $e'_{s,r} = \phi_e(e_{s,r}, v_s, v_r, u)$, where $e_{s,r}$ represents the original edge attributes, v_s reflects the sender node attributes, and v_r indicates the receiver node attributes. Next, a node-update function ϕ_v computes new node attributes v'_r for a receiver node r from the updated edge attributes (specifically, edge attributes summed for each sender node s), input node attributes, and input global attributes: $v'_r = \phi_v(\sum_s e'_{s,r}, v_r, u)$. Finally, a global-update function ϕ_u computes updated global attributes from the updated edge attributes (specifically, edge attributes summed over all pairs of sender node s and receiver node r), updated node attributes (specifically, node attributes summed over each receiver node r), and input global attributes: $u' = \phi_u(\sum_{s,r} e'_{s,r}, \sum_r v'_r, u)$.

Because GraphNets take identical structures as inputs and outputs, multiple GraphNet modules can be combined in sequence: the output of one module becomes the input to the next, and so on. Our agent sequences two GraphNet modules, comprising two "message passing steps" with update functions ϕ_e^1, ϕ_v^1, ϕ_u^1, ϕ_e^2, ϕ_v^2, and ϕ_u^2 (see Figure 1c). The second node-update function, ϕ_v^2, is modified so that its inputs do not include updated edge attributes. The overall network serves simultaneously as a policy function and value function (see Table S5.5 and Figure 1c). We compute recommendations from the updated edge attributes E' and derive the value estimate from the updated global attribute u'. Our architecture is non-recurrent (i.e., "memoryless"). We designed this agent with a purely feedforward architecture to simplify the process of interpreting its policy. Despite the lack of recurrence, the agent could learn a time-conditional policy—for example, by decoding time information from player capital levels or by encoding time information in the structure of the graph itself. Nevertheless, the agent's policy and value estimate cannot directly depend on the graph history: all information must be deduced from the current state of the system.

For more details on graph neural networks, see Battaglia et al. (2018).

S5.2. Advantage-actor critic

We train our GraphNet-based social planner using an advantage actor critic (A2C) algorithm. At each state s_t, the agent observes each participant's capital level, previous cooperation decision (cooperate or defect), and a binary bit for edges (active or inactive). The agent outputs a per-edge recommendation $\pi(s_t)$ and a value estimate $\hat{\omega}(s_t)$ for the state.[6] The A2C algorithm starts by letting the agent act in the environment according to its current policy, and collects behavioral trajectories as state, action, and reward tuples $\mathcal{T} = (s_t, a_t, U_{SP_t})_{t=1}^T$. Based on these trajectories, A2C proceeds by updating (1) the policy to reinforce actions that resulted in higher-than-expected rewards, and (2) the value estimates to better reflect what was observed.

More precisely, we let our social planner's edge-update functions ϕ_e^1 and ϕ_e^2 be characterized by parameter vectors $w_{e^1} \in \mathbb{R}^{d_{e^1}}$ and $w_{e^2} \in \mathbb{R}^{d_{e^2}}$, respectively. We similarly use $w_{v^1} \in \mathbb{R}^{d_{v^1}}$ and $w_{v^2} \in \mathbb{R}^{d_{v^2}}$ to parameterize the node-update functions ϕ_v^1 and ϕ_v^2, respectively. We further let $w_{u^1} \in \mathbb{R}^{d_{u^1}}$ and $w_{u^2} \in \mathbb{R}^{d_{u^2}}$ parameterize the global-update functions ϕ_u^1 and ϕ_u^2, respectively. Finally, we let $w \in \mathbb{R}^{d_{e^1}+d_{e^2}+d_{v^1}+d_{v^2}+d_{u^1}+d_{u^2}}$ be the concatenation of the entire set of these parameter vectors.

For each collected trajectory, and on each round, A2C computes an advantage $\mathcal{A}_t$, defined as the difference between the value estimate at state s_t, $\hat{\omega}_w(s_t)$, and the sum of the rewards accumulated from that point forward, $\sum_{\tau=t}^T U_{SP_\tau}$. A2C then updates w in the direction of the policy gradient on the advantage $\mathcal{A}_t$, $\nabla_w \log \pi(s_t)\mathcal{A}_t$, and of the gradient of the $l2$ loss between the estimated and observed state value, $\sum_{\tau=t}^T -\hat{\omega}(s_\tau)\nabla_w \hat{\omega}(s_t)$ (the baseline loss). We further use a standard V-trace

[6] The standard notation for value is V. Given our use of V to represent vertices in both the game theoretic notation (Section S1) and the GraphNet algorithm notation (Section S5), we use ω to denote value throughout this paper.

policy correction to account for our asynchronous actor-learner implementation, and regularize the policy with an entropy loss to promote exploration (Espeholt et al., 2018).

We sum the three gradient components outlined above (policy gradient, baseline loss, and entropy regularization) to obtain our final update.

S5.3. Optimization target

We reward the social planner for maximizing the cooperative capital accrued by node players, with a penalty for making poor recommendations (e.g., see Pielot et al., 2014):

$$U_{\mathrm{SP}}(\vec{d}, a_{\mathrm{SP}}, \vec{a^1}) = \frac{1}{n} \cdot \sum_{i \in V} d_i - P \cdot \left(\frac{1}{m} \cdot \sum_{(i,j) \in E} f(a_{\mathrm{SP}}, \vec{a^1}, i, j) \right) \tag{S3}$$

$$f(a_{\mathrm{SP}}, \vec{a^1}, i, j) = \begin{cases} 1 & \text{if } a_{\mathrm{SP}}(i,j) \neq 0 \text{ and } a^1_{i,j} = a^1_{j,i} = 0 \\ 0 & \text{otherwise} \end{cases} \tag{S4}$$

where P is a parameter normalizing the penalty contribution to the utility function. All remaining variables are defined in Section S1.

S5.4. Simulation methods

We simulate human decision making in the cooperative network game using our analysis of participant behavior in the baseline conditions (Section S4.3). As described in *Methods*, we construct hand-crafted "bots" that make decisions to cooperate or defect and to accept or reject recommendations (see Equations 1 & 2). Table S2 describes the values used to parameterize the simulated bots.

Bot parameter	Value
μ_θ	−0.304
σ_θ	2.410
β_0	1.807
β_1	0.818
β'_0	−0.010
β'_1	−0.193
β'_2	0.370
β'_3	1.521
φ_0	0.774
φ_1	0.085
φ_2	0.287
φ_3	0.909

Table S2. Parameter values used to simulate human decision making for agent training. Values were derived by fitting models to participant behavior in the baseline conditions.

S5.5. Agent and training parameters

We train 30 replicates of the GraphNet agent, each using a different random initialization of the agent's neural network, over 5×10^7 simulated rounds of the cooperative network game. Each replicate trains on one GPU, over approximately 18 hours of wall time. Table S3 describes the variables used to parameterize the GraphNet agent, its architecture, and its training. Each update function $\phi^{\{1,2\}}_{\{e,v,u\}}$ was instantiated through a multilayer perceptron (MLP) with a single layer. We use truncated normal initializers parameterized with $\mu = 0$ and $\sigma = 1/\sqrt{\text{input size}}$ for the MLPs, truncating values at two standard deviations.

Computational unit	Architecture	Output size	Activation function	Initialization function
Edge-update function (ϕ_e^1)	Single-layer MLP	128	tanh	Truncated normal
Node-update function (ϕ_v^1)	Single-layer MLP	128	tanh	Truncated normal
Global-update function (ϕ_u^1)	Single-layer MLP	128	tanh	Truncated normal
Edge-update function (ϕ_e^2)	Single-layer MLP	2	–	Truncated normal
Node-update function (ϕ_v^2)	Single-layer MLP	128	tanh	Truncated normal
Global-update function (ϕ_u^2)	Single-layer MLP	1	–	Truncated normal

Table S3. Parameter values used for the architecture of the GraphNet agent.

Computations in a GraphNet module proceed in stages, passing through a sequence of update functions (see Section S5.1). The overall architecture comprises a total of six layers between the input to the agent and its output. Thus, while the individual computational units are shallow, the resulting architecture is deep.

Table S4 describes the variables used to parameterize training.

Training parameter	Value
Batch size	32
Learning rate (n)	0.0004
Discount (γ)	0.99
Normalization weight (P)	1.0
Entropy regularization	0.004
Baseline cost	0.5

Table S4. Parameter values used for training the GraphNet agent with reinforcement learning.

S5.6. Training results

We observe reliable learning among the replicates of the GraphNet agent (Figure S7). Performance (estimated as mean cooperation level over all rounds within a game) increases over training, with 90.0% of replicates achieving a performance of 0.70 by the end of 5×10^7 simulated training rounds.

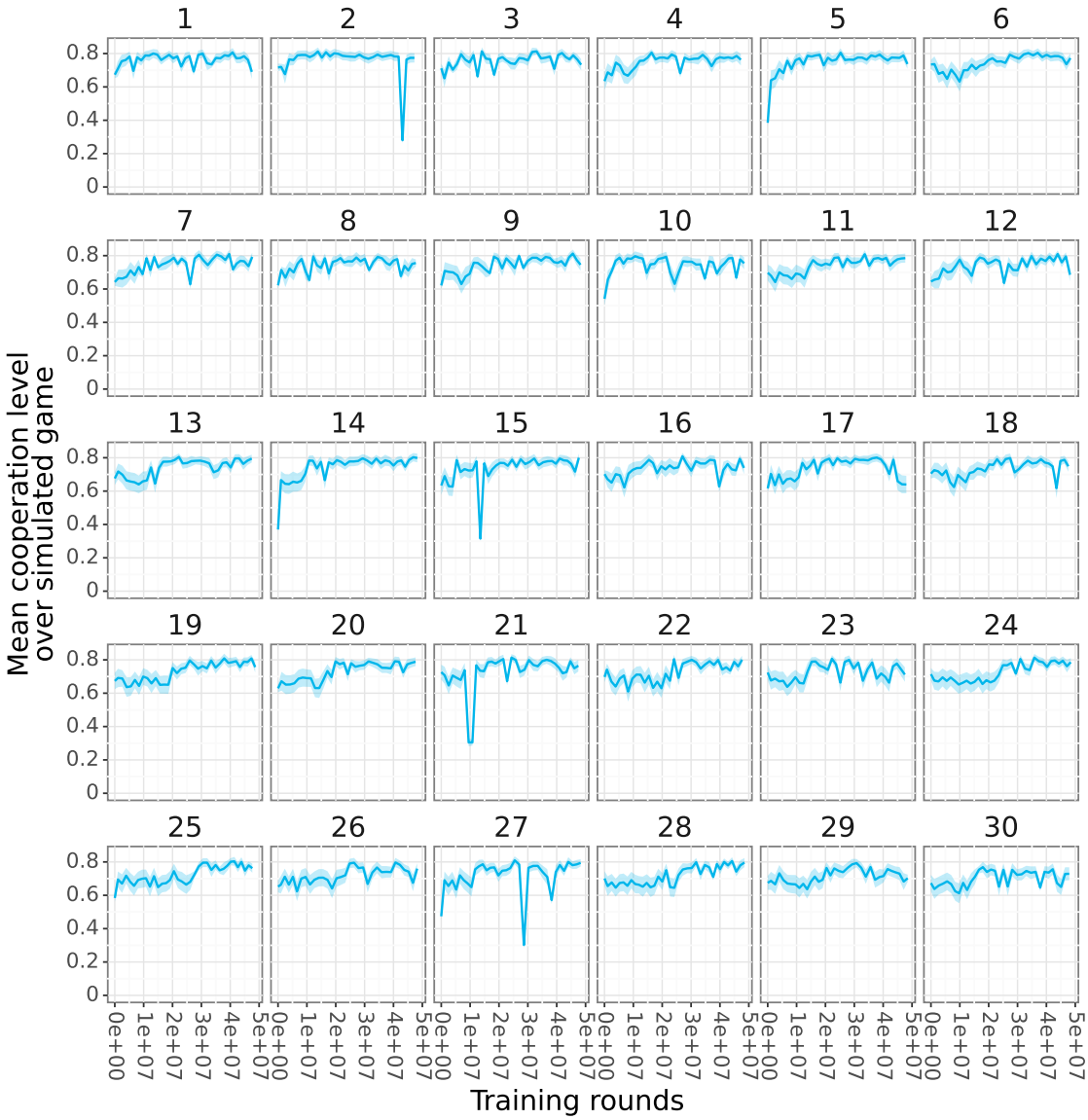

Figure S7. Training curves showing the GraphNet agent's performance in simulated games as a function of the cumulative number of simulated training rounds. Figure facets depict training runs started with different random initializations of the agent's network. During training, we save copies of the agent's policy at regular "checkpoints". We construct training curves by evaluating each checkpoint in 100 simulated games using the same bot settings as in training episodes. Error bands thus represent 95% confidence intervals over 100 simulated games at each checkpoint.

S6. Evaluation study

S6.1. Demographics

We recruited $N = 208$ participants (13 sessions) for the GraphNet planner condition, with a mean age of 36.3 years ($sd = 12.8$). Approximately 44.9% of the recruited participants identified as female, 52.8% as male, and 1.1% as non-binary. When asked about their education, 11.3% of the sample reported completing a high school degree or equivalent, 4.5% an associate degree, 23.3% some college, 42.0% a bachelor's degree, and 18.2% a graduate degree.

S6.2. Analysis and results

We begin by estimating the effect that the GraphNet planner has on cooperation rates over time and comparing its performance against the baselines. To do so, we fit a generalized linear mixed model with a logistic link, regressing participants' decisions to cooperate or defect on: a joint intercept; a fixed effect for the interaction of each condition with round number; and participant as a random effect. Network rigidity (coeff = −0.24, 95% CI [−0.27, −0.20], $p < 0.001$), random recommendations (coeff = −0.13, 95% CI [−0.16, −0.10], $p < 0.001$), cooperative clustering (coeff = −0.07, 95% CI [−0.10, −0.04], $p < 0.001$), and the GraphNet planner (coeff = 0.04, 95% CI [0.01, 0.07], $p = 0.007$) significantly affected cooperation rates over time (Figure S8). The joint intercept indicates a high level of cooperation at the beginning of the game (coeff = 2.57, 95% CI [2.05, 3.19], $p < 0.001$).

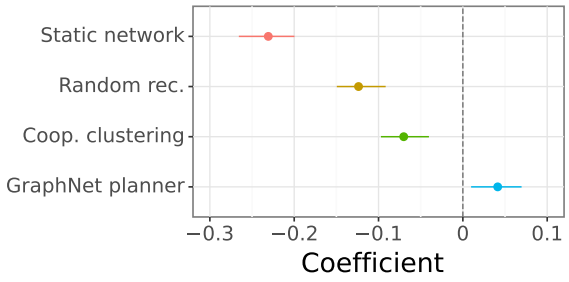

Figure S8. Estimated log odds for the per-round change in participant cooperation caused by the GraphNet social planner and the baseline conditions. Error bars indicate 95% confidence intervals.

We next identify significant differences between conditions by comparing estimated marginal means in the model. We compare the conditions through pairwise contrasts, applying a Tukey adjustment for multiple comparisons.

This individual-level mixed model provides comparability with prior studies of the network cooperation game (Rand et al., 2011, 2014; Shirado and Christakis, 2020; Shirado et al., 2013). To complement this modeling approach, we fit a linear model that analyzes cooperation at the group level, regressing the fraction of the group cooperating in the final round onto study condition. The results from this group-level model complement those of the individual-level model: groups in the static network ($\beta = 0.42$, 95% CI [0.29, 0.56], $p < 0.001$), random recommendations ($\beta = 0.56$, 95% CI [0.44, 0.68], $p < 0.001$), cooperative clustering ($\beta = 0.61$, 95% CI [0.48, 0.75], $p < 0.001$), and the GraphNet planner ($\beta = 0.78$, 95% CI [0.66, 0.90], $p < 0.001$) conditions concluded the study at varying cooperation levels, all significantly above zero. To identify significant differences between conditions, we estimate marginal means and compare the conditions through pairwise contrasts, applying a Tukey adjustment for multiple comparisons.

We next fit a linear model to evaluate the effects of each social planner on group capital levels. The model regresses mean capital level in the final round on condition. Mean capital level significantly exceeded zero with static networks ($\beta = 2.9$, 95% CI [2.0, 3.8], $p < 0.001$), random recommendations ($\beta = 5.7$, 95% CI [4.9, 6.6], $p < 0.001$), cooperative clustering ($\beta = 4.3$, 95% CI [3.4, 5.2, $p < 0.001$), and the GraphNet planner ($\beta = 8.1$, 95% CI [7.3, 9.0], $p < 0.001$). To identify significant differences between conditions, we estimate and contrast marginal means in the model, applying a Tukey adjustment for multiple comparisons.

We subsequently fit a linear model to evaluate the effects of each social planner on group inequality, measured by calculating the Gini coefficient over group capital levels. The model regresses group inequality in the final round on condition. Group inequality significantly exceeded zero with static networks ($\beta = 0.26$, 95% CI [0.21, 0.30], $p < 0.001$), random recommendations ($\beta = 0.18$, 95% CI [0.14, 0.22], $p < 0.001$), cooperative clustering ($\beta = 0.16$, 95% CI [0.12, 0.20, $p < 0.001$), and the GraphNet planner ($\beta = 0.11$, 95% CI [0.07, 0.15], $p < 0.001$). To identify significant differences between conditions, we estimate and contrast marginal means in the model, applying a Tukey adjustment for multiple comparisons.

We conduct likelihood ratio tests for the random recommendation, cooperative clustering, and GraphNet planner conditions to empirically evaluate whether each social planner conditioned its recommendations on participants' choices. The tests

indicate that the random-recommendation planner's actions did not differ as a function of participants' choices, $\chi^2(2) = 0.9$, $p = 0.64$. In contrast, recommendations varied as a function of participants' decisions with cooperative clustering, $\chi^2(2) = 92.0$, $p < 0.001$, and the GraphNet planner, $\chi^2(2) = 3451.8$, $p < 0.001$.

To confirm that the GraphNet planner is learning to condition its recommendations on the participants' cooperation choices, we set up and run a representation analysis. That is, we leverage the natural structure of the GraphNet's representations to interpret what it is learning (e.g., Sanchez-Lengeling et al., 2020; Zambaldi et al., 2018; see also Gilpin et al., 2018). The GraphNet computes representations of the game's nodes, edges, and global features. The agent directly uses the edge and global features for the policy and value outputs, respectively, but does not directly use the representation of the network nodes for reinforcement learning (see Figure 1c). We find that the node representations encode participants' next cooperation choice with an area under curve (AUC) score of 0.93, 95% CI [0.92 – 0.94] (Figure S9a). We cross-validate the model with five k-fold splits, obtaining a mean accuracy of 0.85 ($sd = 0.01$) over the splits.

Given the high likelihood of participants who cooperate on one round to choose cooperation on the next round (Rand et al., 2011), we compare the predictiveness of the planner's representations against predictions made based on previous-round cooperation (Figure S9b). Bootstrapping over 10,000 replicates, the node representations reliably offer higher AUC scores for participants' cooperation decisions than those from cooperation decisions in the previous round, $p < 0.001$. Though the GraphNet planner is not explicitly incentivized to predict cooperation decisions, its neural network learns to track and represent the cooperativeness of the node players.

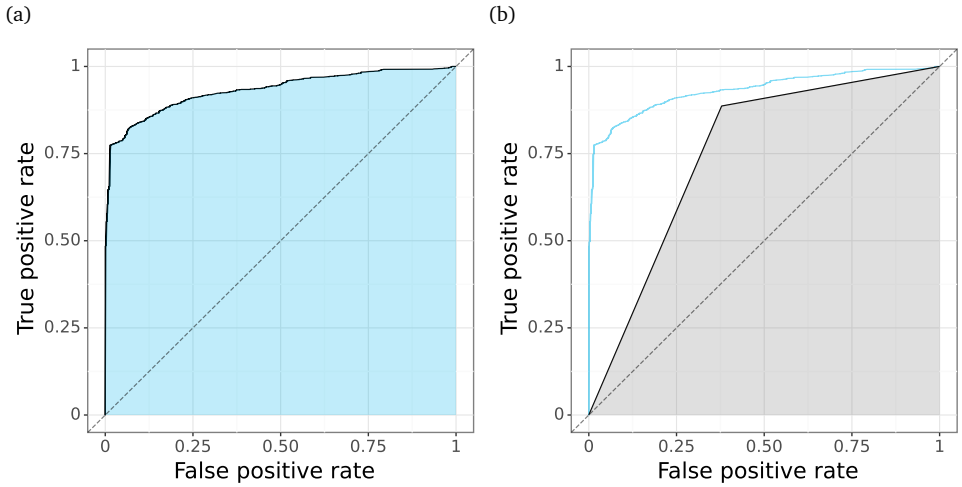

Figure S9. Analysis of the information encoded in the GraphNet social planner's node representations. (a) The representations of network nodes encoded by the GraphNet (V' in Figure 1) provide strong predictive accuracy for a participant's cooperation choice in the next round, as shown in this receiver operator characteristic curve. The representation achieves an AUC score of 0.93 for predicting a participant's decision. (b) In contrast, the participant's previous decision is not as predictive, achieving an AUC of only 0.75. For direct comparison, the blue line indicates the receiver operator characteristic curve for the node representations.

We next fit a linear model to assess the effects of each social planner on cooperator-defector assortative mixing between cooperators and defectors. We compute cooperator-defector assortativity following the formulation by Newman (2003). The model regresses assortative mixing in the final round on condition. Static networks ($\beta = 0.09$, 95% CI $[0.01, 0.17]$, $p = 0.036$) and cooperative clustering ($\beta = 0.10$, 95% CI $[0.02, 0.19]$, $p = 0.015$) exert a positive and significant effect on cooperator-defector assortativity. In contrast, random recommendations ($\beta = -0.03$, 95% CI $[-0.10, 0.05]$, $p = 0.45$) and the GraphNet planner ($\beta = -0.04$, 95% CI $[-0.13, 0.04]$, $p = 0.30$) have no significant effect on assortative mixing. To identify significant differences between conditions, we estimate marginal means and compare the conditions through pairwise contrasts, applying a Tukey adjustment for multiple comparisons.

As a robustness check, we evaluate three alternative specifications for assortative mixing.

Rand et al. (2014) compute assortment as the average fraction of cooperative neighbors for cooperators minus the average fraction of cooperative neighbors for defectors. We calculate and refer to this as "Rand assortativity". A linear model regressing Rand assortativity on condition partially matches the patterns we observed with the original assortativity measure, with the exception of the effect of network rigidity. The Rand-assortativity model shows significant effects for cooperative clustering ($\beta = 0.11$, 95% CI $[0.03, 0.20]$, $p = 0.023$), and non-significant effects for network rigidity ($\beta = 0.09$, 95% CI $[0.00, 0.18]$, $p = 0.06$), random recommendations ($\beta = -0.05$, 95% CI $[-0.13, 0.03]$, $p = 0.22$), and the GraphNet planner ($\beta = -0.06$, 95% CI $[-0.14, 0.02]$, $p = 0.17$).

Shirado and Christakis (2020) calculate assortativity as the average correlation between neighbors' strategies over all edges on the network. We compute and refer to this as "Shirado assortativity". A linear model regressing Shirado assortativity on condition again replicates the dynamics observed with the original assortativity measure. The model demonstrates significant effects for network rigidity ($\beta = 0.14$, 95% CI $[0.05, 0.23]$, $p = 0.002$) and cooperative clustering ($\beta = 0.13$, 95% CI $[0.04, 0.22]$, $p = 0.006$), and non-significant effects for random recommendations ($\beta = -0.03$, 95% CI $[-0.11, 0.06]$, $p = 0.50$) and the GraphNet planner ($\beta = -0.03$, 95% CI $[-0.12, 0.05]$, $p = 0.45$).

Finally, we compute a "defector disassortativity" (or "defector separation") measure based on Wang et al. (2012). Defector disassortativity reflects the difference between the fraction of defector-defector links in the network expected under a random permutation of node choices and the actual observed fraction. We estimate the expected fraction over 10,000 random replicates for each network. This disassortativity measure proves complementary to the prior assortment measures. A linear model regressing defector separation on condition indicates that levels of separation among defectors did not differ significantly from zero with random recommendations ($\beta = 0.02$, 95% CI $[0.00, 0.05]$, $p = 0.06$) or cooperative clustering ($\beta = 0.00$, 95% CI $[-0.03, 0.02]$, $p = 0.79$). In contrast, static networks induced negative levels of defector separation ($\beta = -0.05$, 95% CI $[-0.08, -0.02]$, $p < 0.001$), while the GraphNet planner ($\beta = 0.04$, 95% CI $[0.02, 0.07]$, $p = 0.007$) caused positive levels.

We subsequently fit a linear model to evaluate the effects of each social planner on the relative degree of cooperators within the network. The model regresses the difference in mean degree of cooperators and the mean degree of defectors in the final round on condition. Static networks caused a level of cooperator connectivity that did not differ significantly from zero ($\beta = -0.2$, 95% CI $[-1.2, 0.9]$, $p = 0.75$). In contrast, random recommendations ($\beta = 2.5$, 95% CI $[1.6, 3.5]$, $p < 0.001$), cooperative clustering ($\beta = 2.5$, 95% CI $[1.4, 3.5$, $p < 0.001$), and the GraphNet planner ($\beta = 6.2$, 95% CI $[5.3, 7.2]$, $p < 0.001$) each induced significant and outsize levels of cooperator connectivity. To identify significant differences between conditions, we estimate and contrast marginal means in the model, applying a Tukey adjustment for multiple comparisons.

We assess the degree to which the network in each round exhibits a core-periphery structure through a bimodular surprise measure (de Jeude et al., 2019). This approach estimates how closely a graph fits a core-periphery structure using only its structure (i.e., it does not take node choice into account). We subsequently fit a linear model to evaluate the effects of each social planner on core-periphery structure. The model regresses core-periphery structure fit in the final round on condition. Network rigidity ($\beta = 0.16$, 95% CI $[0.04, 0.29]$, $p = 0.010$), random recommendations ($\beta = 0.35$, 95% CI $[0.24, 0.47]$, $p < 0.001$), cooperative clustering ($\beta = 0.32$, 95% CI $[0.20, 0.45$, $p < 0.001$), and the GraphNet planner ($\beta = 0.46$, 95% CI $[0.35, 0.58]$, $p < 0.001$) all exerted a positive and significant effect on core-periphery structure. To identify significant differences between conditions, we estimate and contrast marginal means in the model, applying a Tukey adjustment for multiple comparisons.

We next evaluate the concordance between core-periphery categorization and participant cooperation. Core and periphery status offer a fairly accurate prediction of cooperation and defection, respectively: 84.6% of participants are correctly classified on the basis of their core-periphery location. We permute participants' choices in each round over 10,000 resamples: for each resample, we calculate the proportion of the overall network where cooperators are classified as core and defectors are classified as peripheral. This permutation test indicates that the observed concordance between core-periphery structure and participant cooperation is highly unlikely to arise by chance, $p < 0.001$.

To better understand the incentives induced by each social planner, we calculate the mean payoffs earned by cooperators and defectors throughout the game in each condition (Figure S10). Echoing previous research, static networks and random recommendations cause cooperators to earn less than defectors, whereas cooperative clustering induces the opposite pattern (Shirado and Christakis, 2020). Under the GraphNet planner, defectors outearn cooperators throughout the game, on average.

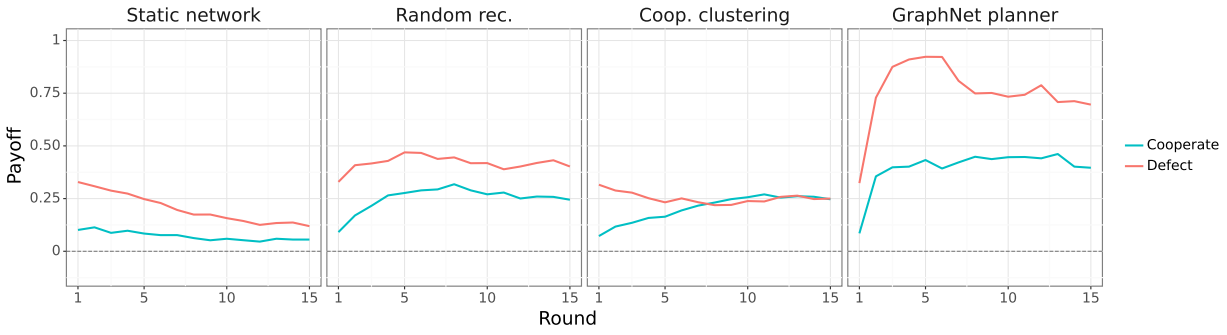

Figure S10. Per-round payoff for participants by cooperation choice in each condition. Blue lines indicate the mean payoff that cooperating participants received in each round. Red lines reflect the payoffs of defecting participants.

As a final, informal evaluation of core-periphery structure, we present snapshots of all sessions from midway through the game (on round 10; see Figure S11).

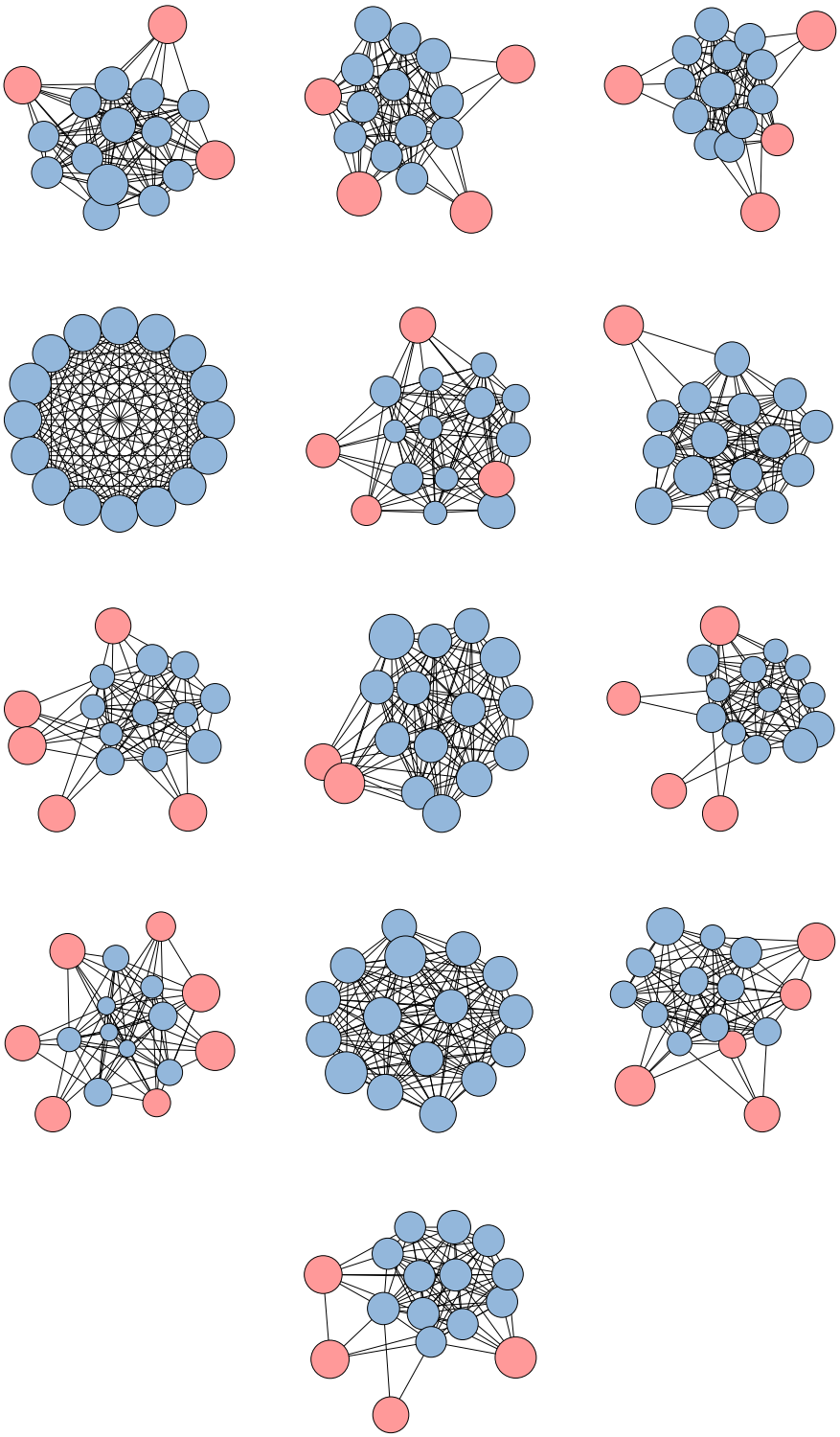

Figure S11. Network snapshots from round 10 of all sessions in the GraphNet planner condition. Node color represents the participant's previous choice (blue, cooperate; red, defect). Node size reflects cumulative cooperative capital (larger nodes indicate a greater amount of capital).

S7. Validation studies

S7.1. Social planners

The validation studies comprised three conditions: an "encouragement planner", a "neutral planner", and "maximum connectivity". This section describes the implementation of each of these planners.

We first construct a new "encouragement" social planner based on analysis of the GraphNet planner's policy (see Figure 3). In contrast with the complex and opaque computations in the GraphNet planner's policy, the encouragement planner makes recommendations as a simple function of player cooperation choices, the recommendation valence, and the round number (Tables S5–S7).

Cooperate-cooperate

t	Add connection	Delete connection
1	1.000	0.000
2	1.000	0.000
3	1.000	0.000
4	1.000	0.000
5	1.000	0.000
6	1.000	0.000
7	1.000	0.000
8	1.000	0.010
9	1.000	0.010
10	1.000	0.011
11	1.000	0.028
12	0.991	0.035
13	0.954	0.073
14	1.000	0.108

Table S5. Conditional probabilities parameterizing the encouragement social planner's recommendations for cooperate-cooperate edges. The encouragement planner makes recommendations as a probabilistic function of the current round number, the referent players' previous actions, and current connection status.

Cooperate-defect

t	Add connection	Delete connection
1	0.993	0.048
2	0.973	0.029
3	0.914	0.145
4	0.791	0.213
5	0.644	0.318
6	0.594	0.508
7	0.463	0.608
8	0.429	0.745
9	0.366	0.802
10	0.372	0.753
11	0.361	0.741
12	0.371	0.774
13	0.328	0.706
14	0.408	0.722

Table S6. Conditional probabilities parameterizing the encouragement social planner's recommendations for cooperate-defect edges. The encouragement planner makes recommendations as a probabilistic function of the current round number, the referent players' previous actions, and current connection status.

Defect-defect

t	Add connection	Delete connection
1	0.000	1.000
2	0.000	1.000
3	0.000	1.000
4	0.000	1.000
5	0.000	1.000
6	0.000	1.000
7	0.000	1.000
8	0.000	1.000
9	0.000	1.000
10	0.000	1.000
11	0.000	1.000
12	0.000	1.000
13	0.000	1.000
14	0.000	1.000

Table S7. Conditional probabilities parameterizing the encouragement social planner's recommendations for defect-defect edges. The encouragement planner makes recommendations as a probabilistic function of the current round number, the referent players' previous actions, and current connection status.

As a second follow-up, we build a social planner that aims to produce the same group connectivity dynamics as the GraphNet planner, without regard for player's choices. The encouragement planner makes recommendations as a simple function of the recommendation valence and the round number (Table S8).

t	Add connection	Delete connection
1	0.891	0.119
2	0.841	0.054
3	0.656	0.084
4	0.642	0.102
5	0.608	0.117
6	0.549	0.204
7	0.545	0.215
8	0.538	0.224
9	0.520	0.239
10	0.504	0.213
11	0.532	0.215
12	0.518	0.237
13	0.529	0.232
14	0.522	0.317

Table S8. Conditional probabilities parameterizing the neutral social planner's recommendations for all edges. The neutral planner makes recommendations as a probabilistic function of the current round number and the current connection status.

Finally, we construct a social planner that attempts to maximize connectivity throughout the game. In every round of the maximum connectivity condition, the social planner recommends that each unlinked pair of players in the graph establish a connection. This social planner never recommends the deletion of any edges.

S7.2. Demographics

We recruited $N = 624$ participants (39 sessions) for the encouragement planner condition, with a mean age of 36.8 years ($sd = 12.2$). Approximately 42.0% of the recruited participants identified as female, 55.4% as male, and 1.8% as non-binary, trans, genderqueer, demigender, agender, asexual, and aromantic. When asked about their education, 13.3% of the sample reported completing a high school degree or equivalent, 10.2% an associate degree, 24.3% some college, 36.7% a bachelor's degree, and 14.6% a graduate degree.

S7.3. Analysis and results

We first fit a generalized linear mixed model to evaluate the effects of each social planner on cooperation rates over time. Network rigidity (coeff = −0.23, 95% CI [−0.27, −0.20], $p < 0.001$), random recommendations (coeff = −0.12, 95% CI [−0.15, −0.09], $p < 0.001$), cooperative clustering (coeff = −0.07, 95% CI [−0.10, −0.04], $p < 0.001$), the GraphNet planner (coeff = 0.04, 95% CI [0.01, 0.07], $p = 0.005$), the encouragement planner (coeff = 0.04, 95% CI [0.00, 0.06], $p = 0.005$), the neutral planner (coeff = −0.17, 95% CI [−0.19, −0.14], $p < 0.001$), and maximum connectivity (coeff = −0.51, 95% CI [−0.55, −0.46], $p < 0.001$) significantly influenced cooperation rates over time (Figure S12). The joint intercept indicates a high level of cooperation at the beginning of the game (coeff = 2.04, 95% CI [1.62, 2.50], $p < 0.001$). To identify significant differences between conditions, we estimate and contrast marginal means in the model, applying a Tukey adjustment for multiple comparisons.

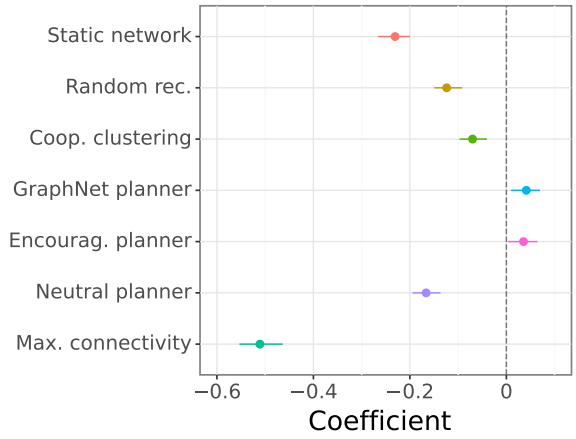

Figure S12. Estimated log odds for the per-round change in participant cooperation caused by the GraphNet social planner, the encouragement planner, and the baseline conditions. Error bars reflect 95% confidence intervals.

To complement this group-level model, we fit a linear model that evaluates cooperation at the group level, regressing the fraction of the group cooperating in the final round onto condition. The results from this group-level model are broadly consistent with those of the individual-level model: groups in the static networks ($\beta = 0.42$, 95% CI [0.29, 0.56], $p < 0.001$), random recommendations ($\beta = 0.56$, 95% CI [0.44, 0.68], $p < 0.001$), cooperative clustering ($\beta = 0.61$, 95% CI [0.48, 0.75], $p < 0.001$), GraphNet planner ($\beta = 0.78$, 95% CI [0.66, 0.90], $p < 0.001$), encouragement planner ($\beta = 0.71$, 95% CI [0.59, 0.83], $p < 0.001$), and neutral planner ($\beta = 0.47$, 95% CI [0.34, 0.59], $p < 0.001$) conditions achieved varying cooperation levels, all significantly above zero, on the final round. In contrast, groups in the maximum connectivity condition cooperated at levels that did not significantly differ from zero ($\beta = 0.12$, 95% CI [0.00, 0.25], $p = 0.05$). To identify significant differences between conditions, we estimate marginal means and compare the conditions through pairwise contrasts, applying a Tukey adjustment for multiple comparisons.

Next, we fit a linear model to evaluate the effects of each social planner on assortative mixing between cooperators and defectors. The model regresses assortative mixing in the final round on condition. Static networks ($\beta = 0.09$, 95% CI [0.02, 0.16], $p = 0.018$) and cooperative clustering ($\beta = 0.10$, 95% CI [0.03, 0.17, $p = 0.007$) induced positive and significant levels of cooperator-defector assortativity in the graph. The encouragement planner produced negative and significant levels of assortatitivity ($\beta = -0.09$, 95% CI [−0.15, −0.02], $p = 0.006$). In contrast, random recommendations ($\beta = -0.05$, 95% CI [−0.12, 0.02], $p = 0.13$), the GraphNet planner ($\beta = -0.06$, 95% CI [−0.13, 0.01], $p = 0.07$), the neutral planner ($\beta = -0.01$, 95% CI [−0.08, 0.06], $p = 0.84$), and maximum connectivity ($\beta = -0.06$, 95% CI [−0.16, 0.02], $p = 0.15$) exerted no significant effect on assortative mixing. To identify significant differences between conditions, we estimate and contrast marginal means in the model, applying a Tukey adjustment for multiple comparisons.

We subsequently fit a linear model to evaluate the effects of each social planner on the relative degree of cooperators within the network. The model regresses relative degree in the final round on condition. Static networks ($\beta = -0.1$, 95% CI [−1.0, 0.9], $p = 0.85$) and maximum connectivity ($\beta = -0.1$, 95% CI [−1.3, 1.1], $p = 0.87$) precipitated levels of cooperator connectivity that did not differ significantly from zero. In contrast, random recommendations ($\beta = 2.5$, 95% CI [1.6, 3.4], $p < 0.001$), cooperative clustering ($\beta = 2.5$, 95% CI [1.5, 3.4, $p < 0.001$), the GraphNet planner ($\beta = 6.2$, 95% CI [5.4, 7.1], $p < 0.001$), the encouragement planner ($\beta = 6.0$, 95% CI [5.2, 6.8], $p < 0.001$), and the neutral planner ($\beta = 1.6$, 95% CI [0.7, 2.5], $p < 0.001$) each induced significant and outsize levels of cooperator connectivity. To identify significant differences between conditions, we estimate and contrast marginal means in the model, applying a Tukey adjustment for multiple comparisons.

We next fit a linear model to evaluate the effects of each social planner on core-periphery structure. The model regresses core-periphery structure fit in the final round on condition. Network rigidity ($\beta = 0.16$, 95% CI [0.04, 0.29], $p = 0.005$),

random recommendations ($\beta = 0.37$, 95% CI $[0.26, 0.47]$, $p < 0.001$), cooperative clustering ($\beta = 0.31$, 95% CI $[0.19, 0.42$, $p < 0.001$), the GraphNet planner ($\beta = 0.46$, 95% CI $[0.36, 0.57]$, $p < 0.001$), the encouragement planner ($\beta = 0.58$, 95% CI $[0.48, 0.68]$, $p < 0.001$), and the neutral planner ($\beta = 0.22$, 95% CI $[0.11, 0.32]$, $p < 0.001$) all exerted a positive and significant effect on core-periphery structure. In contrast, the effect of maximum connectivity on core-periphery structure was not statistically significant ($\beta = 0.16$, 95% CI $[-0.05, 0.38]$, $p = 0.14$). To identify significant differences between conditions, we estimate and contrast marginal means in the model, applying a Tukey adjustment for multiple comparisons.

Finally, we fit a linear model to evaluate the effects of each social planner on network connectivity. The model regresses network density in the final round on condition. Static networks ($\beta = 0.30$, 95% CI $[0.28, 0.33]$, $p < 0.001$), random recommendations ($\beta = 0.64$, 95% CI $[0.56, 0.70]$, $p < 0.001$), cooperative clustering ($\beta = 0.47$, 95% CI $[0.39, 0.56$, $p < 0.001$), the GraphNet planner ($\beta = 0.75$, 95% CI $[0.69, 0.81]$, $p < 0.001$), the encouragement planner ($\beta = 0.66$, 95% CI $[0.58, 0.74]$, $p < 0.001$), the neutral planner ($\beta = 0.67$, 95% CI $[0.60, 0.73]$, $p < 0.001$), and maximum connectivity ($\beta = 1.00$, 95% CI $[0.99, 1.00]$, $p < 0.001$) all produced network densities that significantly exceeded zero. To identify significant differences between conditions, we estimate and contrast marginal means in the model, applying a Tukey adjustment for multiple comparisons.

As before, we calculate the mean payoffs earned by cooperators and defectors throughout the game in each condition (Figure S13). Across the various conditions, we observe an inconsistent relationship between the relative payoff for cooperation and expected group cooperation (see Figure S1).

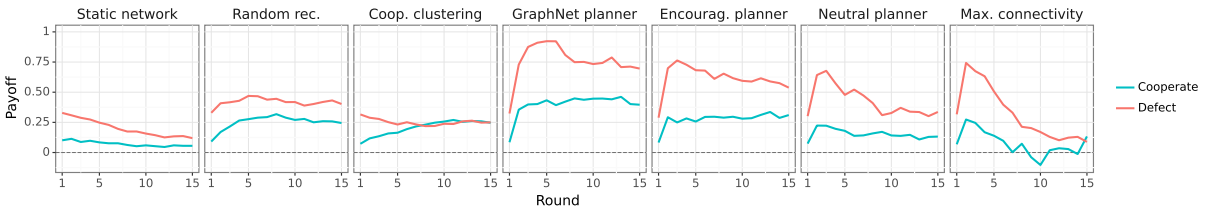

Figure S13. Per-round payoff for participants by cooperation choice in each condition. Blue lines indicate the mean payoff that cooperating participants received in each round. Red lines reflect the payoffs of defecting participants.

Finally, to informally evaluate the core-periphery dynamics in the encouragement planner condition, we present snapshots of all sessions from midway through the game (on round 10; Figure S14).

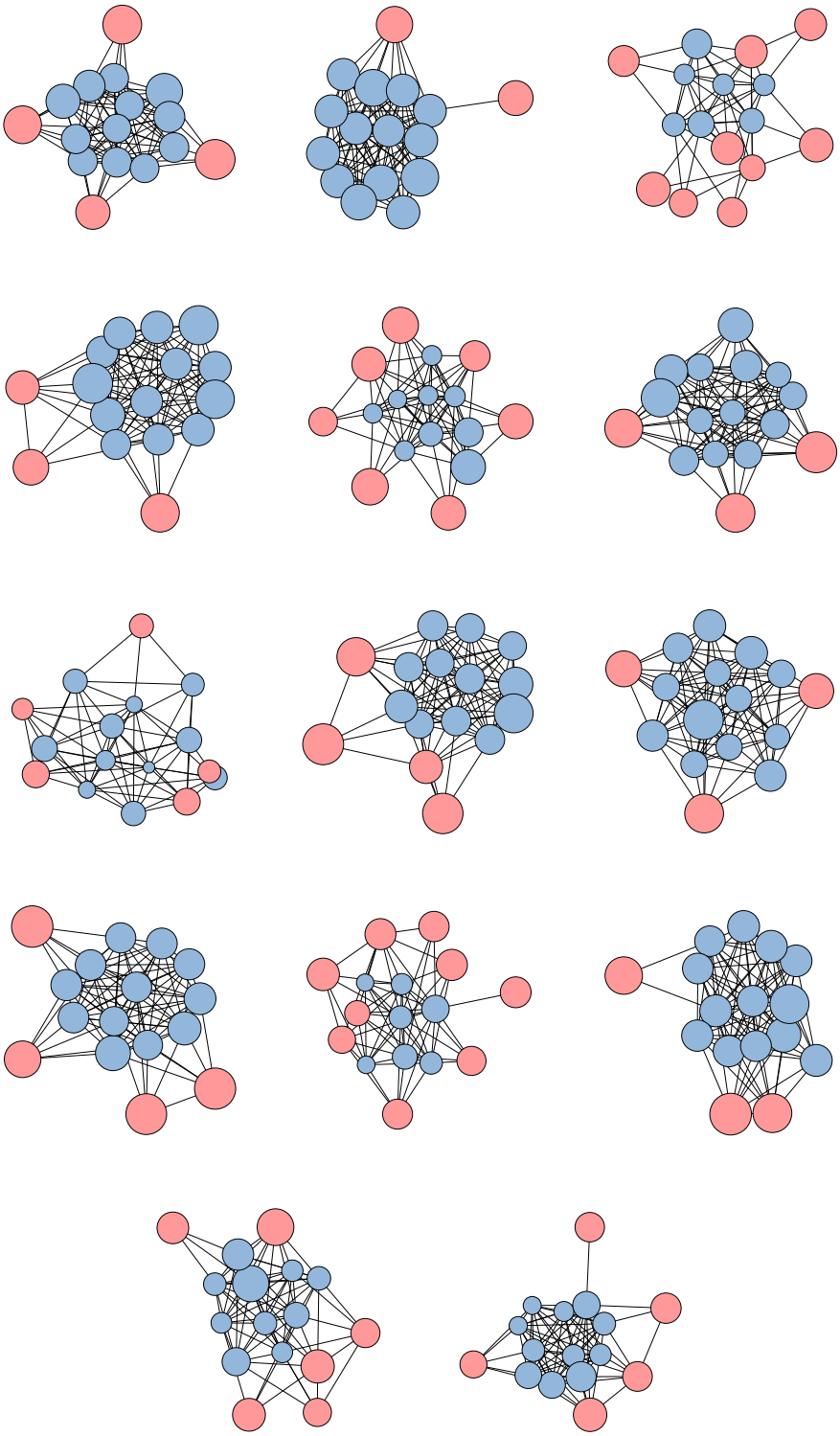

Figure S14. Network snapshots from round 10 of all sessions in the encouragement planner condition. Node color represents the participant's previous choice (blue, cooperate; red, defect). Node size reflects cumulative cooperative capital (larger nodes indicate a greater amount of capital).

S8. Study screenshots

(a)

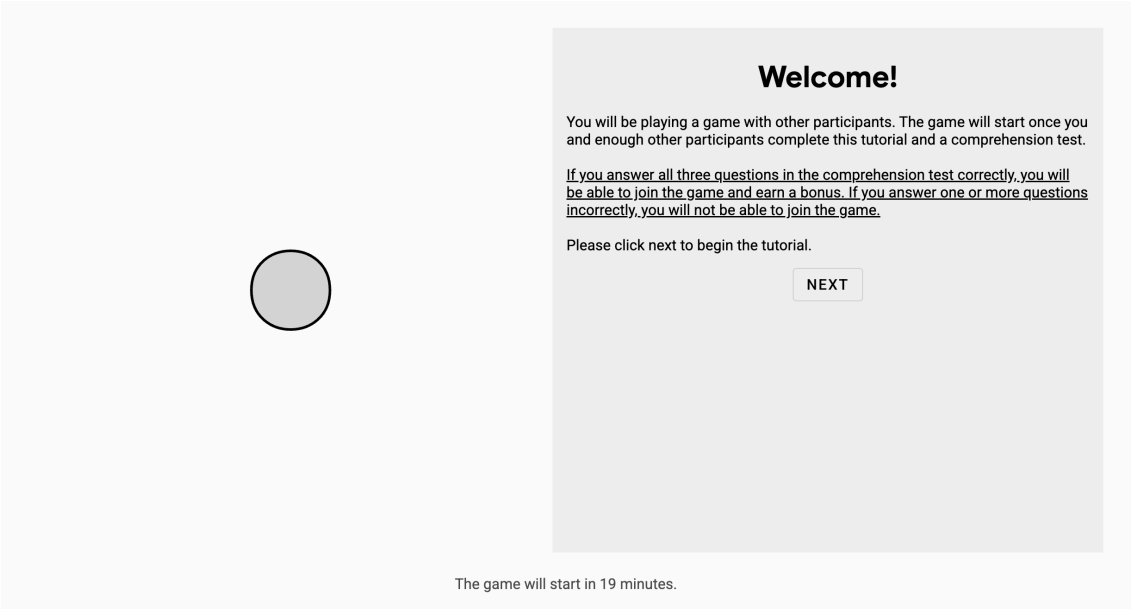

(b)

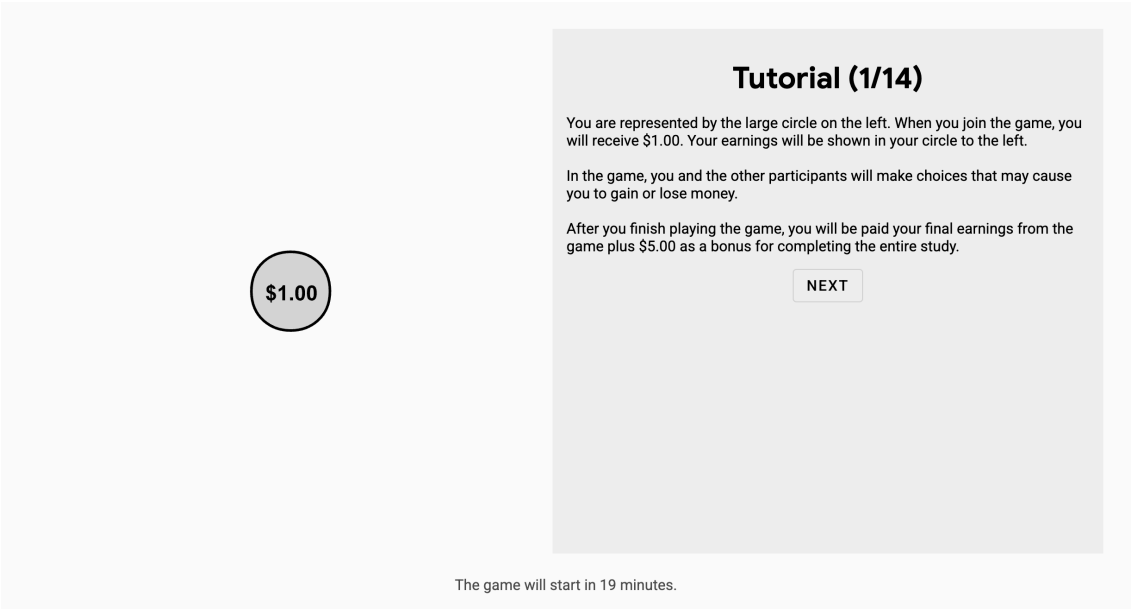

Figure S15. Screenshots of the participant interface for the cooperative network game. (a) The participant reads general study information. (b) The participant reads tutorial information about the game.

(a)

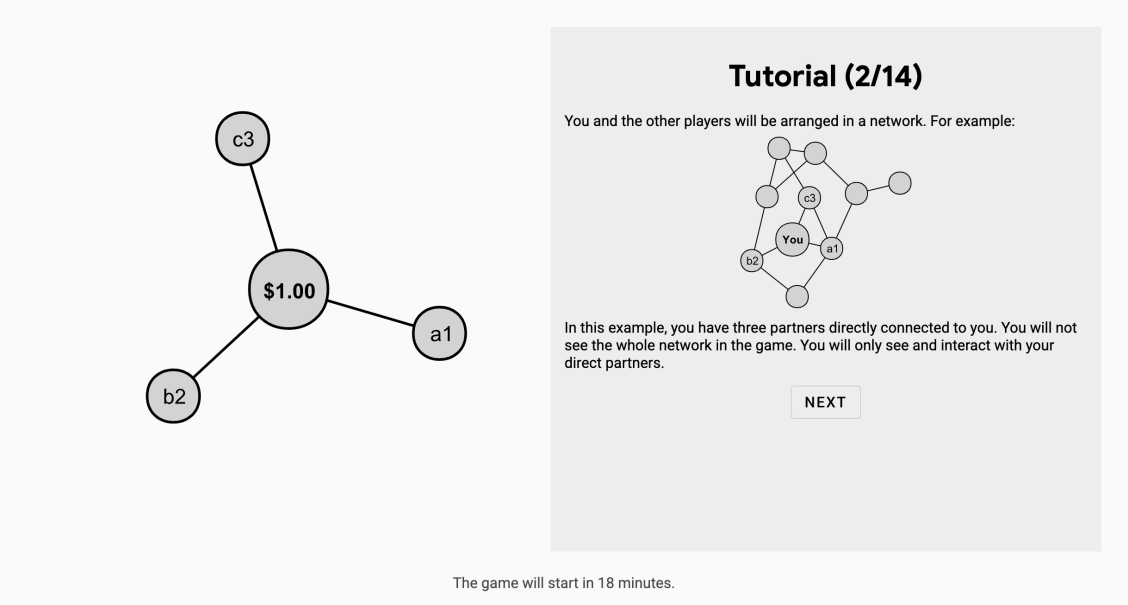

(b)

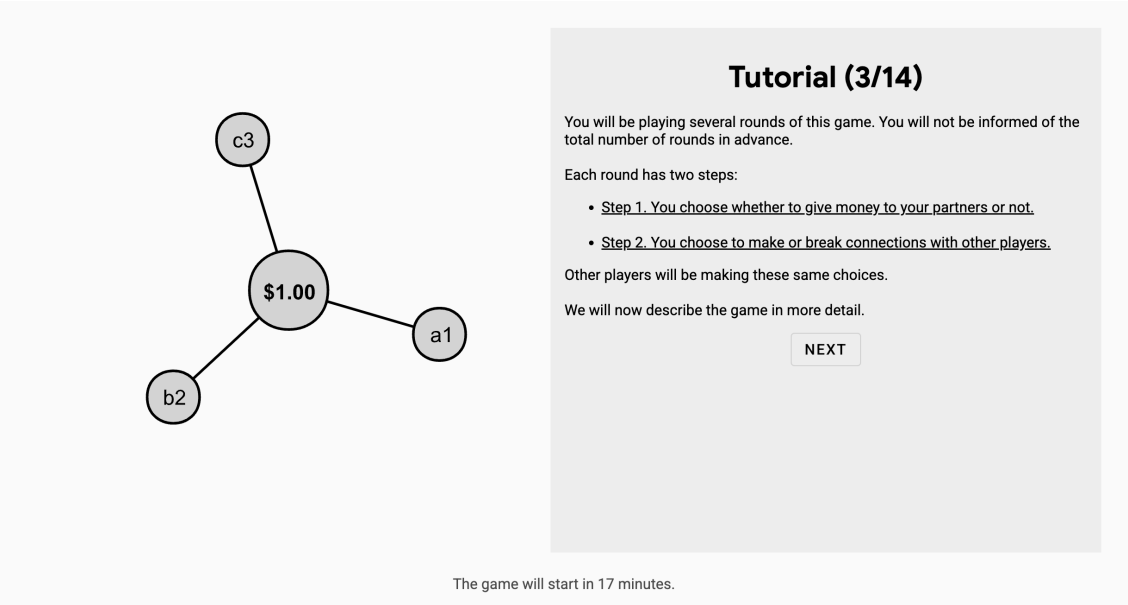

Figure S16. Screenshots of the participant interface for the cooperative network game. (a) The participant reads tutorial information about the game. (b) The participant reads tutorial information about the game.

(a)

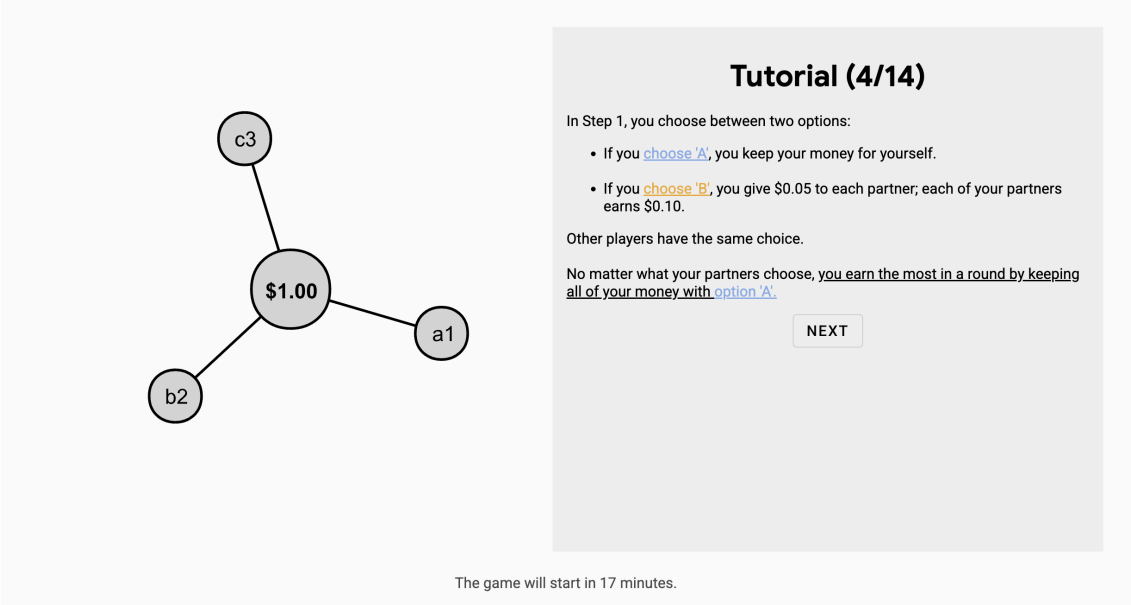

(b)

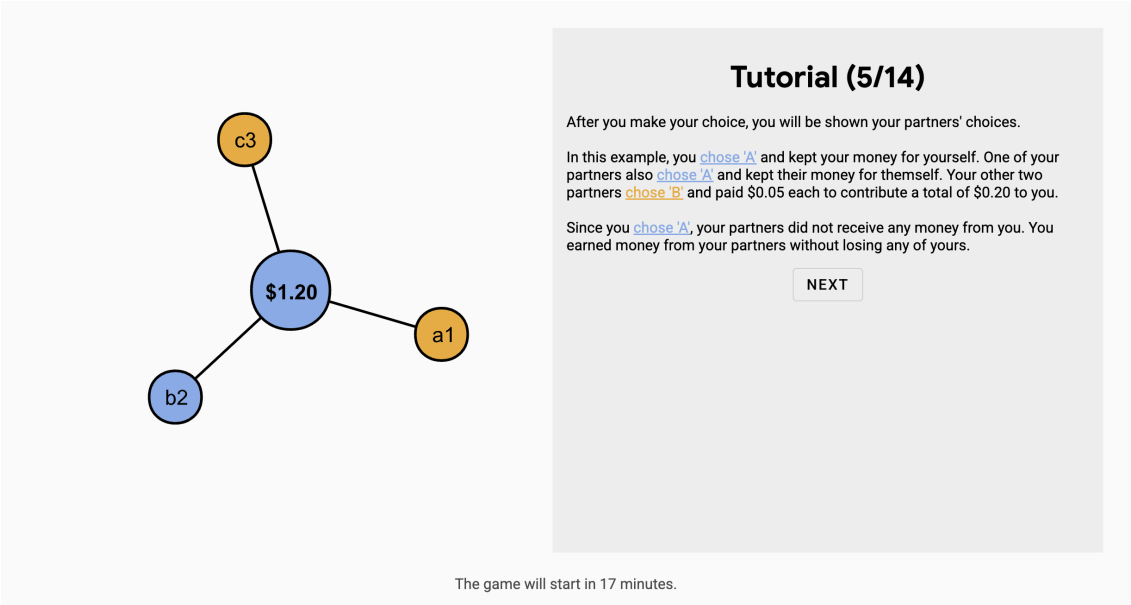

Figure S17. Screenshots of the participant interface for the cooperative network game. (a) The participant reads tutorial information about the game. (b) The participant reads tutorial information about the game.

(a)

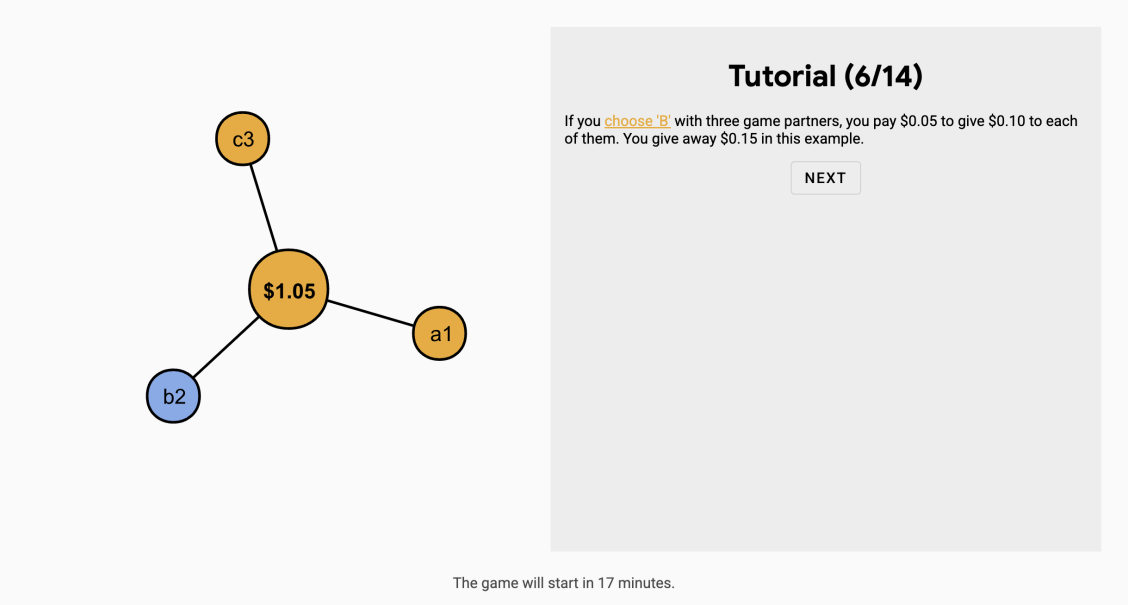

(b)

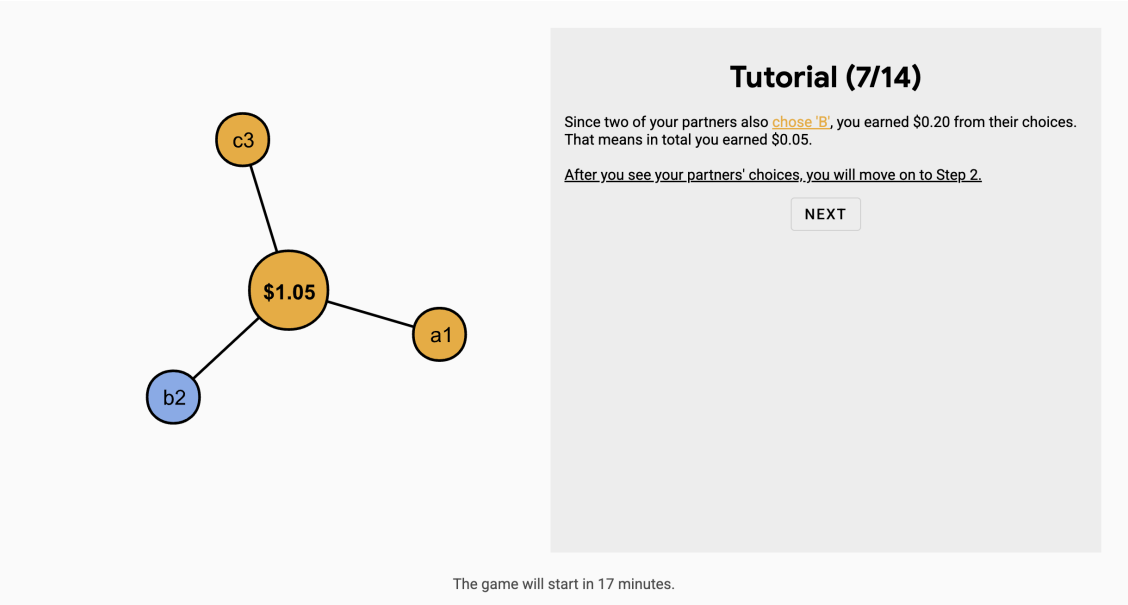

Figure S18. Screenshots of the participant interface for the cooperative network game. (a) The participant reads tutorial information about the game. (b) The participant reads tutorial information about the game.

(a)

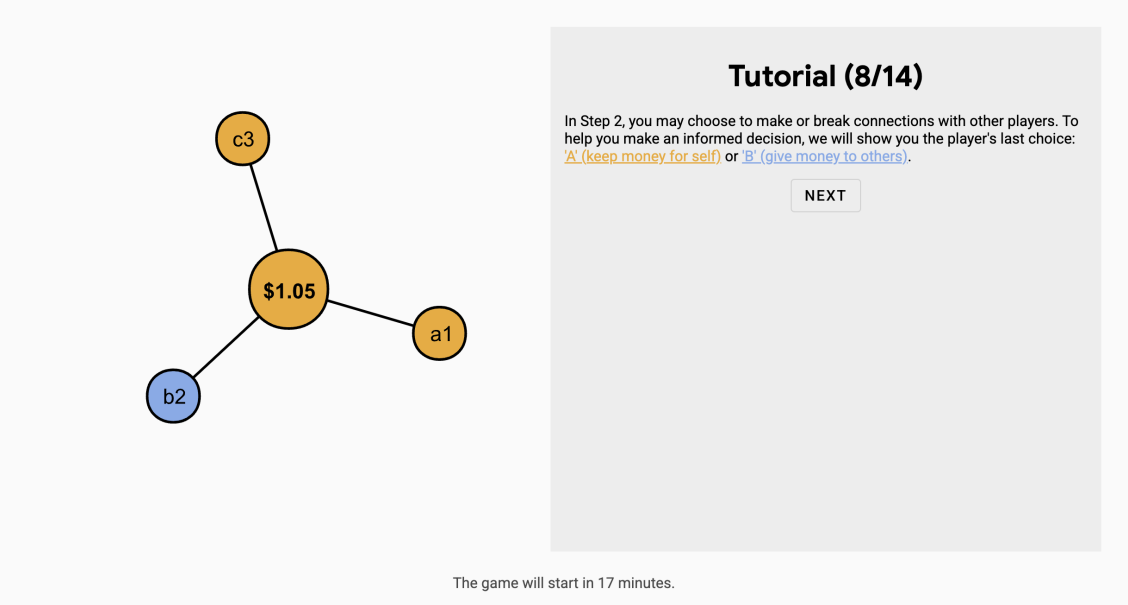

(b)

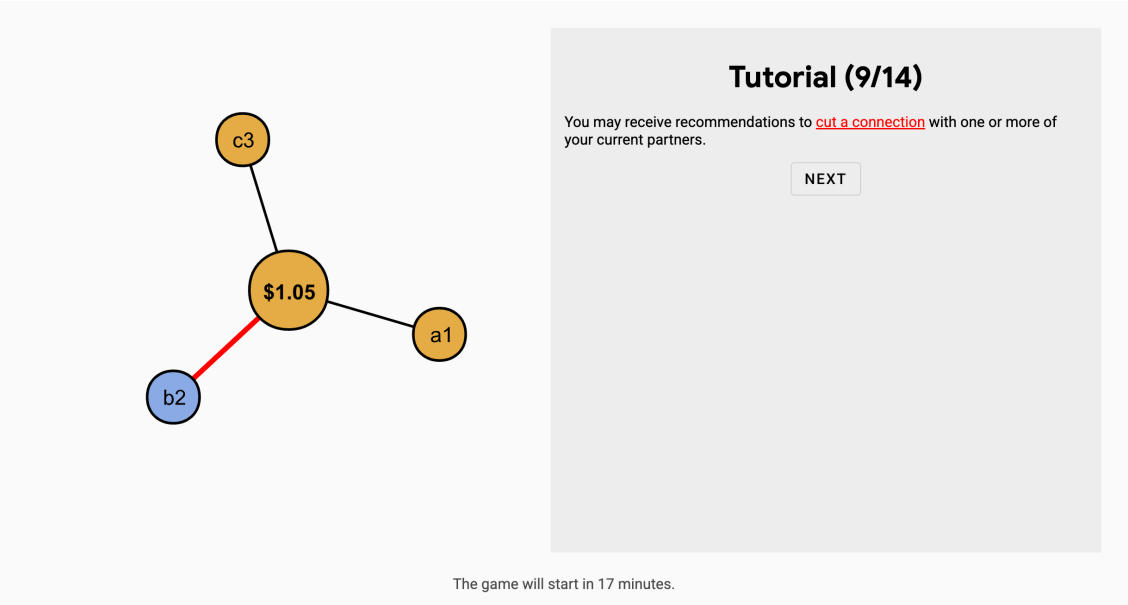

Figure S19. Screenshots of the participant interface for the cooperative network game. (a) The participant reads tutorial information about the game. (b) The participant reads tutorial information about the game.

(a)

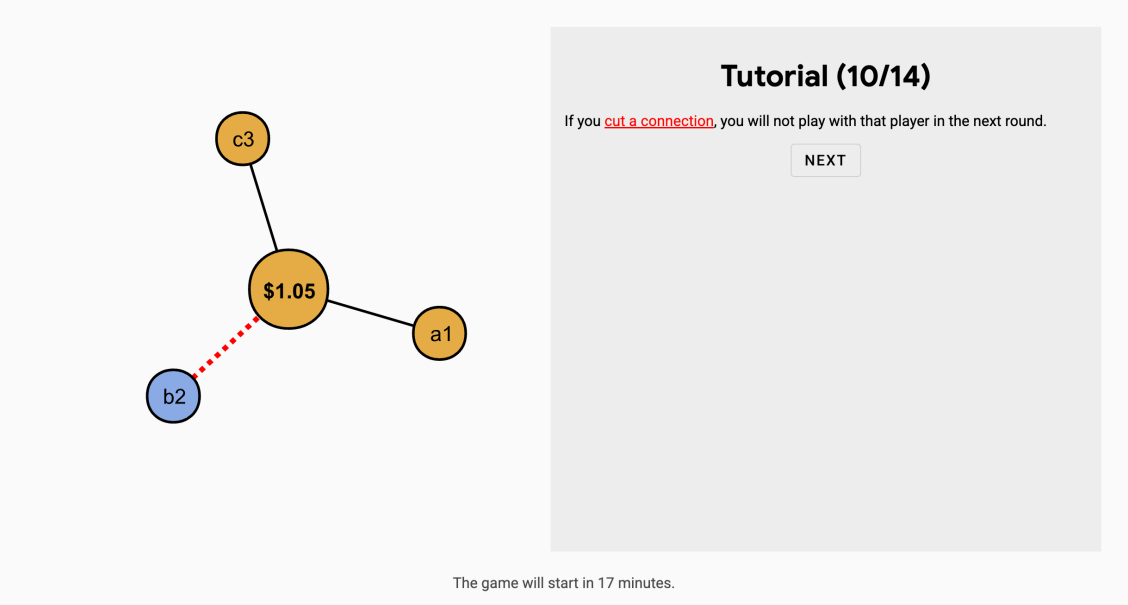

(b)

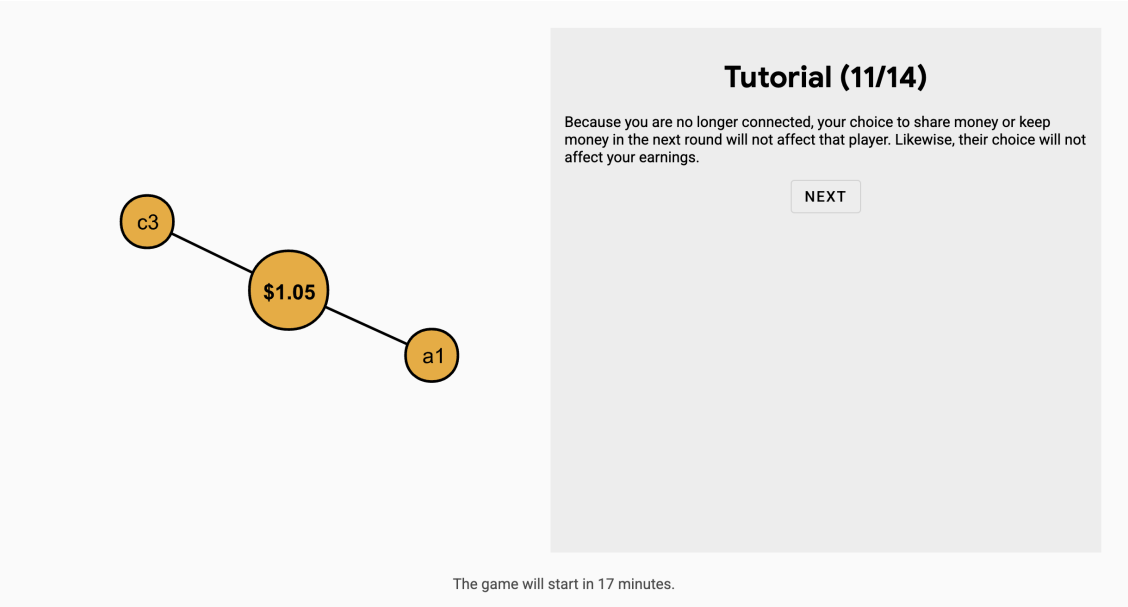

Figure S20. Screenshots of the participant interface for the cooperative network game. (a) The participant reads tutorial information about the game. (b) The participant reads tutorial information about the game.

(a)

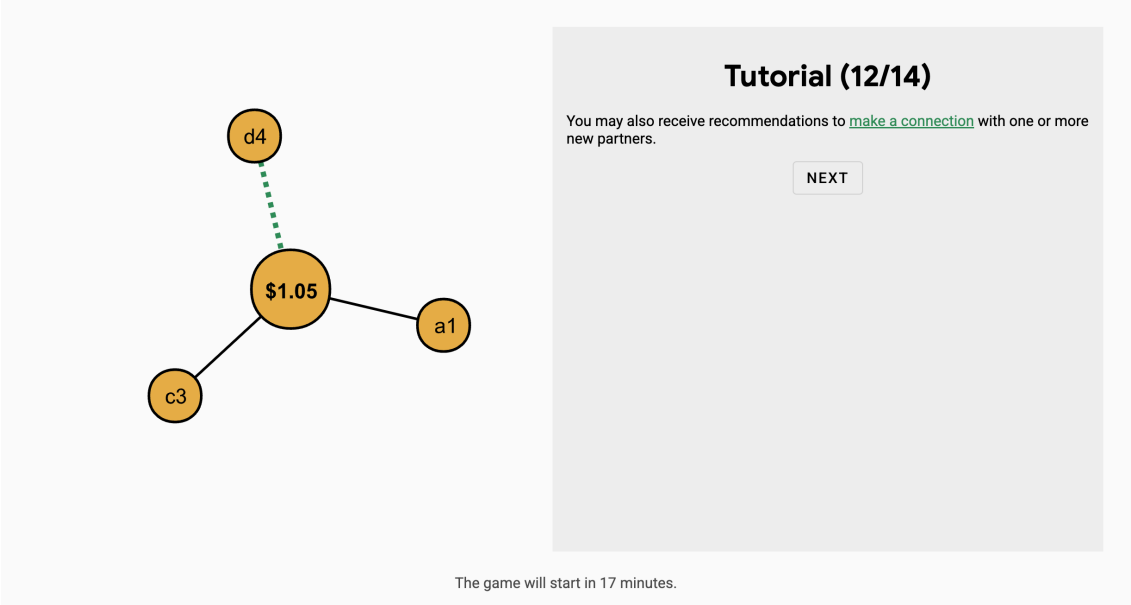

(b)

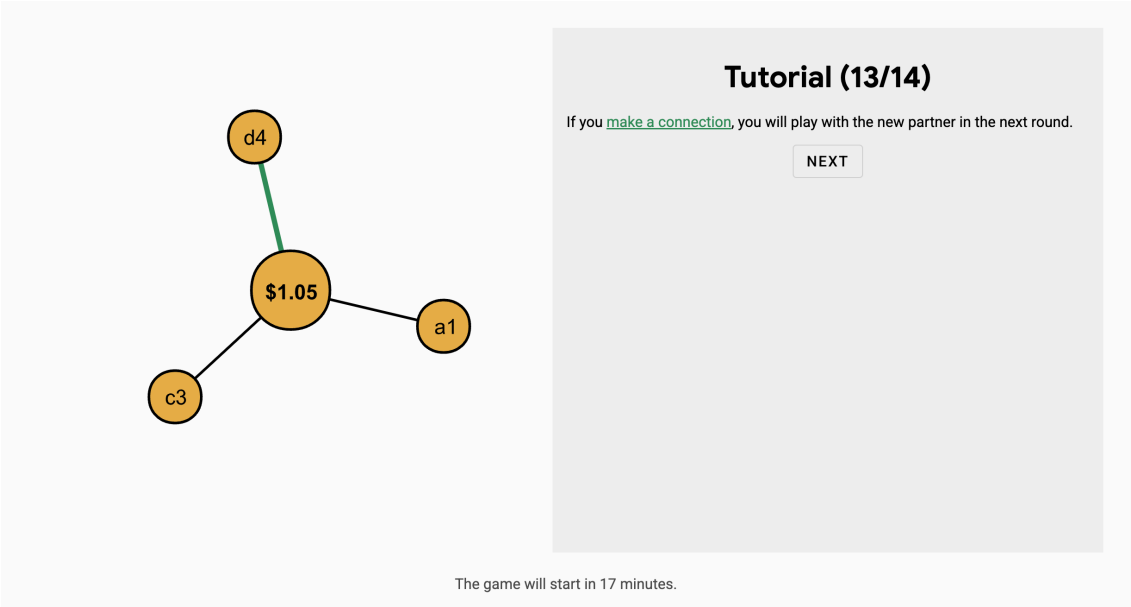

Figure S21. Screenshots of the participant interface for the cooperative network game. (a) The participant reads tutorial information about the game. (b) The participant reads tutorial information about the game.

(a)

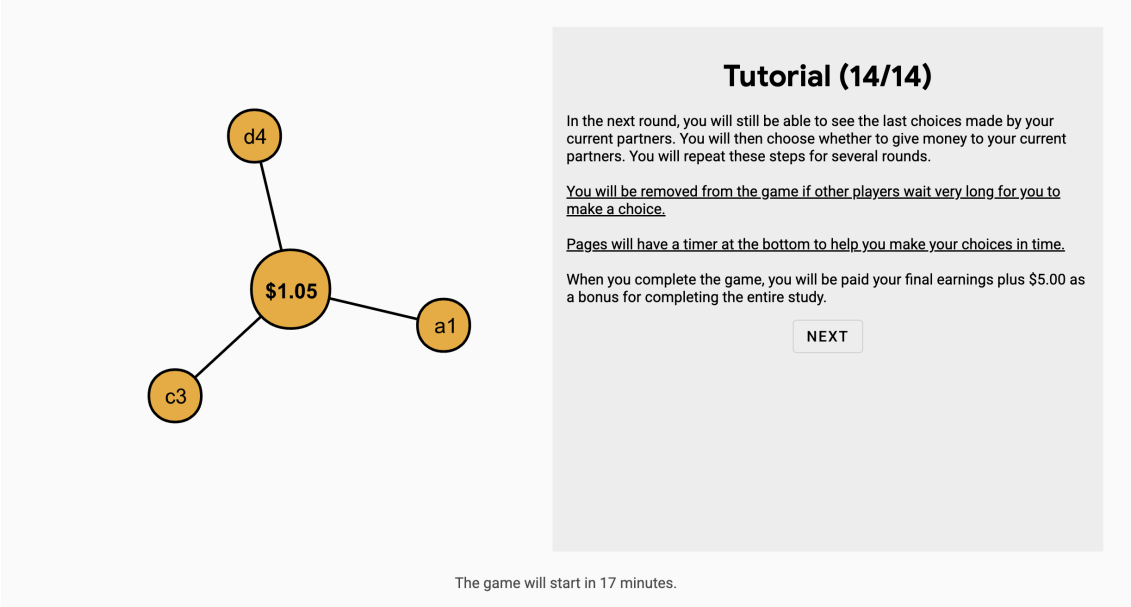

(b)

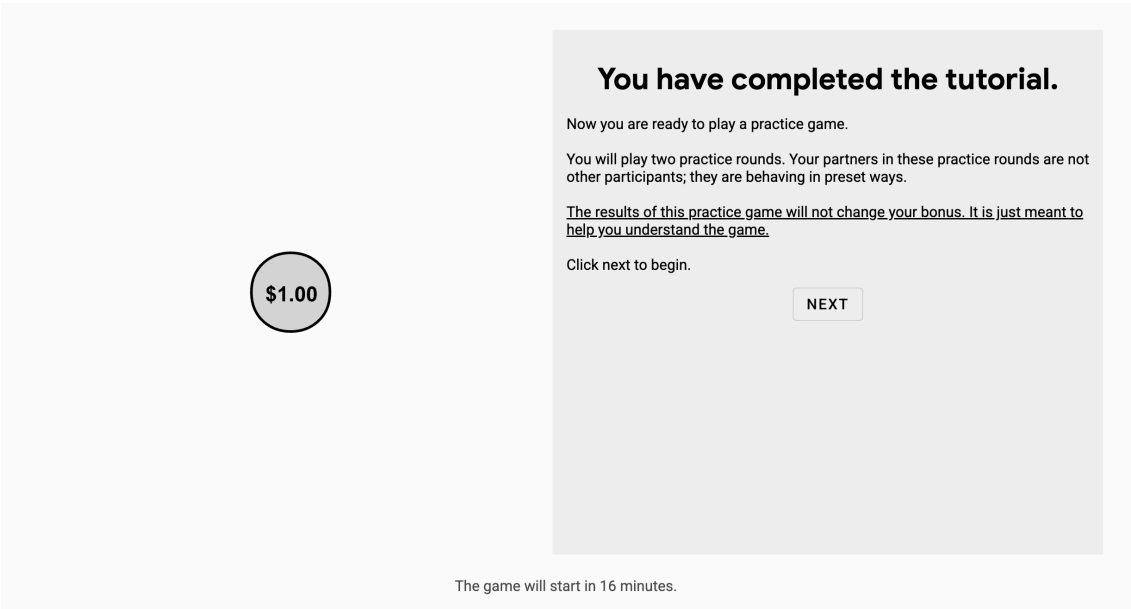

Figure S22. Screenshots of the participant interface for the cooperative network game. (a) The participant reads tutorial information about the game. (b) The participant reads information about the practice game.

(a)

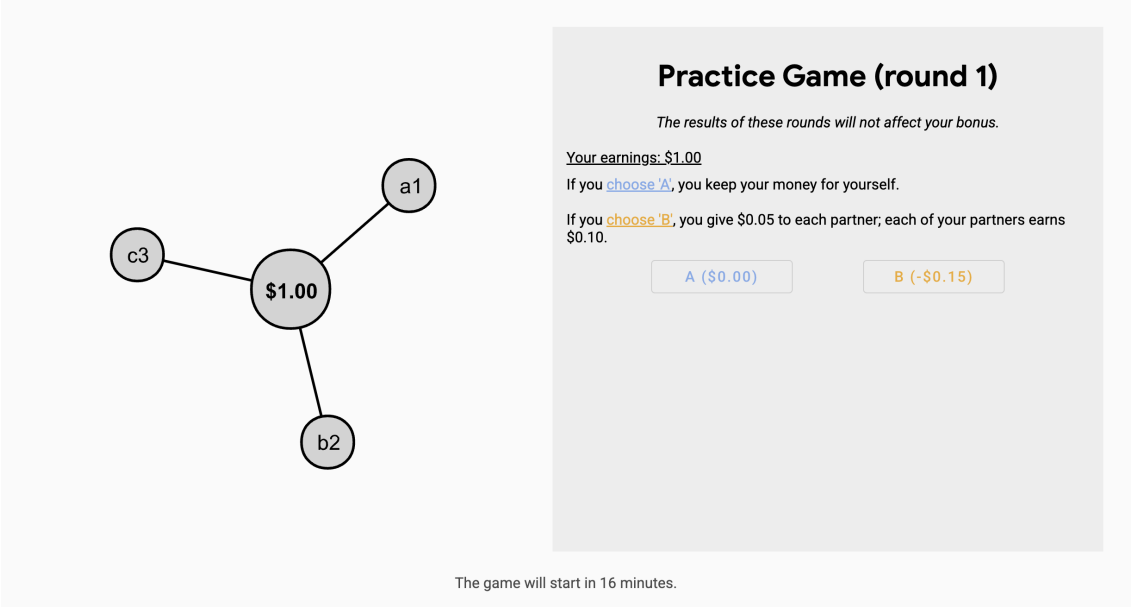

(b)

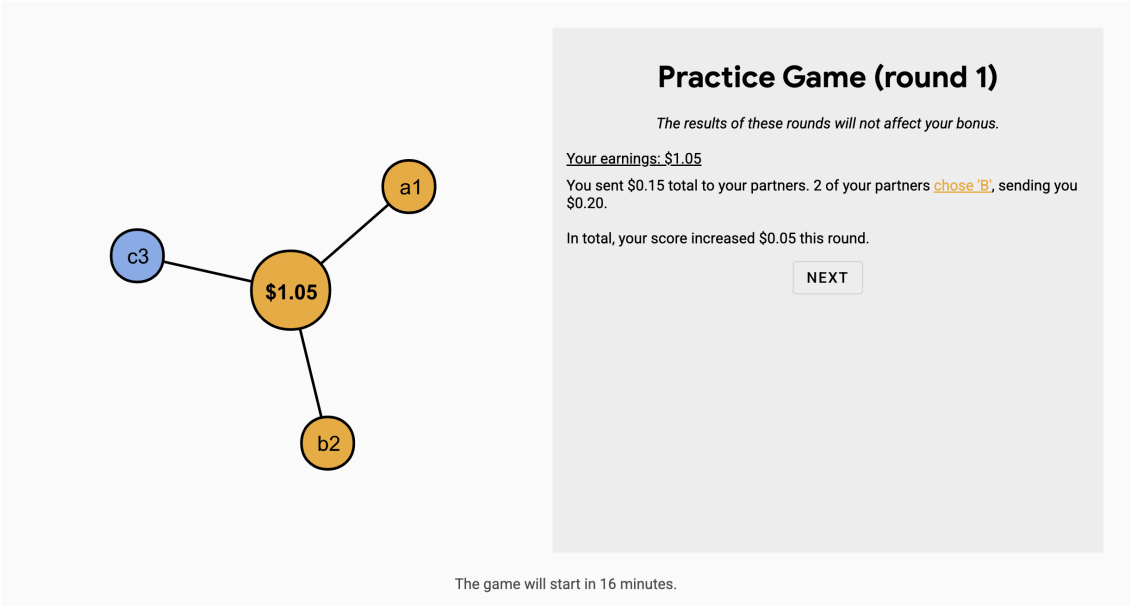

Figure S23. Screenshots of the participant interface for the cooperative network game. (a) The participant observes their neighbors and chooses to cooperate or defect (practice game). (b) The participant sees their earnings and their neighbors' choices (practice game).

(a)

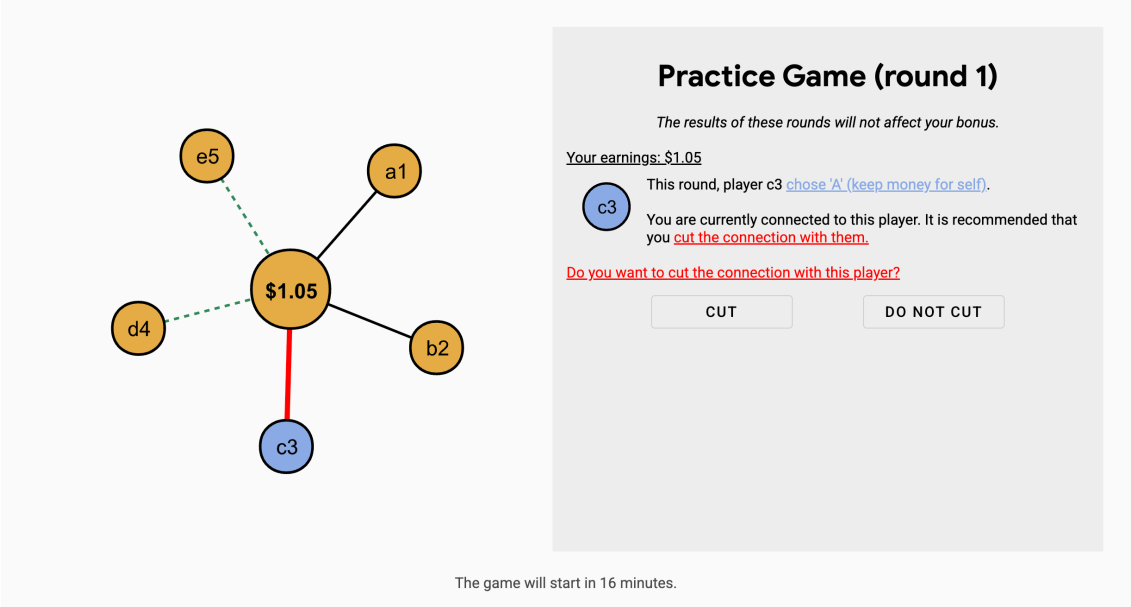

(b)

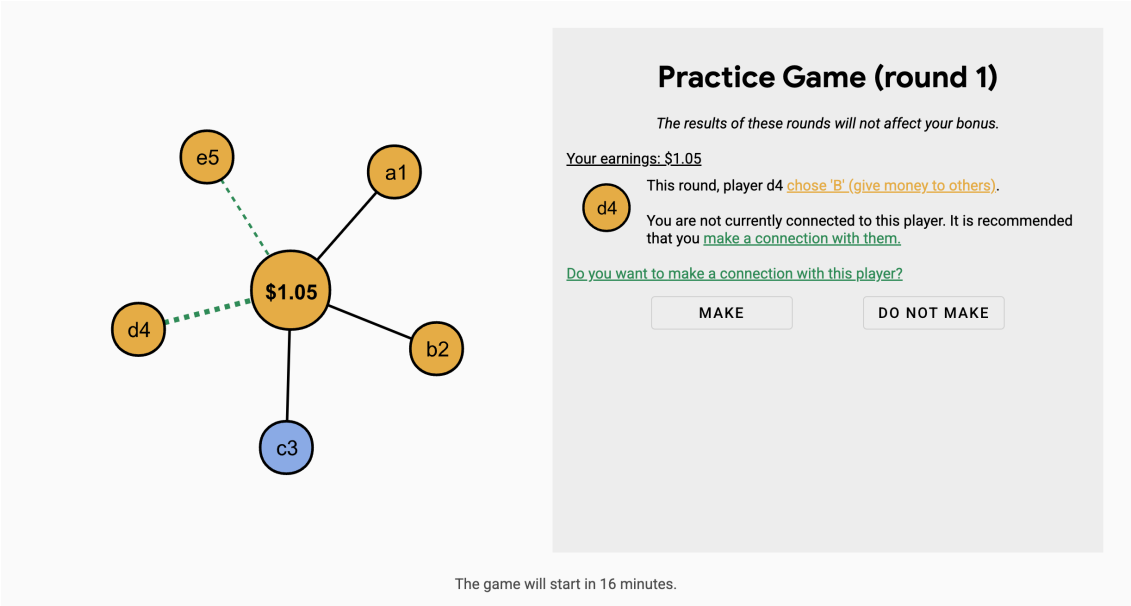

Figure S24. Screenshots of the participant interface for the cooperative network game. (a) The participant sees their pending recommendations and chooses to accept or reject the focal recommendation (practice game). (b) The participant sees their pending recommendations and chooses to accept or reject the focal recommendation (practice game).

(a)

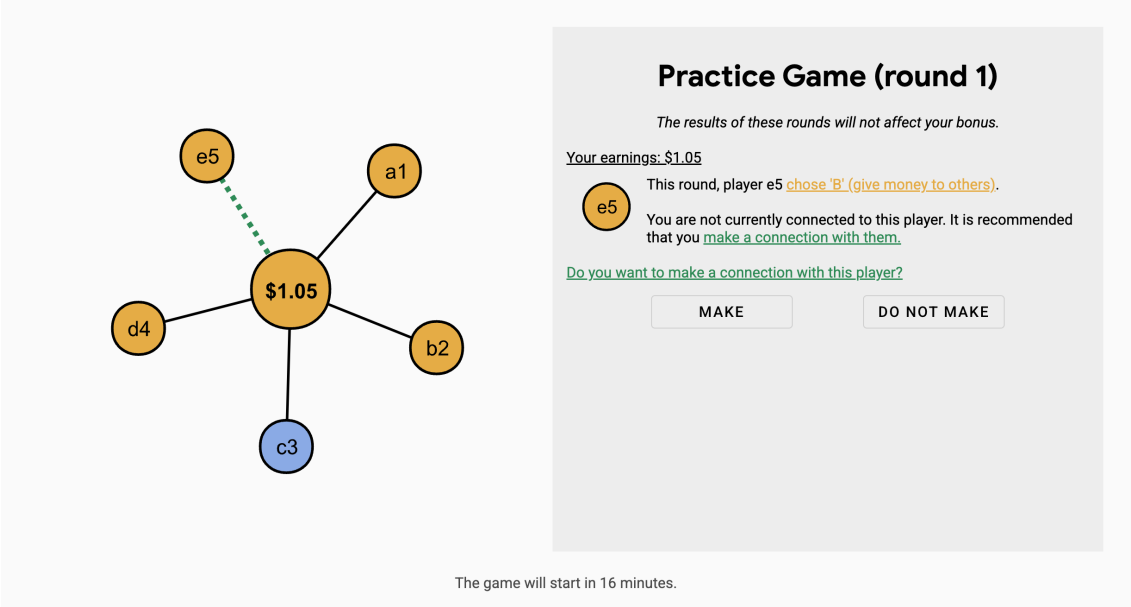

(b)

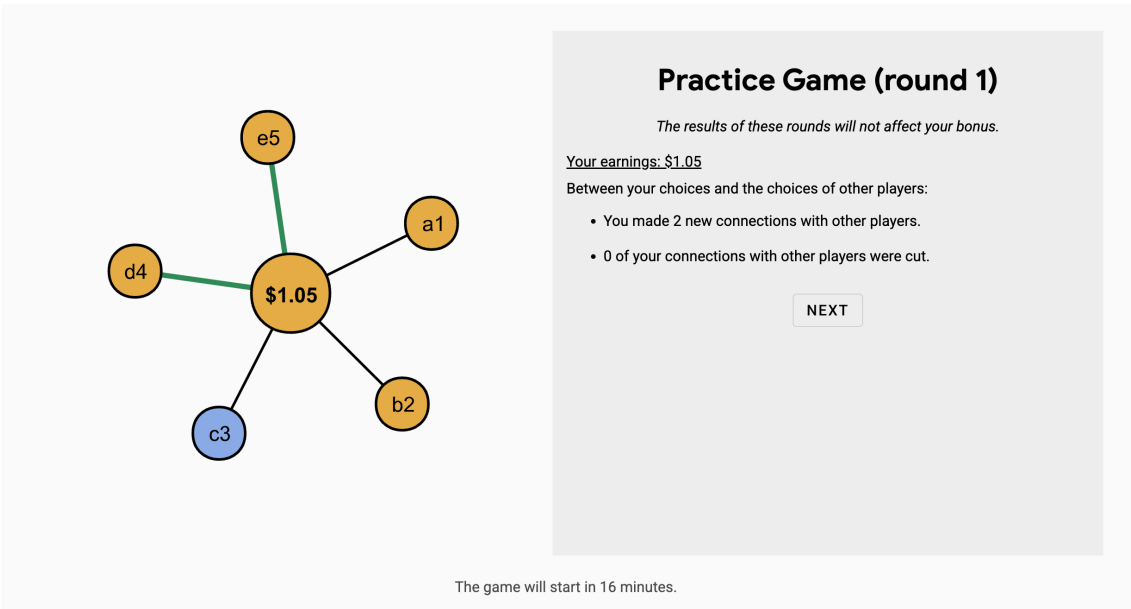

Figure S25. Screenshots of the participant interface for the cooperative network game. (a) The participant sees their pending recommendations and chooses to accept or reject the focal recommendation (practice game). (b) The participant observes the overall set of changes to their neighborhood (practice game).

(a)

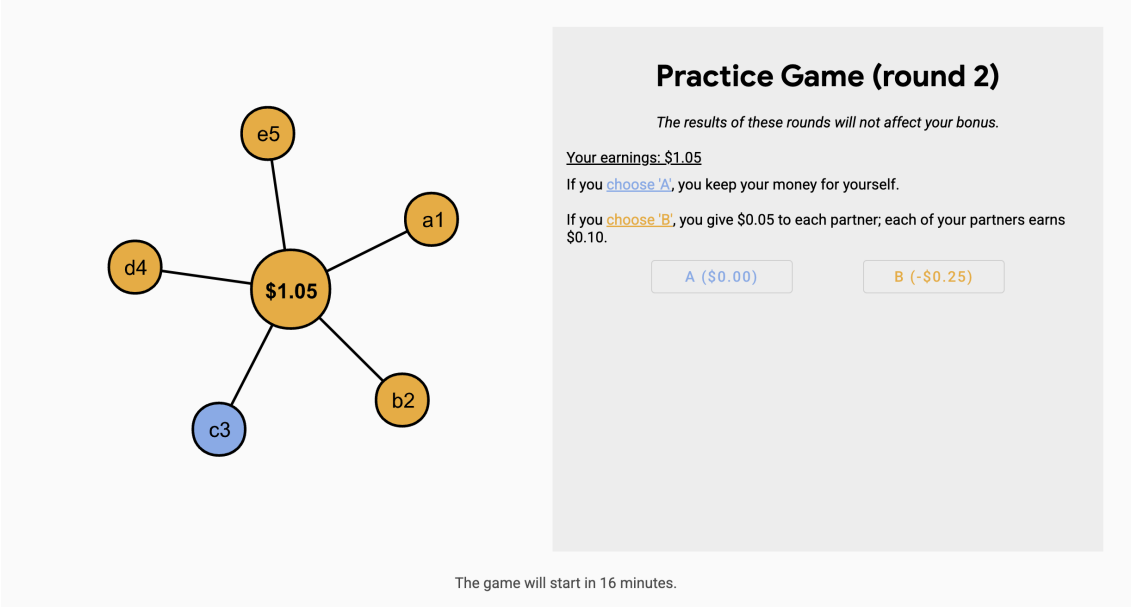

(b)

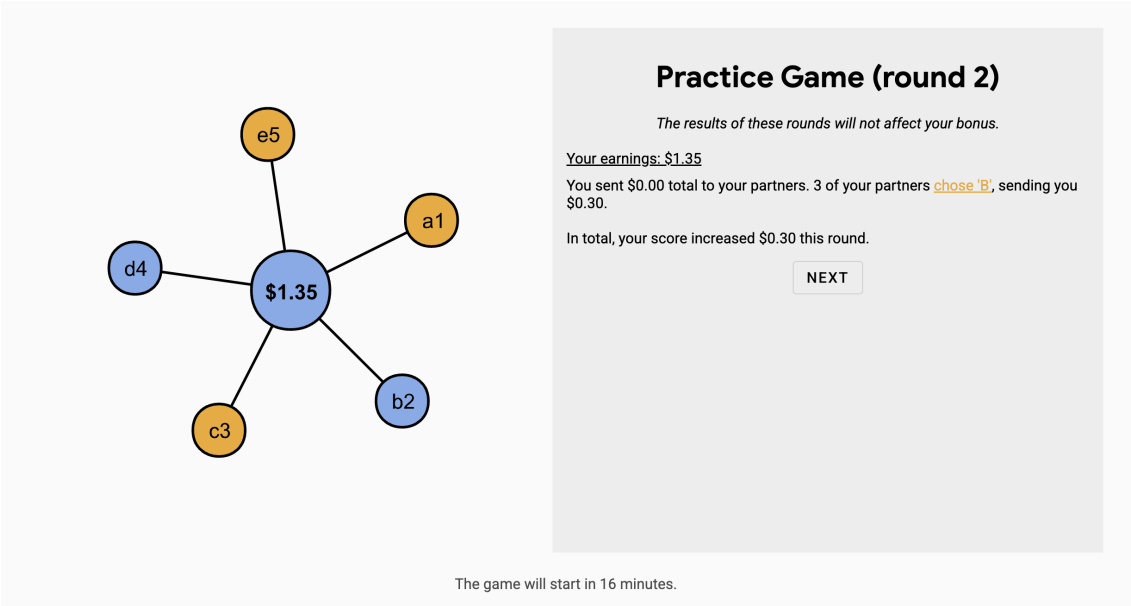

Figure S26. Screenshots of the participant interface for the cooperative network game. (a) The participant observes their neighbors and chooses to cooperate or defect (practice game). (b) The participant sees their earnings and their neighbors' choices (practice game).

(a)

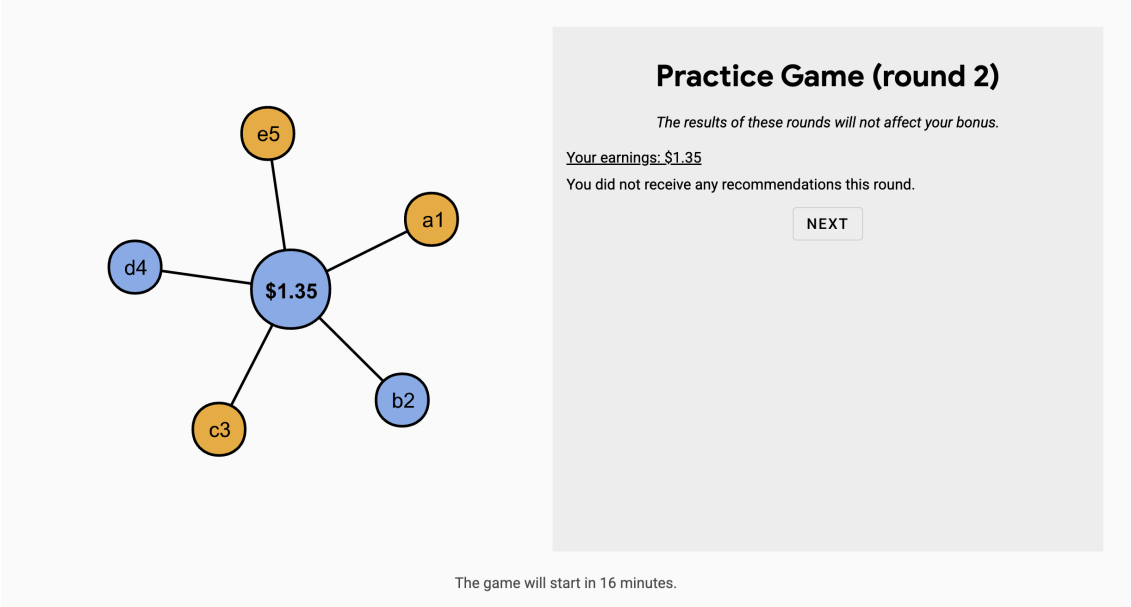

(b)

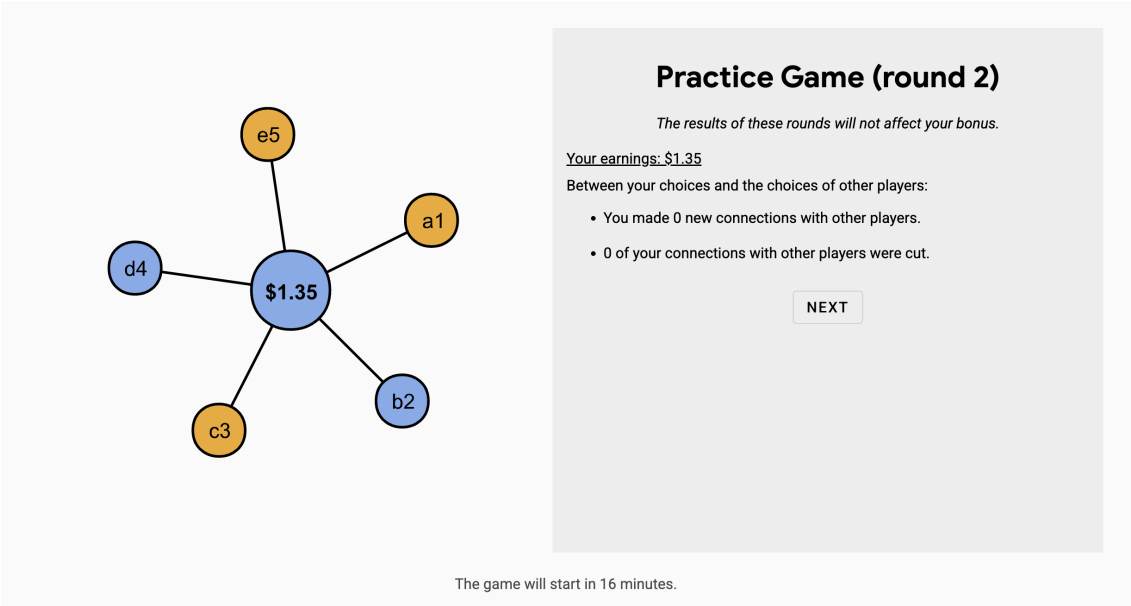

Figure S27. Screenshots of the participant interface for the cooperative network game. (a) The participant sees their pending recommendations and chooses to accept or reject the focal recommendation (practice game). (b) The participant observes the overall set of changes to their neighborhood (practice game).

(a)

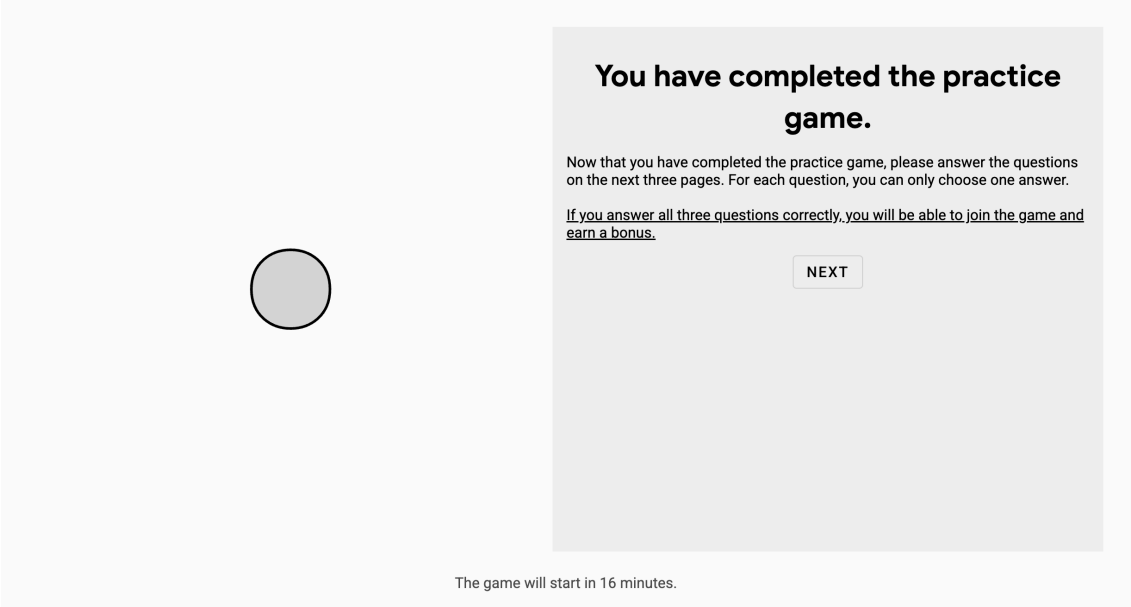

(b)

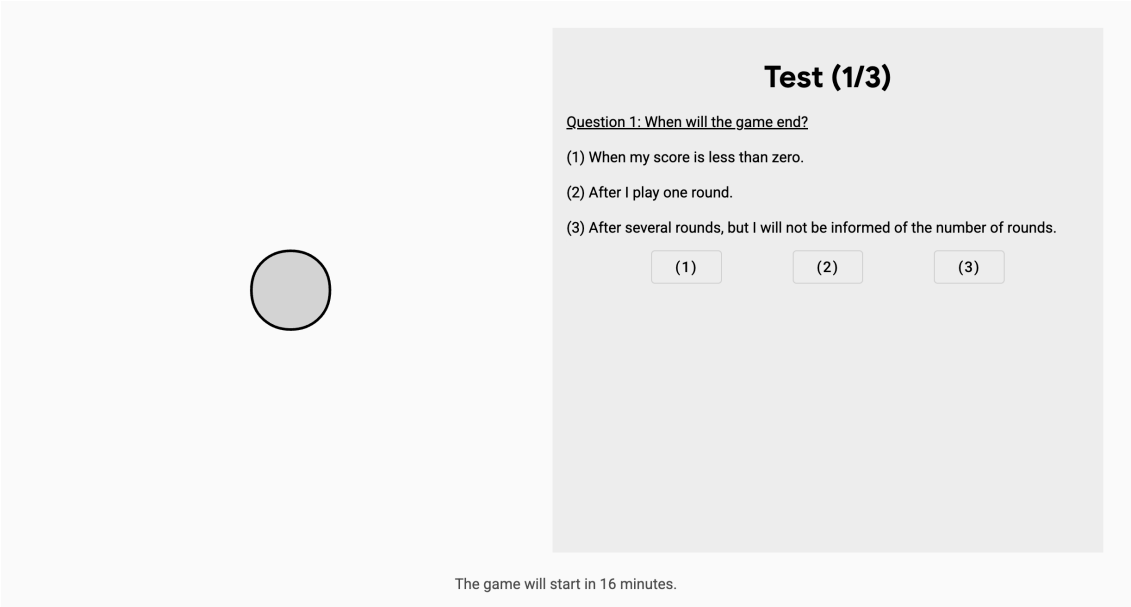

Figure S28. Screenshots of the participant interface for the cooperative network game. (a) The participant reads information about the comprehension test. (b) The participant takes the comprehension test.

(a)

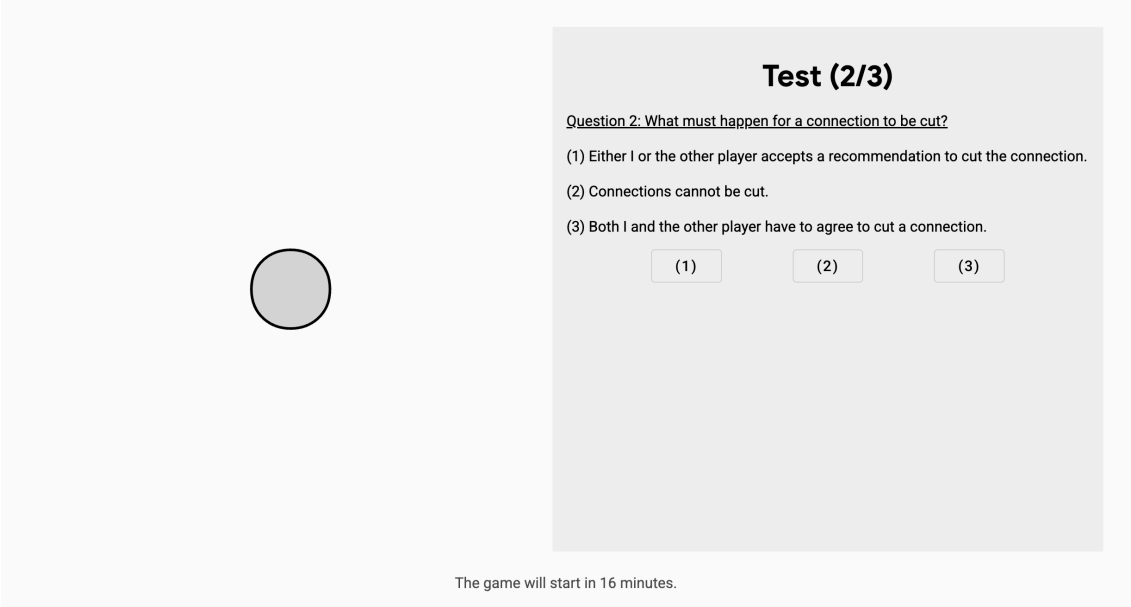

(b)

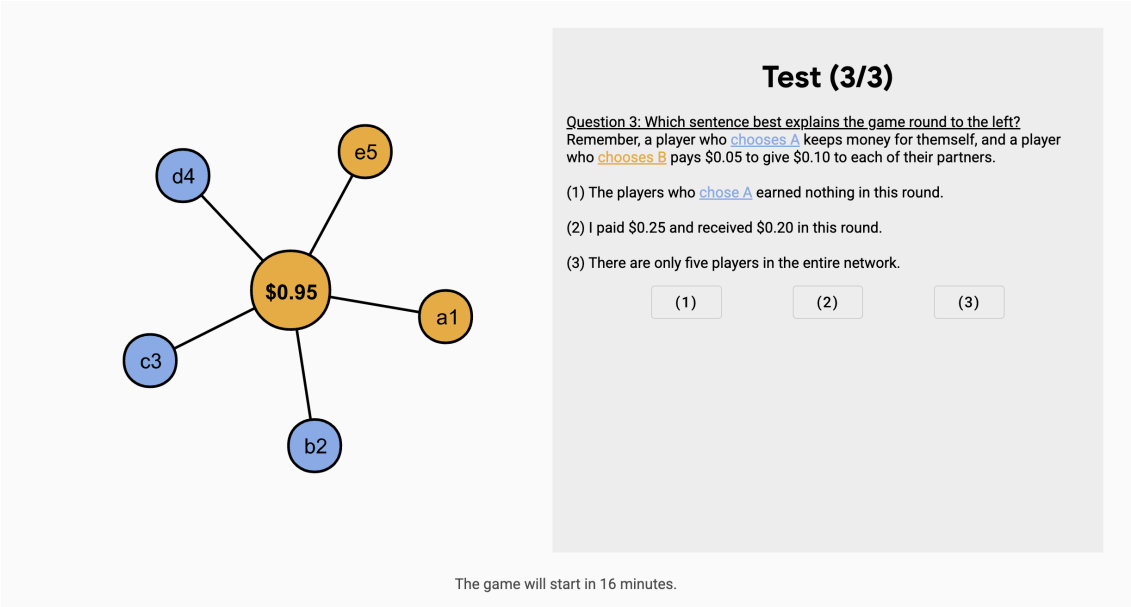

Figure S29. Screenshots of the participant interface for the cooperative network game. (a) The participant takes the comprehension test. (b) The participant takes the comprehension test.

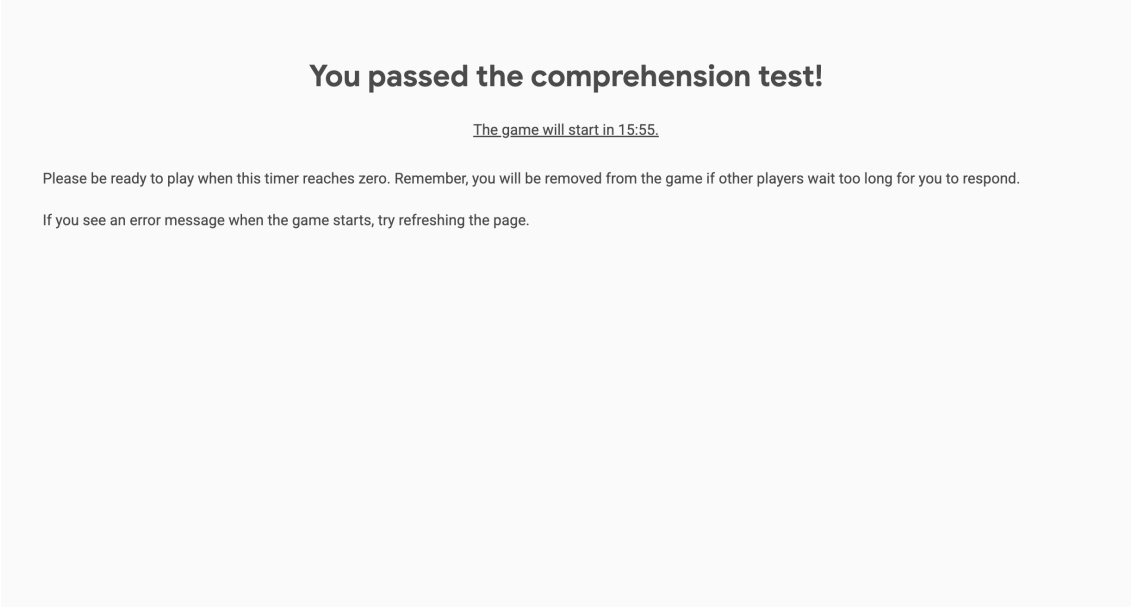

Figure S30. Screenshots of the participant interface for the cooperative network game. The participant sees their results for the comprehension test. If they answered all three questions correctly, the participant waits to be randomly assigned to a game session.

(a)

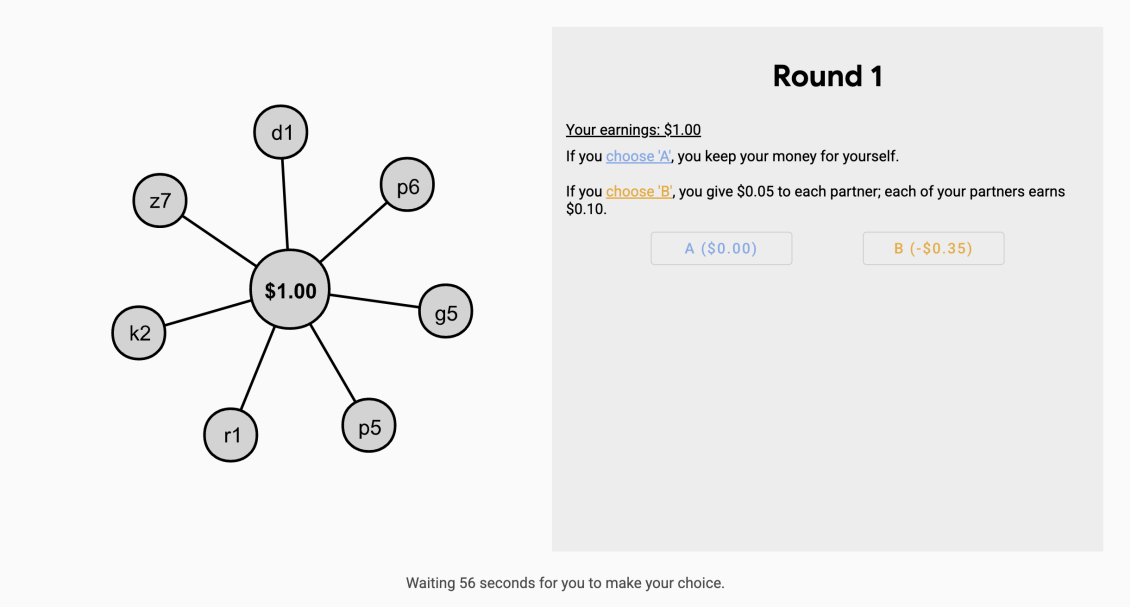

(b)

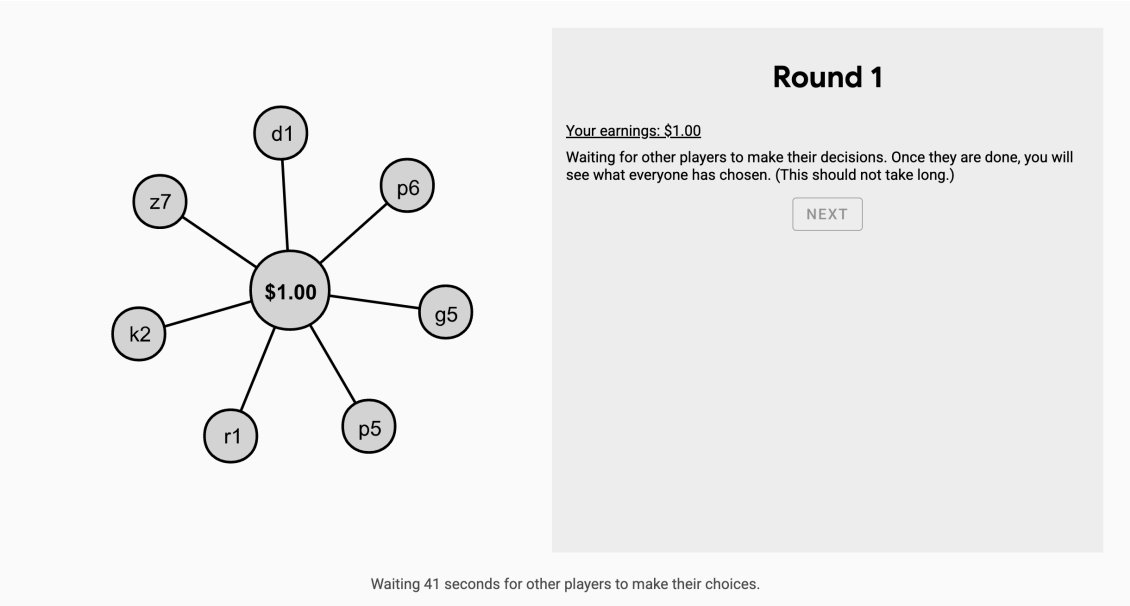

Figure S31. Screenshots of the participant interface for the cooperative network game. (a) The participant observes their neighbors and chooses to cooperate or defect. (b) The participant waits for other participants in the session to make their choices.

(a)

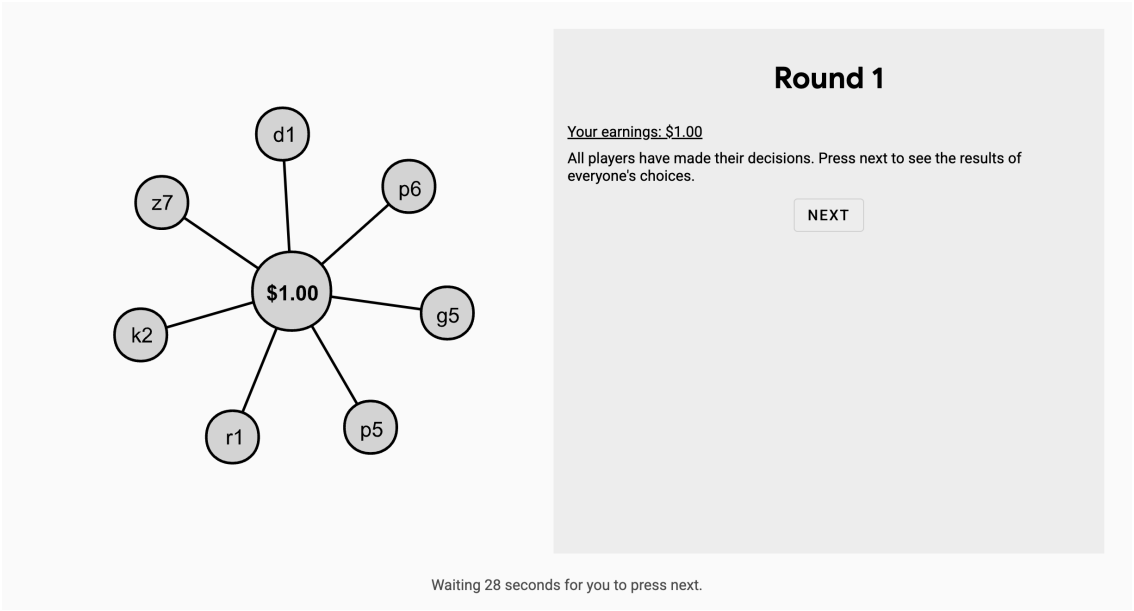

(b)

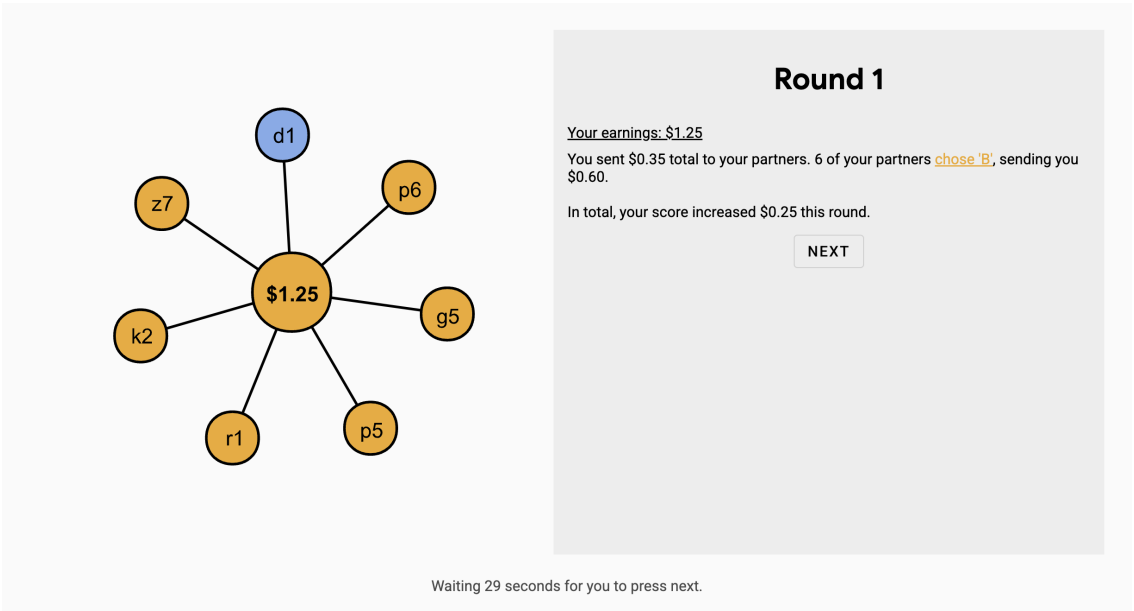

Figure S32. Screenshots of the participant interface for the cooperative network game. (a) The participant clicks to moves on. (b) The participant sees their earnings and their neighbors' choices.

(a)

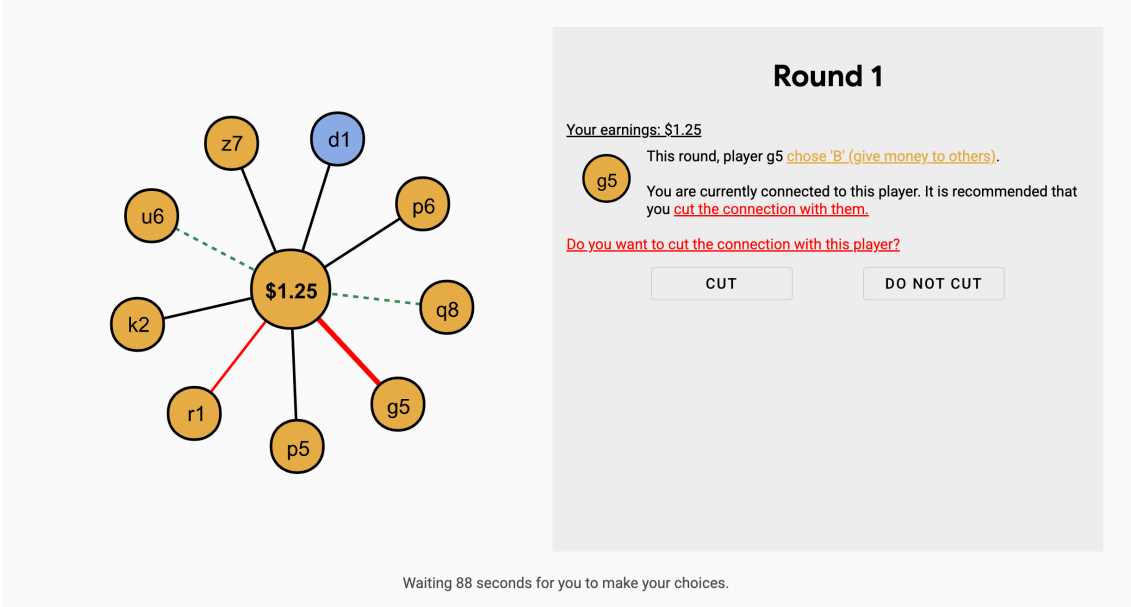

(b)

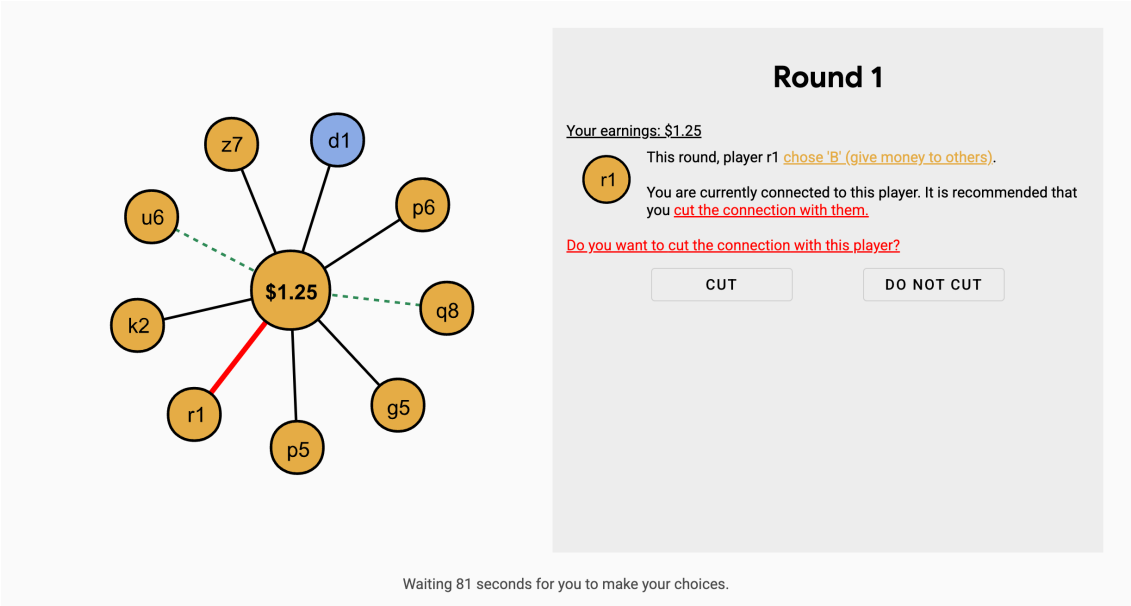

Figure S33. Screenshots of the participant interface for the cooperative network game. (a) The participant sees their pending recommendations and chooses to accept or reject the focal recommendation. (b) The participant sees their pending recommendations and chooses to accept or reject the focal recommendation.

(a)

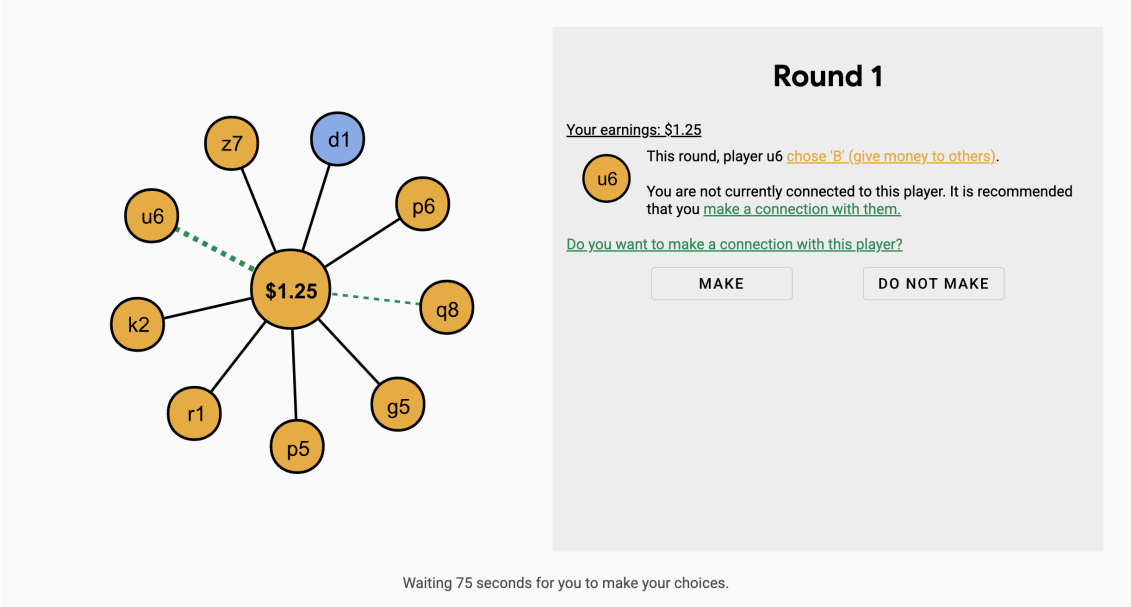

(b)

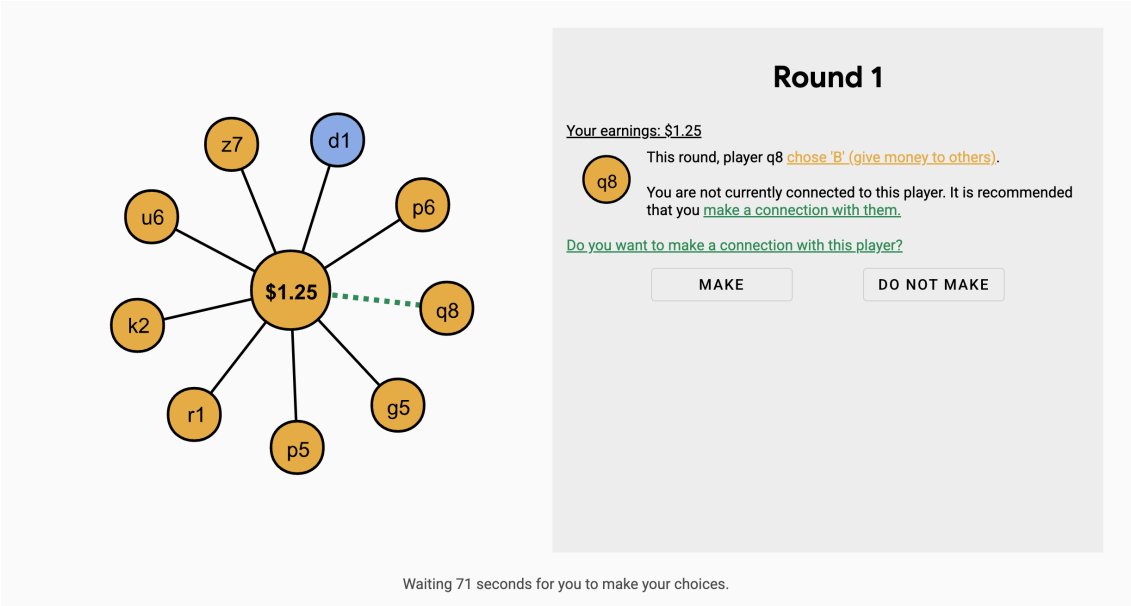

Figure S34. Screenshots of the participant interface for the cooperative network game. (a) The participant sees their pending recommendations and chooses to accept or reject the focal recommendation. (b) The participant sees their pending recommendations and chooses to accept or reject the focal recommendation.

(a)

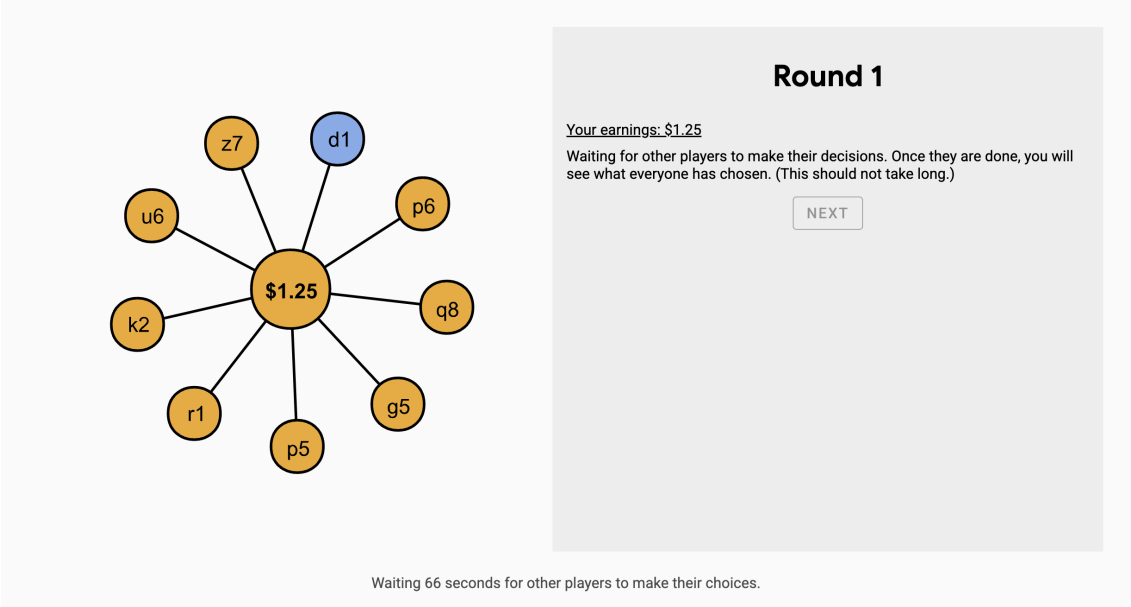

(b)

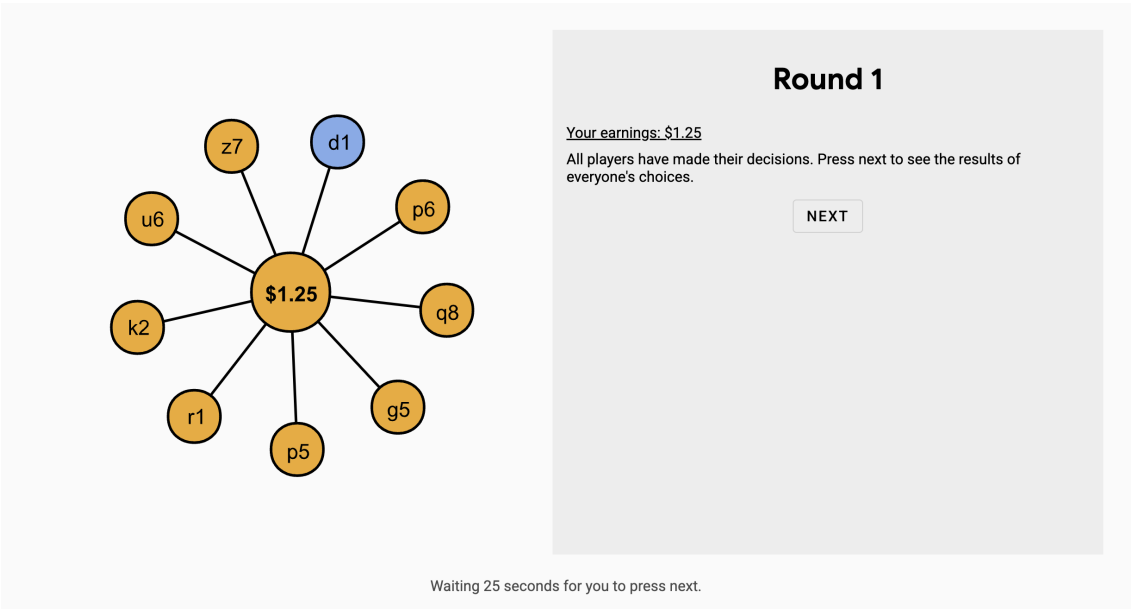

Figure S35. Screenshots of the participant interface for the cooperative network game. (a) The participant waits for other participants in the session to make their choices. (b) The participant clicks to moves on.

(a)

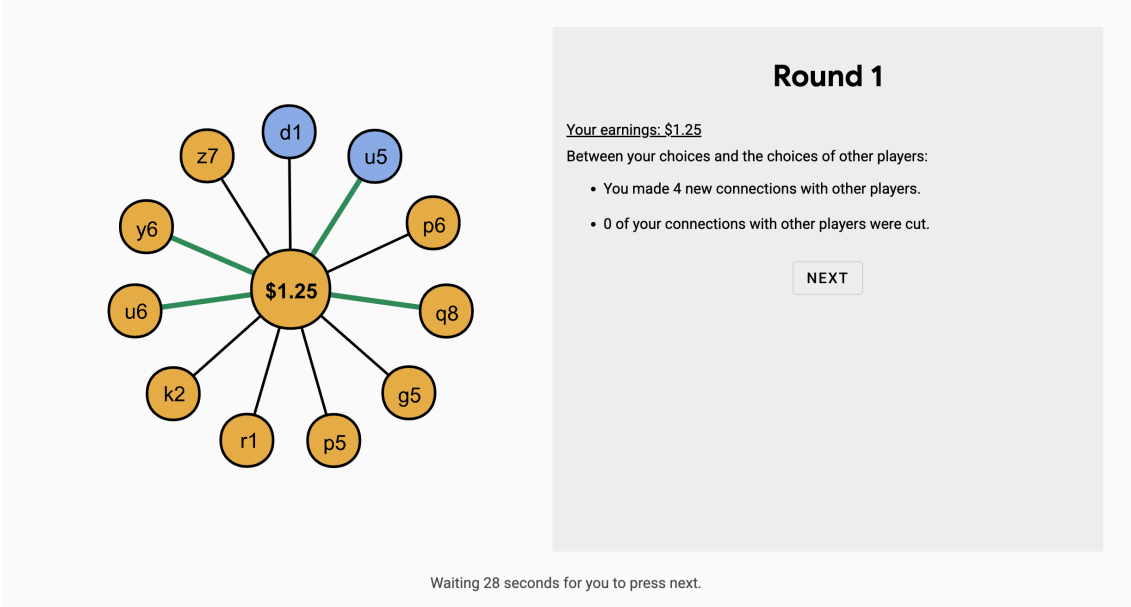

(b)

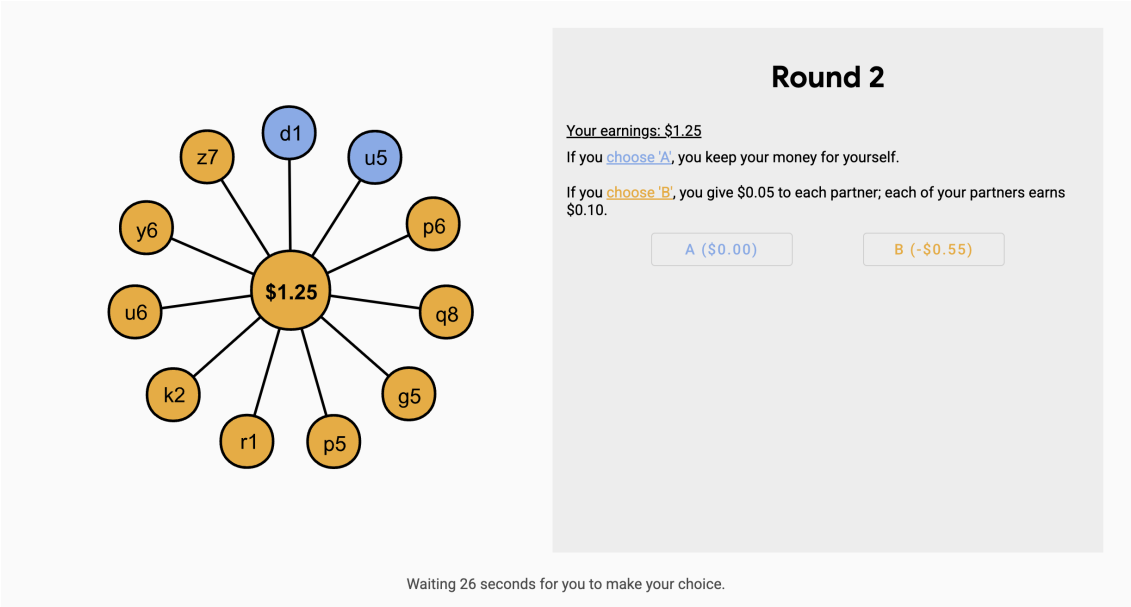

Figure S36. Screenshots of the participant interface for the cooperative network game. (a) The participant observes the overall set of changes to their neighborhood. (b) The participant observes their neighbors and chooses to cooperate or defect.

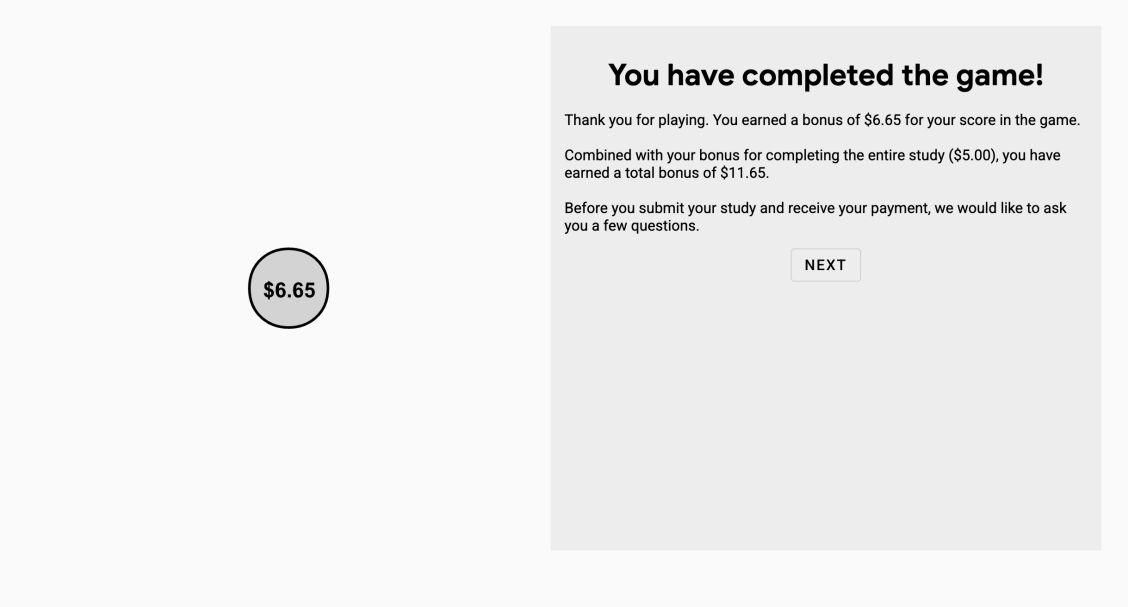

Figure S37. Screenshots of the participant interface for the cooperative network game. The participant learns their total earnings and reads about the post-game questionnaire.